Cape Peninsula
University of Technology

Power allocation for multiple input multiple output systems

by

Rifqah Press

Thesis submitted in fulfilment of the requirements for the degree

Master of Engineering: Electrical Engineering

in the Faculty of Engineering and the Built Environment

at the Cape Peninsula University of Technology

Supervisor: Dr Vipin Balyan

Bellville
September 2021

CPUT Copyright Information
The dissertation/thesis may not be published either in part (in scholarly, scientific or technical journals), or as a whole (as a monograph), unless permission has been obtained from the university

DECLARATION

I, Rifqah Press, declare that the contents of this dissertation/thesis represent my own unaided work, and that the dissertation/thesis has not previously been submitted for academic examination towards any qualification. Furthermore, it represents my own opinions and not necessarily those of the Cape Peninsula University of Technology.

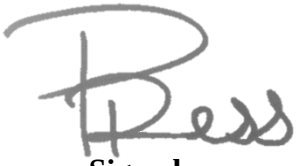

Signed

30/09/2021
Date

ABSTRACT

Mobile communication systems face power consumption issues, specifically multiple input multiple output (MIMO) systems, due to the vast number of antennas. Research shows the movement towards greener mobile communications, whereby utilising more energy-efficient systems. This research aims to design and develop an approach to improve the power allocation of a broadcast MIMO system.

A literature review highlights the current power allocation schemes advantages and disadvantages of said schemes. Analysis shows the effectiveness of current schemes and the design of a new power allocation approach to fill the gap in the current scheme. The implementation of non-orthogonal multiple acess (NOMA) into a broadcast MIMO system significantly improves the system's energy and spectral efficiency. A power allocation algorithm is implemented into a NOMA-based relay system, where relays aid cell-edge users. The cell center users connect directly to the base station, whereas the cell edge users connect via relay. The user equipment (UEs) and relays successfully employ successive interference cancellation (SIC) to cancel and decode unintended signals. Outage probability and ergodic rate simulations show the effectiveness of the power allocation scheme, where user fairness is also considered.

Energy harvesting relays are a step closer to greener communications, where the relays harvest energy from the received signal and utilises the harvested energy to forward the signals to the connected users. Simulation results show improvements in the outage probability of the users.

ACKNOWLEDGMENTS

I wish to thank:

- My creator, for granting me this blessing and opportunity
- Dr. Vipin, for all the contribution, guidance, and support
- My family, for all the encouragement, prayers, and sustenance
- The Erasmus plus program for allowing me to complete part of my studies in Bulgaria at the University of Sofia.
- The financial assistance of the National Research Foundation towards this research is acknowledged. Opinions expressed in this thesis and the conclusions arrived at are those of the author and are not necessarily to be attributed to the National Research Foundation.

DEDICATION

I dedicate this to my husband, daughter and especially mother-in-law and father-in-law. I make particular thanks to my in-laws, without whom this would not be possible. Thank you for all the ways you have supported me, for all the motivation, love and confidence.

TABLE OF CONTENTS

LIST OF FIGURES

LIST OF TABLES

GLOSSARY

3GPP	Third-Generation Partnership Project
5G	Fifth Generation
AF	Amplify -and-Forward
AMPS	Advanced Mobile Phone Services
BS	Base Station
BW	Bandwidth
CDMA	Code Division Multiple Access
CPS	Cyber-Physical System
D2D	Device-to-Device
DFT	Discreet Fourier Transform
DFT	Discreet Fourier Transform
DFTS-OFDM	Discrete Fourier Transform-Spread Orthogonal Frequency Division Multiplexing
EDGE	Enhanced Data rates for GSM Evolution
eMBB	Enhanced Mobile Broadband
E-UTRA	Evolved Universal Terrestrial Radio Access
FBMC	Filter Bank Multi-Carrier
FDD	Frequency Division Duplex
FDMA	Frequency Division Multiple Access
FFT	Fast Fourier Transform
F-OFDM	Filtered OFDM
GFDM	Generalised Frequency Division Multiplexing
GPRS	General Packet Radio Services
GSM	Global System for Mobile Communications
HSDPA	High-Speed Downlink Packet Access
HSPA	High-Speed Packet Access
HSUPA	High-Speed Uplink Packet Access
IDMA	Interleave Division Multiple Access
IoT	Internet of Things
ITU	International Telecommunications Union
LDS	Low-Density Spreading
LOS	Line OF Sight
LTE	Long-Term Evolution
MA	Multiple Access
MCS	Modulation and Coding Scheme
MEC	Multi-access Edge Computing
MIMO	Multiple Input Multiple Output
MISO	Multiple-Input Single-Output
mMTC	Massive Machine Type Communications
mmWave	Millimeter-Wave
MRC	Maximum Ratio Combining
NFV	Network Function Virtualisation
NMT	Nordic Mobile Telephone
NOMA	Non-Orthogonal Multiple Access
OFDM	Orthogonal Frequency Division Multiplexing
OFDMA	Orthogonal Frequency Division Multiple Access

OMA	Orthogonal Multiple Access
OP	Outage Probability
PA	Power Allocation
PHY	Physical Layer
PN	Pseudo-Noise
PSR	Power Splitting Relaying
QAM	Quadrature Amplitude Modulation
QoS	Quality of Service
QPSK	Quadrature Phase Shift Keying
RAN	Radio Access Network
RAT	Radio Access Technology
RB	Resource Block
RE	Resource Element
RF	Radio Frequency
SC	Superposition Coding
SC-FDM	Single-Carrier Frequency Division Multiplexing
SCMA	Sparse Code Multiple Access
SDN	Software-Defined Networking
SIC	Successive Interference Cancellation
SIMO	Single-Input Multiple-Output
SINR	Signal to Interference plus Noise Ratio
SMS	Short Message Service
TACS	Total Access Communication Systems
TDD	Time Division Duplex
TDMA	Time Division Multiple Access
TSR	Time Switching Relaying
UAV	Unmanned Air Vehicle
UE	User Equipment
UFMC	Universal Filtered Multi-Carrier
UMTS	Universal Mobile Technology System
URLLC	Ultra-Reliable and Low Latency Communications
VR	Virtual Reality
WCDMA	Wideband Code Division Multiple Access
WCS	Wireless Communication Systems
WET	Wireless Energy Transfer
WiMAX	Worldwide interoperability for Microwave Access
ZF	Zero-Forcing

Chapter 1

INTRODUCTION

1.1. Introduction to Problem

Mobile communications have increased over the years, with people using their mobile devices daily for work, video streaming, and online gaming. Every day the amount of mobile users increases, and due to the limited resources, the mobile communication system is struggling to accommodate all the users. Therefore, the communication system must adapt and evolve to provide services to the daily influx of users (Cai et al., 2021). The technology for wireless communication systems (WCS) has significantly improved over the years (Yang et al., 2017, chap.1). Fifth-generation (5G) wireless networks are the latest wireless communication technology, requiring increased data rates and energy conservation. Multiple input multiple-output (MIMO) is a technology that utilises multiple antennas at the transmitter and receiver. It is a 3G and 4G mobile technology and a candidate technology for 5G to alleviate the strain on the communication system and provide higher data rates (Alexiou, 2017).

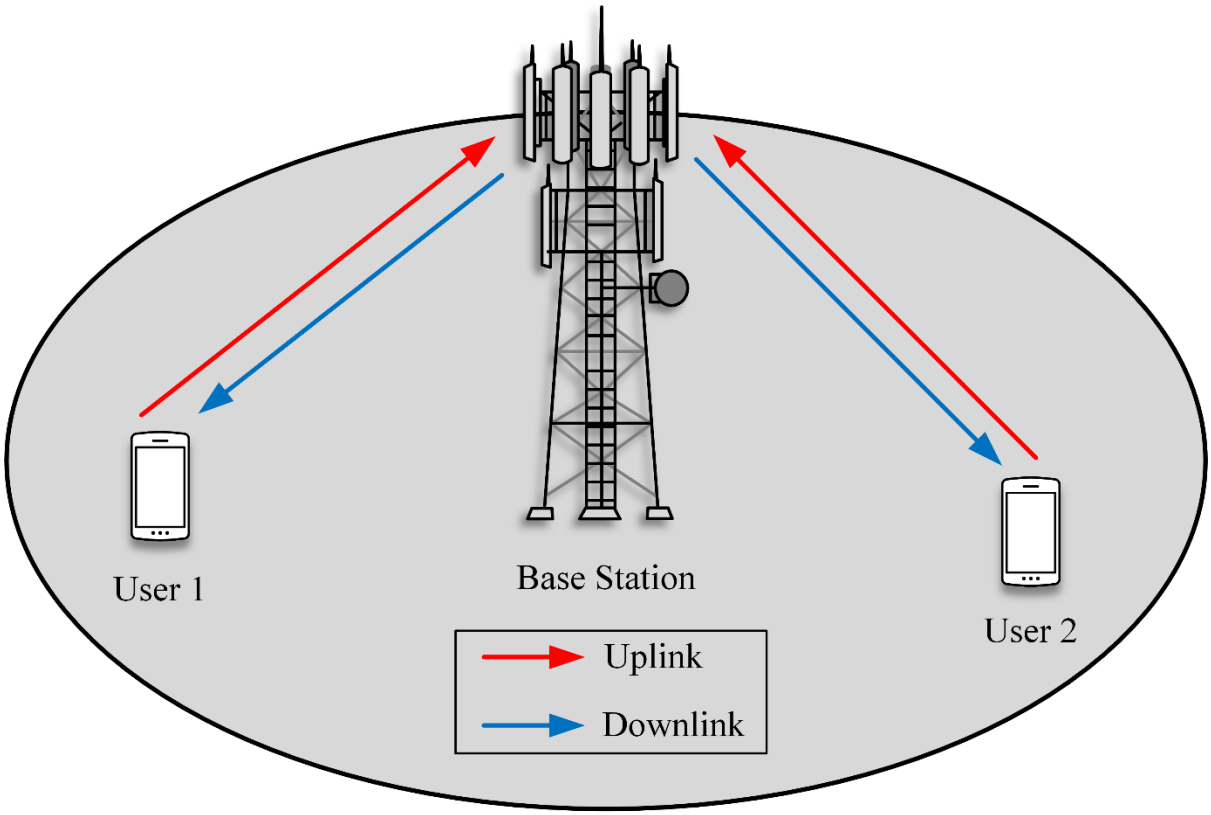

Figure 1.1: Base station coverage area

A cellular network consists of many base stations servicing single or multiple users in a given area. Figure 1.1 shows the coverage area of a single base station communicating with two users on the uplink and downlink. Given the allocated resources, the base station aims to provide reliable wireless communication to connected users. A significant performance metric of a WCS is throughput spectral efficiency, defined as the total data rate transmitted over a given bandwidth. Increasing the spectral efficiency of a mobile communication system provides increased: data rates, service reliability, and coverage. By taking advantage of the spatial dimension, MIMO allows us to improve the communication system's spectral efficiency, resulting in; channel interference mitigation, spectral resource reuse, signal power gains, and robustness (Huang et al., 2011).

For MIMO, the multiple inputs are multiple transmit antennas, and multiple outputs are multiple receive antennas, so MIMO is a combination of multiple antennas at the transmitter and receiver, as seen in Figure 1.1. MIMO uses spatial multiplexing to transmit multiple data streams in parallel, thus increasing the data rate.

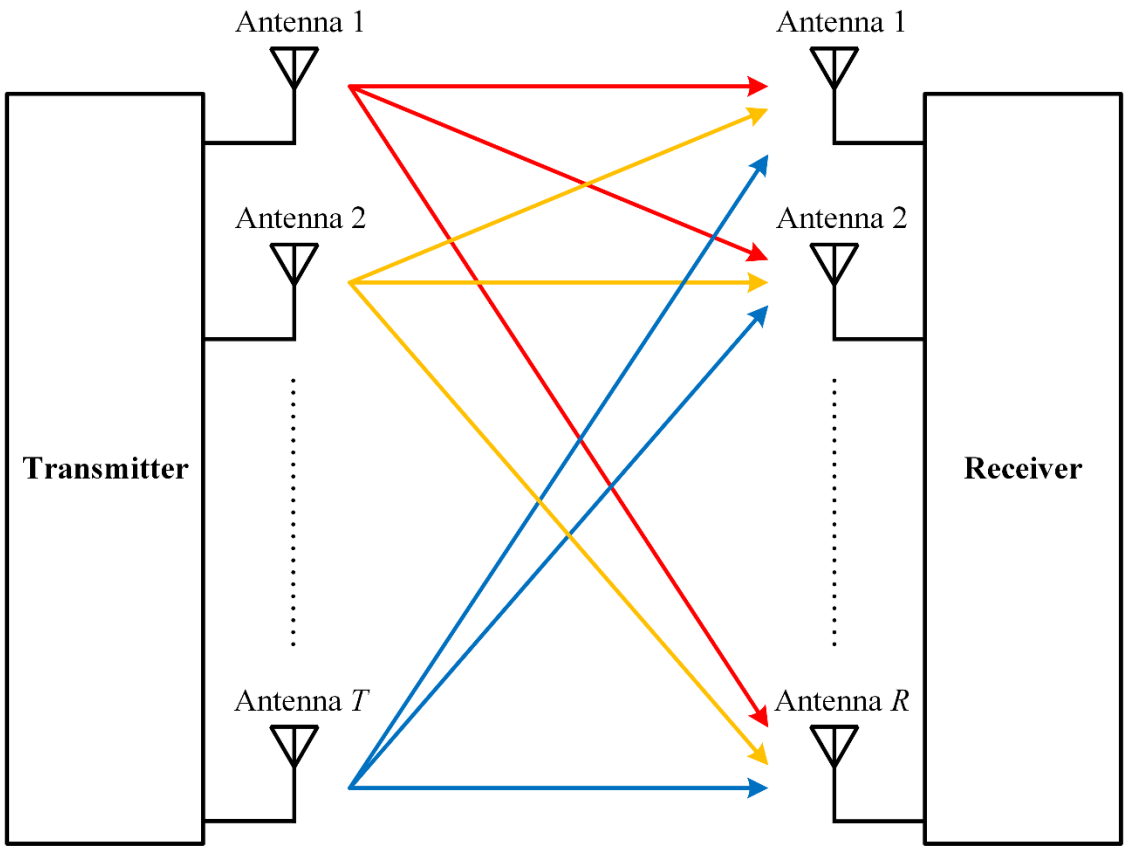

Figure 1.2: MIMO channel block diagram

Although MIMO provides many performance benefits by utilising many antennas, there is also a downside. The MIMO communication system's power consumption increases as the number of antennas increases; thus, the power requirements for transmission present a challenge for the mobile communication system (Sboui et al., 2017; Mishra & Alexandropoulos, 2018; Chinnadurai et al., 2017; Zhang et al., 2018).

1.2. Problem Statement

MIMO has proven to be an effective technology to combat the influx of mobile users and provide a good quality of service. However, to keep up with demand, the number of antennas increases, thus increasing the power consumption of the MIMO system. The limited available resources make maintaining a power-hungry system such as MIMO increasingly tricky. This research aims to reduce the power consumption of the MIMO system by improving the system's energy efficiency. Improving the system's power allocation (PA) increases its energy efficiency, thus reducing power consumption. Therefore this research aims to improve the power allocation of the MIMO system by investigating current schemes and developing a new power allocation scheme based on the current scheme's shortfalls.

1.3. Objectives and Aims

1.3.1. Aim

The research project's objective is to design and develop an approach to improve the power allocation of the MIMO system.

1.3.2. Objectives

- Study the current PA in MIMO systems literature and review the schemes and methodologies
- Perform an analysis of the schemes and evaluate the results to determine any shortfalls in the current schemes
- Model and simulate the novel schemes found in the reviewed literature using MATLAB
- Extensively investigate the modelled scheme and determine a new approach to improve the PA
- Design and implement an improved PA approach based on the investigation findings
- Evaluate the proposed scheme by performing simulations of the critical performance parameters
- Perform a comparison using the simulations on MATLAB of the proposed scheme with other novel schemes

1.4. Design and Methodology

This section describes the methods and steps used to design and simulate the improved PA approach.

1.4.1. Current Literature Review

A detailed literature review of current power allocation schemes gives the types of schemes used in MIMO systems. This literature review enables the design of a new power allocation scheme while considering existing schemes.

1.4.2. Analyse Current Schemes

Analysis of the current schemes highlights the effectiveness of the schemes as well as the shortfalls. The derivation of a new power allocation approach can improve the highlighted shortfalls.

1.4.3. Model and Design

A model of the new approach to improve the PA is designed using a software simulation package.

1.4.4. Simulation of Design

Simulations of the improved PA approach are conducted and compared to current PA schemes. Simulations are performed using MATLAB and or LABView.

1.5. Delineation of the Research

The outcomes of this research are simulation-based, using real-time data.

1.6. Significance

This research will improve the power allocation of the MIMO system, thus improving the performance of the MIMO system as a whole.

1.7. Expected Outcomes

- MEng Thesis
- At least one article from conference proceedings
- At least one article in accredited journals

1.8. Thesis Outline

The outline of the thesis is as follows:

Chapter 1: gives a brief overview of the communication system and introduces the problem statement, proposed solution, research objectives, design methodology, and significance of the research.

Chapter 2: presents the topic relevant literature with emphasis on critical performance areas, parameters, and methodologies utilised in MIMO, specifically NOMA based systems.

Chapter 3: discusses the history of mobile system technologies specifically, the multiple access techniques, the mobile generation evolution, and the drivers for the new generation.

Chapter 4: discusses NOMA as a multiple access technique for 5G, presenting the concept, benefits, and application within a communication system.

Chapter 5: presents the focus of the research specifically, the implementation, results, and benefits of the proposed power allocation scheme in a four-user NOMA based network utilising relays.

Chapter 6: builds on the research presented in chapter 5 by implementing energy harvesting relays and discusses the benefits and results of utilising energy harvesting relay nodes.

Chapter 7: concludes the presented research by discussing the proposed power allocation scheme, simulated results, and benefits. It highlights the scheme's effectiveness with and without energy harvesting relay nodes. It also presents possible future work in the physical layer security and NOMA 5G applications.

1.9. Summary

This research aims to find an approach to improve the power allocation of the MIMO system. A detailed literature review of current PA schemes is given. The objective is to design and develop an approach to improve PA in the MIMO system. The methodology includes implementing and analysing existing schemes, developing an approach to improve the PA, and simulating the new approach. The expected outcomes are; an MEng thesis, one article in an accredited journal, and one article from conference proceedings.

Chapter 2

LITERATURE REVIEW

Recently resource allocation in MIMO systems has been widely researched, particularly power allocation. This section highlights the critical performance areas, parameters, methodologies, and results associated with power allocation in MIMO, with great emphasis on non-orthogonal multiple access (NOMA) based systems. Extensive research into NOMA as a solution to increased data demands is underway where NOMA improves the system's sum rate and spectral efficiency (Fang, Zhang, Cheng, Roy, et al., 2017; Xu & Cumanan, 2017). NOMA utilises the power domain to service multiple users simultaneously by multiplexing them over the same resource, however, with varying power levels (Yang et al., 2016; Choi, 2017b).

2.1. Energy Efficiency

Energy efficiency measures how well energy is used, consuming the least energy possible while preserving system performance. Power consumption in a MIMO system is significantly increased due to many antennas; thus, maximising efficiency improves system performance.

To maximize a MIMO-based system's energy efficiency, (Sboui et al., 2017) found that the conventional water-filling power allocation method is not practical. Therefore, further investigation led to developing a non-complex algorithm based on optimal power expressions, which results in a proportional increase in energy efficiency and the number of antennas. Like (Sboui et al., 2017; H. Li et al., 2019) and (Chinnadurai et al., 2017) also propose an algorithm to maximize a MIMO systems' energy efficiency. However, (H. Li et al., 2019) propose an algorithm that incorporates the optimal transmit antenna selection based on linear constraints, whereas (Chinnadurai et al., 2017) proposes a user allocation algorithm for a NOMA-based MIMO system. Results show that the joint scheme presented by both (Chinnadurai et al., 2017) and (H. Li et al., 2019) yields improvements in the energy efficiency of their systems. Unlike (Sboui et al., 2017), (Jia et al., 2018) utilises the conventional water-filling power allocation method with multiple levels combined with user pairing. Authors (Zhang et al., 2017) and (Zeng et al., 2018b) focus on the user's quality of service while achieving energy efficiency maximisation of the system, whereas (Zeng & Fodor, 2018) and (Shi et al., 2019) proposes a joint resource allocation scheme, focusing on; computational and radio resource allocation and user clustering and power allocation. However, (Zeng et al., 2018b) computes the feasibility of the energy efficiency maximisation and presents two different approaches based on the outcome. The scheme proposed by (Zeng & Fodor, 2018) is way more complex than that of

(Zhang et al., 2017); however, results indicate that both schemes result in superior performances when compared to orthogonal multiple access (OMA) schemes. Some authors, such as (Fang, Zhang, Cheng & Leung, 2017) and (Shi et al., 2019), propose more than one algorithm to achieve the desired results of the specific performance parameter, i.e., energy efficiency maximisation. The utilisation of two algorithms proposed by (Fang, Zhang, Cheng & Leung, 2017) performs different tasks, .i.e. user scheduling and power allocation, whereas (Shi et al., 2019) proposes two resource allocating algorithms with varying complexity. Results presented by (Fang, Zhang, Cheng & Leung, 2017) and (Shi et al., 2019) show performance superiority over orthogonal frequency division multiple access (OFDMA) and traditional OMA. Figure 2.1 shows the minimum energy efficiency of an algorithm proposed by (Huang et al., 2019). A comparison between three algorithms, namely energy efficiency maximisation algorithm (EEMA), spectral efficiency maximisation algorithm (SEMA), and the proposed power allocation algorithm shows the increase in the number of users decreases the energy efficiency. This shows the correlation between energy and spectral efficiency and the related trade-off

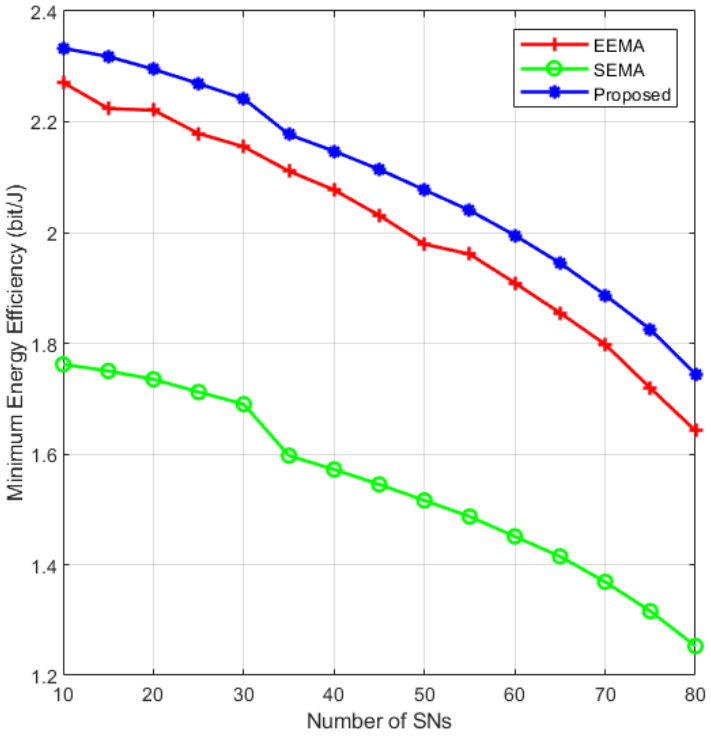

Figure 2.1: Energy efficiency of users (adapted from Huang et al., 2019)

2.2. Spectral Efficiency

The maximum rate at which information can be transmitted over a specified bandwidth is spectral efficiency.

After investigating the spectral efficiency of a multi-user MIMO system, (Saatlou et al., 2019) found a joint data and power allocation scheme to maximise the spectral efficiency. Like (H. Li et al., 2019), (Saatlou et al., 2019) also increases the number of base station antennas; however, (H. Li et al., 2019) focuses on energy efficiency while (Saatlou et al., 2019) focuses on spectral efficiency. In comparison (Jia et al., 2018; Zeng et al., 2018a; Saatlou et al., 2019; H. Li et al., 2019) implements power constraints to achieve their objectives, however, achieving different results; such as improvements in energy efficiency and spectral efficiency as well as spectral efficiency preservation. Moreover, (Zhang et al., 2018) explores single and multi-cell systems utlising zero-forcing (ZF) and maximum ratio combining (MRC) detectors to obtain achievable spectral efficiency in an uplink massive MIMO system.

2.3. NOMA

NOMA implements superposition coding (SC) and successive interference cancellation (SIC) at the transmitter and receiver, respectively (Timotheou & Krikidis, 2015; Oviedo & Sadjadpour, 2018), and capitalises on the varying channel conditions of the users.

Authors (Zuo & Tao, 2017) and (Manglayev et al., 2016) report an increase in the system throughput; however, (Zuo & Tao, 2017) implements a scheme focusing on sum-throughput maximisation whereby the user's minimum rate requirements and total transmission power are considered, whereas (Manglayev et al., 2016) and (Yuan et al., 2019) implement an optimal power allocation algorithm to maintain the fairness of the system. Much like (Manglayev et al., 2016) (Di et al., 2016) also focuses on user fairness; however, the proposed iterative algorithms are based on matching game theory to perform the resource allocation; whereas (Yuan et al., 2019) improves energy and spectral efficiency using a rate constrained power allocation algorithm. The schemes presented by both (Zuo & Tao, 2017) and (Sun et al., 2015) highlights the importance of power and minimum rate constraints. It shows the different utilisation of constraints to achieve different results, such as sum-throughput maximisation and ergodic capacity maximisation. Like (Sun et al., 2015), (Zhang et al., 2019) focuses on the system's capacity where a joint resource allocation scheme in conjunction with zero-forcing beamforming effectively increases the system's capacity.

Research into a cognitive environment led (Balyan, 2020) to implement NOMA into a cognitive radio system whereby primary users mitigate the secondary user's interference. It capitalises on NOMAs SIC detection and derives outage probability expressions that evaluate the system's performance.

The main focus for (Ding et al., 2016) and (Zeng et al., 2019) is the power allocation of their respective systems. However, the user's quality of service (QoS) is an essential metric, where (Ding et al., 2016) implements two sets of QoS requirements and (Zeng et al., 2019) implements the user's QoS in a cluster millimeter-wave (mmWave) network to improve the energy efficiency. Results show the effectiveness of the respective schemes where (Ding et al., 2016) analyses the scheme's accuracy and the system's energy efficiency by (Zeng et al., 2019) outperform conventional OMA schemes.

After implementing an antenna selection scheme for NOMA-based networks (Shrestha et al., 2016), improved the system's total sum rate by implementing multiple antennas at the base station compared to systems with single antennas. Whereas (Nasser et al., 2019) utilise a power allocation scheme to mitigate interference to improve the system's total sum rate.

2.4. Cooperative Relaying Networks

Many cooperative relaying systems either implement dedicated relay nodes or utilise users as relay nodes to communicate with the base station.

Recent studies show an increase in system capacity and coverage within a network due to the ultilisation of cooperative relaying networks. Relays within a network facilitate cell edge users and improve their performance, such as (Zhai et al., 2021) and (Xu et al., 2021); (Zhai et al., 2021) employs a UAV as a relay along with a joint resource allocation algorithm to maximise the cell edge user's data rates whereas (Xu et al., 2021) evaluates the ergodic capacity of the system based on the number of cell center and cell-edge users. Much like (Zhai et al., 2021), (Song et al., 2018) explores a UAV-aided relay network where the UAV relay utilises a decode-and-forward protocol along with zero-forcing beamforming and power allocation combination. Consequently, the outage probability analysis validates the proposed scheme.

Authors (Liu et al., 2018; Zhai et al., 2021; Song et al., 2018) implements the decode and forward relaying protocol in their systems, whereas (Huang et al., 2020; Xie et al., 2019) employ two relaying protocols, amplify-and-forward and decode-and-forward. The proposed

schemes of (Huang et al., 2020) and (Xie et al., 2019) evaluate both protocol's performances, and results show that the latter protocol attains a superior performance.

Research into schemes and technologies to support 5G applications and use cases such as device-to-devive (D2D) and mmWave communication yields promising results, as seen by (Young Bae Song et al., 2016) and (Kaur & Singh, 2019). The authors (Young Bae Song et al., 2016) implement NOMA into a D2D relay system where a device assists the far user and improves the signal to interference noise ratio and data rate. Moreover, (Kaur & Singh, 2019) reports the superior performance of the proposed system where users cooperate and assist other users in a massive MIMO system for mmWave communication.

Implementing NOMA into the communication system allows the utilisation of SIC such as (Zhao et al., 2019) and (Xie et al., 2020). Authors (Zhao et al., 2019) utilise a SIC-enabled relay in the downlink communication, whereas (Xie et al., 2020) utilise SIC at the base station in the uplink communication.

2.5. Energy Harvesting

Recently energy harvesting has garnered much attention, specifically in cooperative networks. Research shows the benefits of energy harvesting nodes, such as an increase in the life span of the nodes and the self-sustainability of a communication network, especially for 5G applications. The energy harvesting employs different receiver architectures, power splitting and time switching, thus enabling two protocols: power splitting relaying (PSR) and time switching relaying (TSR).

Authors (Mondal et al., 2020; Guo et al., 2019; Alsharoa et al., 2017) and (Wang et al., 2018) utilise the most widely used PSR protocol, whereas (F. Li et al., 2019) utilises the TSR protocol. However, (Du et al., 2015) and (Nasir et al., 2013) utilises both protocols and evaluates the performance of each. Moreover (Du et al., 2015) report the superiority of the PSR protocol, whereas (Nasir et al., 2013) reports that the latter is more superior.

Many researchers only implement one energy harvesting scheme into their system model; however, (Mondal et al., 2020) and (Salem et al., 2020) implement three different relay schemes. To explore the comparison of the proposed schemes (Mondal et al., 2020), implements adaptable PSR schemes, whereas (Salem et al., 2020) increases the security of the communication system. Like (Salem et al., 2020), (Le & Kong, 2019) focuses on the physical

layer security of the communication system where the base station transmits a jamming signal to mitigate interference from the eavesdropper node.

Analysis of the presented schemes shows the immense power of joint resource allocation schemes, whereby the scheme or algorithm joins different resources to achieve the required performance of the chosen metric. Researchers also explore many relay schemes, resulting in many scheme combinations based on specific performance metrics. The research presented in this paper focuses on the allocation of resources in a NOMA-enabled relay network.

2.6. Summary

The literature discusses resource allocation in MIMO based systems, specifically power allocation with emphasis on NOMA based systems. The authors present various power allocation schemes while focusing on specific performance parameters such as energy efficiency, spectral efficiency, and energy harvesting. Analysis of the proposed schemes highlights their implementation, efficacy, and complexity. Scheme comparisons show the proposed schemes' superiority over conventional power allocation schemes. Specific authors also implemented more than one scheme to reduce complexity or achieve their desired outcome.

Chapter 3

HISTORY OF MOBILE SYSTEM TECHNOLOGIES

3.1. Background

Mobile communications have evolved tremendously over the years, starting with the most basic and limited communication to highly advanced and sophisticated modes of communication. The release of each mobile generation addressed the shortfalls of its predecessors and provided the user with new features and capabilities. The utilisation of various multiple access (MA) techniques resulted in each generation exceeding the previous generation's data rates and spectral efficiency. The MA techniques allow users to share the wireless channel without interfering with each other. However, there are certain limitations with each technique, such as the allocated available resources. The limitation of each MA technique resulted in the exploration and design of new techniques, able to meet the ever-increasing wireless communication demands. The four main MA techniques are frequency division multiple access (FDMA), time division multiple access (TDMA), code division multiple access (CDMA), and OFDMA. Table 3.1 gives the four multiple access techniques utilised by different cellular generations.

Table 3.1: Multiple access techniques (adapted from Vaezi et al., 2018)

Generation	MA Technique	Resource
1G	FDMA	Frequency
2G	TDMA	Time
3G	CDMA	PN Codes
4G	OFDMA	Time/Frequency

3.2. Multiple Access Techniques

There are two categories of MA techniques, orthogonal multiple access and non-orthogonal multiple access. This section explores the OMA techniques.

3.2.1. Frequency Division Multiple Access

In this technique, multiple users communicate over the same channel by making use of sub-bands or sub-carriers. The sub-carriers are created by dividing the channel bandwidth into individual bands and allocated to individual users. Thus, each user has a specific frequency band in which to communicate.

3.2.2. Time Division Multiple Access

In this technique, multiple users communicate over the same channel by making use of sub-slots. The sub-slots are created by dividing the time into individual slots and allocated to individual users. Thus, each user has a specific time slot in which to communicate.

3.2.3. Code Division Multiple Access

Multiple users communicate simultaneously over the entire channel using pseudo-noise (PN) codes in this technique. The orthogonal PN codes are created by assigning different codes to each transmitter and spreading it over the frequency.

3.2.4. Orthogonal Frequency Division Multiple Access

In this technique, each user communicates over a specific frequency band and time slot. It combines FDMA and TDMA by allocating sub-carriers and sub-slots to each user. Thus each user communicates over a specific sub-carrier for a limited time.

3.2.5. Comparison of Multiple Access Techniques

Figure 3.1 gives a graphical representation of the four MA techniques and shows the utilisation and allocation of the resources for each technique, i.e., frequency and time.

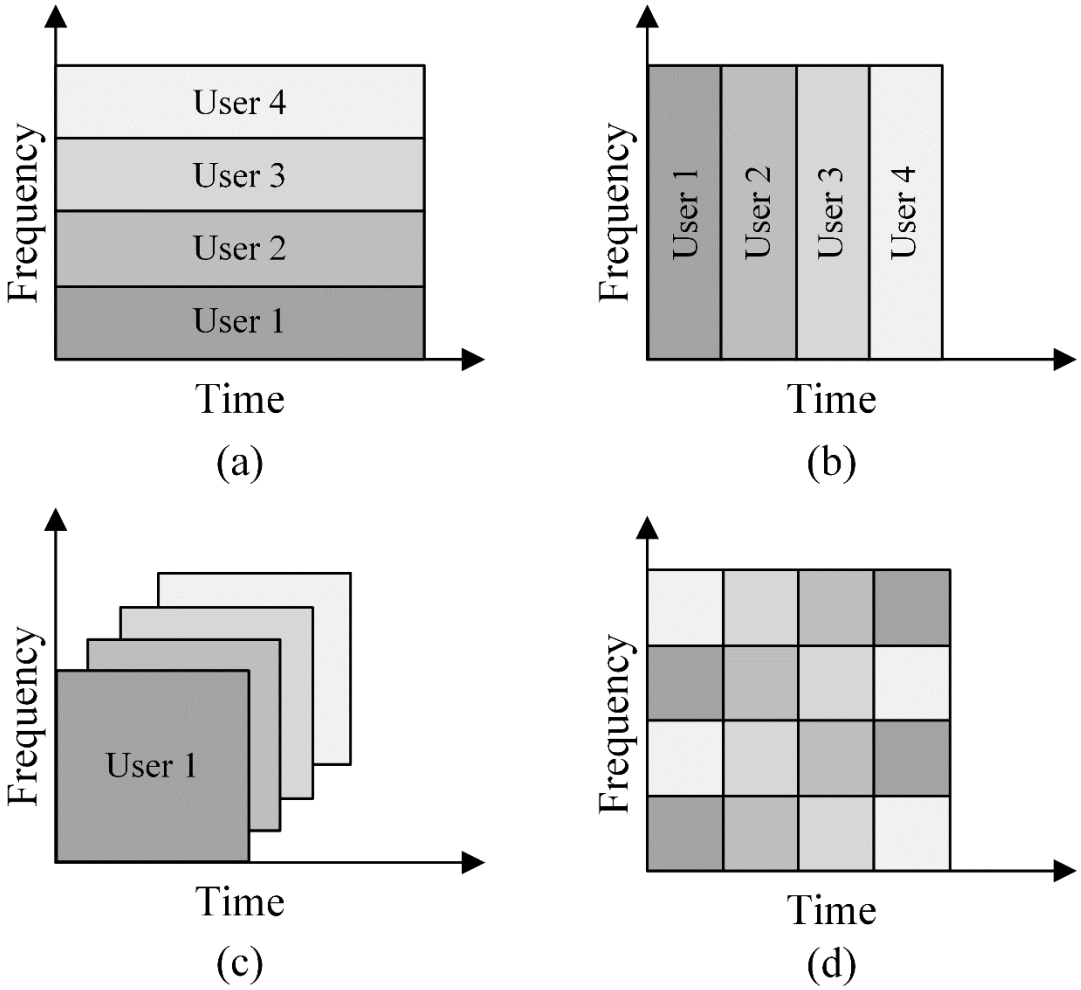

Figure 3.1: (a) FDMA, (b) TDMA, (c) CDMA, (d) OFDMA (adapted from Belleschi, 2008: 43)

3.3. Mobile Generation Evolution

The early stages of mobile communication and devices were only accessible to a select group of people due to the cost, size, and capability of mobile devices. As mobile technology developed, the demand, complexity, features, and capabilities increased, which resulted in an unprecedented increase in mobile devices and wireless applications. Today, mobile devices are easily affordable and diverse, depending on cost and features. This section explains the evolutionary roadmap from the first generation to the fourth mobile generation; it covers each generation's key technologies, applications, benefits, and shortfalls (Dahlman et al., 2016). The last section explores the emerging technologies and applications for the fifth-generation mobile communication system.

3.3.1. First Generation (1G)

The first-generation mobile system was analog-based and only had voice communication capability. It enabled the user to input the desired telephone number and converse with the recipient. It utilised frequency modulation and provided multiplexing by using the FDMA technique. The widely used 1G global standards were advanced mobile phone services (AMPS), Nordic mobile telephone (NMT), and total access communication system (TACS). The 1G mobile system quickly gained popularity with an increase in the number of users. However, this mobile system was very rudimentary and had specific shortfalls such as poor; security, voice quality, handover, and low traffic capacity (Das, 2017).

3.3.2. Second Generation (2G)

The second-generation mobile system was digitally based and offered primary and supplementary services such as voice calls, short message service (SMS), facsimile, and call management. It utilised digital modulation and provided multiplexing by using FDMA and TDMA techniques. Global system for mobile communications (GSM) and CDMA-One were two of the most widely used 2G standards. GSM also introduced general packet radio services (GPRS) and enhanced data rates for GSM evolution (EDGE) to improve packet-switched data transmission and enable increased data rates. Due to the advancement of the internet and cellular generation, an opportunity to incorporate the two presented itself. GPRS incorporated packet-switched data transmission, resulting in mobile devices capable of downloading data. EDGE utilised an adaptable modulation and coding scheme (MCS) dependent on the channel conditions, resulting in increased data rates and reduced latency. Like 1G, 2G also gained tremendous popularity with many users. As the number of users increased, particular shortfalls came to light, such as the capacity of the network, the high latency, and low data rates (Das, 2017).

3.3.3. Third Generation (3G)

The development of the third-generation mobile system provided increased data rates and system capacity, which allowed users to utilise; the data services with higher data rates, the voice services with improved voice quality, and Internet browsing. The universal mobile technology system (UMTS) utilised the GSM network to create the 3G mobile system by modifying the air interface technology while preserving the core network.

Thus, allowing the 3G mobile system to work with the existing GSM and GPRS networks. UMTS utilised wideband code division multiple access (WCDMA) to increase system capacity and spectral efficiency. Due to the constant increase in data rate requirements, WCDMA evolved and introduced high-speed packet access (HSPA) for uplink and downlink communications, namely, high-speed uplink packet access (HSUPA) and high-speed downlink packet access (HSDPA), respectively. The addition of HSPA to 3G maintains the baseline 3G standards while providing higher data rates, also known as 3.5G. The third-generation utilised the CDMA multiple access techniques, which comprised the two global standards, WCDMA and CDMA2000. Another technology called worldwide interoperability for microwave access (WiMAX) is the latest 3G technology. It uses point-to-multipoint communications where a base station with an omnidirectional antenna communicates with multiple fixed users. The modification of WiMAX enabled base station handover capability and the mobility of users, called mobile WiMAX.

The third-generation partnership project (3GPP) is an organisation that develops and maintains global mobile standards. This organisation fulfills the requirements set forward by the international telecommunications union (ITU) (Das, 2017; Cox, 2014; Dahlman et al., 2016).

The capability of 3G reached its limit; the further enhancement of WCDMA was not possible. Thus, 3G was no longer able to provide satisfactory performance in terms of video applications, data rates, and system capacity, to name a few. The evolution of technology created a constant demand for better system performances, such as improved data rates, reduced latency, higher capacity, and improved video quality.

3.3.4. Fourth Generation (4G)

Mobile telecommunication networks monitored voice calls and data traffic over the years; while voice calls showed a slow and steady increase from 2007 to 2013, data traffic increased exponentially. Data traffic was low at first because of the mobile system and mobile device technology available. The improvement in the mobile system and mobile device technology allowed the utilisation of data-hungry applications, hence the exponential increase in mobile traffic. Mobile phones became more powerful, compact, and user friendly and referred to as smartphones. The utilisation of smartphones increased the number of users, thus causing mobile network systems to reach capacity. The previous mobile systems could no longer accommodate all the users and traffic; therefore, the need for a new mobile system arose (Cox, 2014).

The fourth-generation mobile system, also known as long-term evolution (LTE), utilises OFDMA for its air interface and packet-switched data services. It also became the single global standard for mobile systems instead of different technologies competing against one another, as experienced by previous generations. Mobile system developers set forward to achieve the 4G objectives set out by the ITU, namely, increasing the system's capacity and user data rates, user experience, and latency improvements. LTE has expanded from mobile communications to device-to-device and machine communications (Das, 2017).

One of the most important developments was the air interface of LTE; it had to meet a specific set of requirements, namely the peak data rate, spectral efficiency, and latency of the system. LTE surpassed the peak downlink and uplink data rates, from 100 Mbps to 300 Mbps and 50 Mbps to 75 Mbps, respectively. However, these peak data rates are under ideal conditions and are unobtainable in reality. Therefore, spectral efficiency provides an excellent measure of system performance; it measures the rate of transmitted information over a specific bandwidth. The spectral efficiency of LTE had to exceed that of Release 6 WCDMA in both uplink and downlink transmissions by a factor of 3 and 4, respectively. The reduction of the latency was critical for LTE to support online gaming and voice communication. Table 3.2 gives a comparison between WCDMA and LTE's air interface features.

Table 3.2: Comparison WCDMA and LTE air interface (adapted from Cox, 2014)

Feature	WCDMA	LTE
Modes of Operation	FDD and TDD	FDD and TDD
Bandwidth	5 MHz	1.4, 3, 5, 10, 15 or 20 MHz
Multiple Access Technique	WCDMA	OFDMA and SC-FDMA
Frame Duration	10 ms	10 ms
MIMO Antennas	From Release 7	Yes
Transmission Time Interval	2 or 10 ms	1 ms

Mobility and coverage was the other focus area for LTE; it supports operations for an increased cell coverage area, increased mobile speed, multiple antenna configurations, and an increased number of bandwidth options (Cox, 2014). Release 10 of LTE is known as LTE-Advanced; it is a modified version of LTE providing higher data rates, higher spectral efficiency, and a better user experience.

3.3.4.1. LTE Technologies

a) OFDM

LTE utilises orthogonal frequency division multiplexing (OFDM) for its downlink transmissions, where it utilises a concatenation of narrowband subcarriers for transmission, thus enabling simultaneous data transmission over many subcarriers.

b) SC-FDM

For the uplink transmissions, LTE utilises single-carrier frequency division multiplexing (SC-FDM) based on OFDM. It combines a discreet Fourier transform (DFT) precoder with the standard OFDM.

c) MIMO

LTE uses a spatial multiplexing technique called multiple-input multiple-output (MIMO), where the transmitter and receiver have multiple antennas.

d) Turbo Coding

LTE utilises turbo coding, a coding technique that uses two parallel encoders separated by an inter-leaver.

3.3.5. Mobile Generation Comparison

Table 3.3 shows the mobile generation evolution from 1G to 4G with the standards used. It also shows an increase in the capabilities of each generation.

Table 3.3: Comparison of mobile generations

Generation	Multiplexing	Standard	Support
1G	FDMA	AMPS, TACS	Voice
2G	TDMA, CDMA	GSM	Voice, Data
2.5G to 2.75G	TDMA, CDMA	GPRS, EDGE	Voice, Data, Web Browsing, Email Services, Low-Speed Streaming
3G	CDMA	CDMA2000, WCDMA, HSDPA/HSUPA	Voice, Data, Video Calling, Web Browsing, TV Streaming
4G	OFDMA	LTE, WiMAX, Wi-Fi	Voice, Data, Video Calling, Online Gaming, HD Streaming

3.4. Physical Layer of LTE

This section provides details of the LTE technology's physical layer (PHY), specifically the utilisation of OFDM, frequency division duplex (FDD), and time division duplex (TDD). It provides the reasoning for the design decisions, which resulted in the exceptional system performance of LTE.

3.4.1. Air Interface

LTE's air interface utilises OFDMA, and in comparison to previously used multiple access techniques such as FDMA, TDMA, and CDMA, the benefits of OFDMA outweigh these techniques. The benefits include mitigation of inter-symbol interference, elevated spectral efficiency, frequency domain scheduling, wideband transmissions, time and frequency allocation flexibility, and MIMO antenna configuration support (Sauter, 2014; Dahlman et al., 2016; Zarrinkoub, 2014).

3.4.2. Frequency Bands

An LTE requirement was to enable transmission over previously standardised and new frequency bands. The addition of frequency bands enabled the ease of mobile roaming worldwide. LTE utilises FDD and TDD modes where uplink and downlink transmissions occur; on different frequencies in the same time slot and on the same frequency in different time slots, respectively. Evolved universal terrestrial radio access (E-UTRA) has a set of operating frequency bands for FDD and TDD operating modes, given in Table 3.4 and Table 3.5, respectively.

Table 3.4: FDD frequency bands (adapted from Zarrinkoub, 2014)

Frequency Bands	Uplink (MHz)	Downlink (MHz)
1	1920 – 1980	2110 – 2170
2	1850 – 1910	1930 – 1990
3	1710 – 1785	1805 – 1880
4	1710 – 1755	2110 – 2155
5	824 – 849	869 – 894
6	830 – 840	875 – 885
7	2500 – 2570	2620 – 2690
8	880 – 915	925 – 960

9	1749.9 – 1784.9	1844.9 – 1879.9
10	1710 – 1770	2110 – 2170
11	1427.9 – 1447.9	1475.9 – 1495.9
12	699 – 716	729 – 746
13	777 – 787	746 – 756
14	788 – 798	758 – 768
15	Reserved	
16	Reserved	
17	704 – 716	734 – 746
18	815 – 830	860 – 875
19	830 – 845	875 – 890
20	832 – 862	791 – 821
21	1447.9 – 1462.9	1495.9 – 1510.9
22	3410 – 3490	3510 – 3590
23	2000 – 2020	2180 – 2200
24	1626.5 – 1660.5	1525 – 1559
25	1850 – 1915	1930 - 1995

Table 3.5: TDD frequency bands (adapted from Zarrinkoub, 2014)

Frequency Band	Uplink and Downlink (MHz)
33	1900 – 1920
34	2010 – 2025
35	1850 – 1910
36	1930 – 1990
37	1910 – 1930
38	2570 – 2620
39	1880 – 1920
40	2300 – 2400
41	2496 – 2690
42	3400 – 3600
43	3600 – 3800

As seen in Table 3.4, the FDD frequency band pairs 1 to 25 range from 699 MHz to 3590 MHz, where frequency bands 15 and 16 are reserved. Table 3.5 shows the unpaired operating frequency bands for TDD mode (Zarrinkoub, 2014).

3.4.3. Time and Frequency Domain

LTE utilises two types of frame structures for OFDM transmissions, type-1 and type-2 for FDD and TDD modes; the time-based type-2 frame structure consists of time frames with a duration of 10 ms each, as seen in Figure 3.2. The division of each time frame results in 10 subframes with a duration of 1 ms each. A subframe consists of two slots, with a duration of 0.5 ms each. Within each slot are OFDM symbols, where the type of cyclic prefix determines the number of OFDM symbols (Dahlman et al., 2016; Das, 2017; Zarrinkoub, 2014).

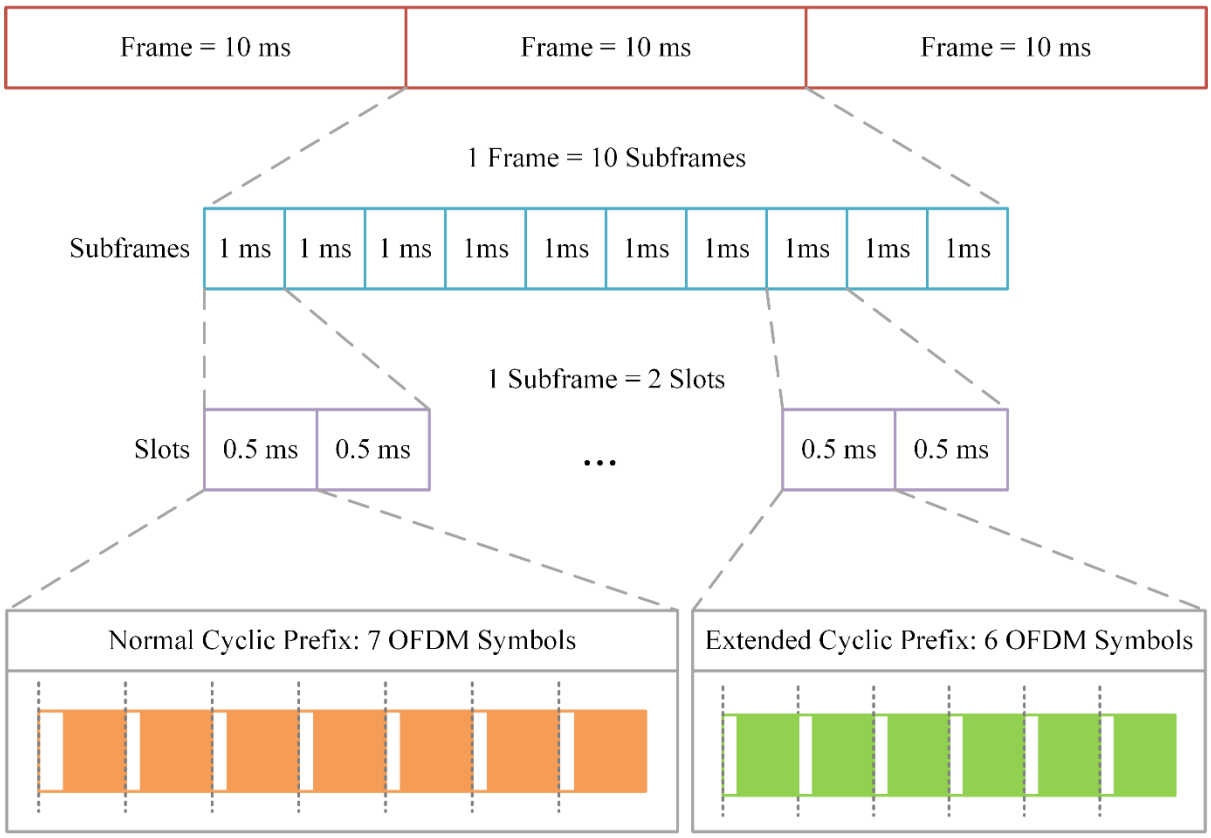

Figure 3.2: LTE time-domain frame structure (adapted from Zarrinkoub, 2014)

The type-1 frame structure allows the simple mapping of data symbols in the time and frequency domain, i.e., a resource element to the resource grid. The resource grid is two-dimensional with; a subcarrier spacing of 15 kHz and each slot duration of 0.5 ms with 7 OFDM symbols in each slot.

A resource element (RE) is a physical resource of time and frequency and consists of a 1-by-1 structure of 1 symbol by 1 subcarrier. Figure 3.3 shows the composition of an LTE resource grid for the downlink transmission using normal cyclic prefixing (Zarrinkoub, 2014).

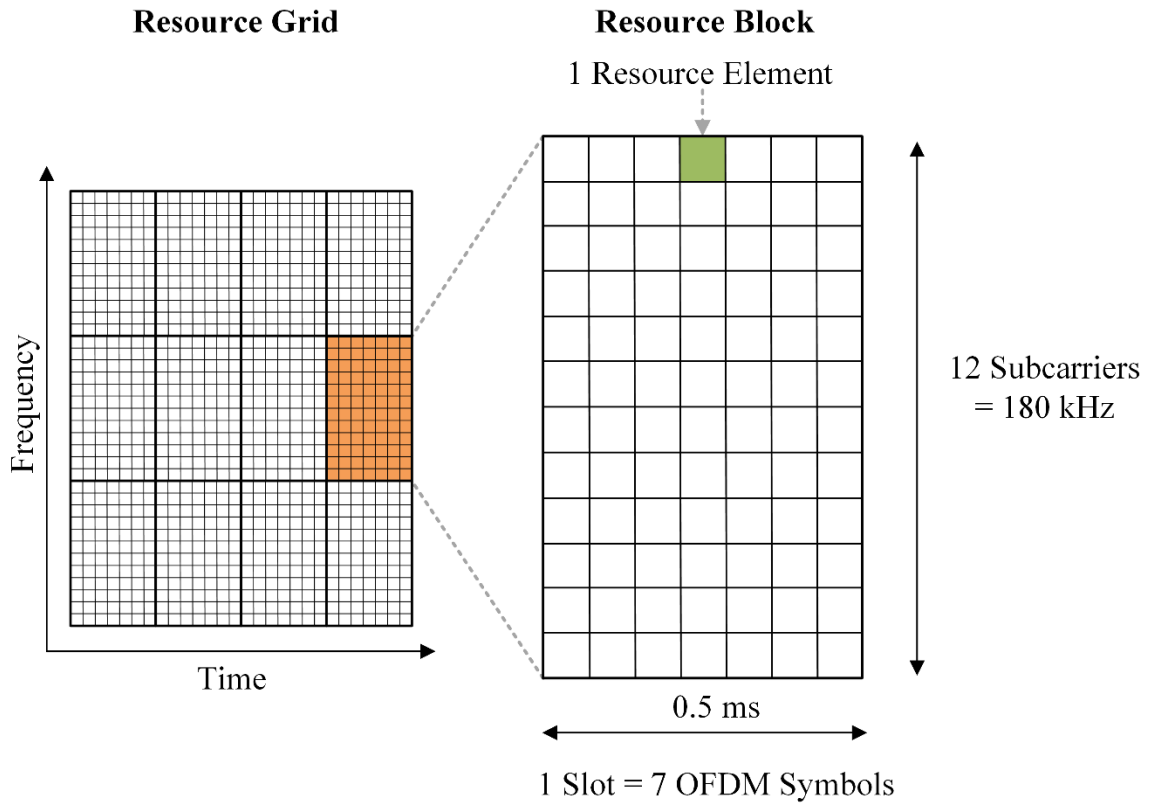

Figure 3.3: Resource grid

A resource block (RB) consists of 84 REs with a (12 subcarrier x 7 OFDM symbol) or (180 kHz x 0.5 ms) dimension. A frequency carrier consists of several resource blocks where the channel bandwidth determines the number of resource blocks the carrier can accommodate.

Table 3.6: LTE channel bandwidths (adapted fromZarrinkoub, 2014)

Channel Bandwidth (MHz)	Number of Resource Blocks
1.4	6
3	15
5	25
10	50
15	75
20	100

Table 3.6 gives the resource block allocation for the various channel bandwidths in LTE. The utilisation of resource blocks enables the flexibility of the spectrum (Cox, 2014; Dahlman et al., 2016; Zarrinkoub, 2014).

3.4.4. OFDM Multicarrier Transmission

This sub-section provides a brief overview of OFDM multi-carrier transmission along with its features and benefits. The generation of signals in the OFDM scheme consists of various processes, starting with the population of the resource grid with modulated data. The transmission of the data symbols occurs on different frequency bands or sub-carriers, as shown in Figure 3.4, with each symbol a_k on its sub-carrier. The bandwidth BW is divided into N subcarriers with a spacing of Δf between the subcarriers.

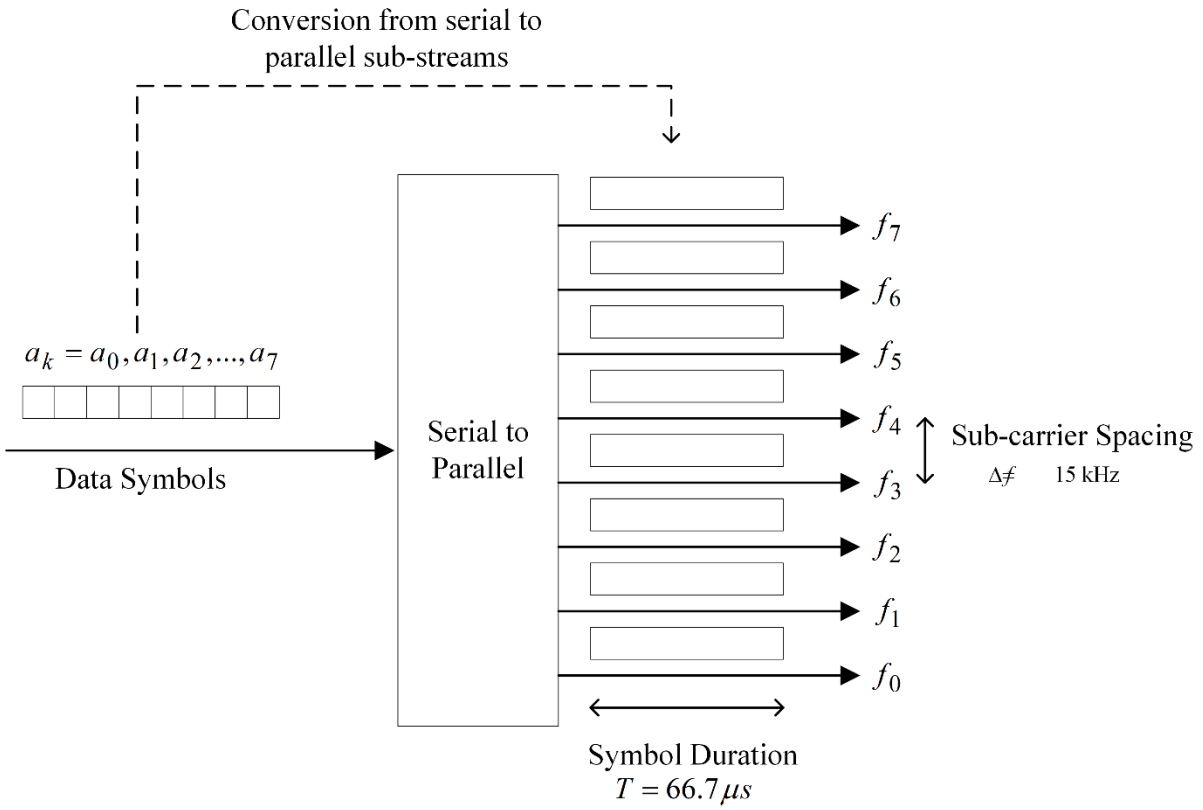

Figure 3.4: Frequency band division (adapted from Cox, 2014)

The subcarrier frequency f_k is an integer multiple of Δf which is 15 kHz; this can be seen by equation (3.1).

$$f_k = k\Delta f \tag{3.1}$$

$$x(t) = \sum_{k=1}^{N} a_k e^{j2\pi f_k t} = \sum_{k=1}^{N} a_k e^{j2\pi k \Delta f t} \tag{3.2}$$

Each subcarrier corresponds to a complex modulator; thus, there are N modulators that make up a bank of complex OFDM modulators with a complex modulated output given by equation (3.2) , and an illustration of the modulator can be seen in Figure 3.5.

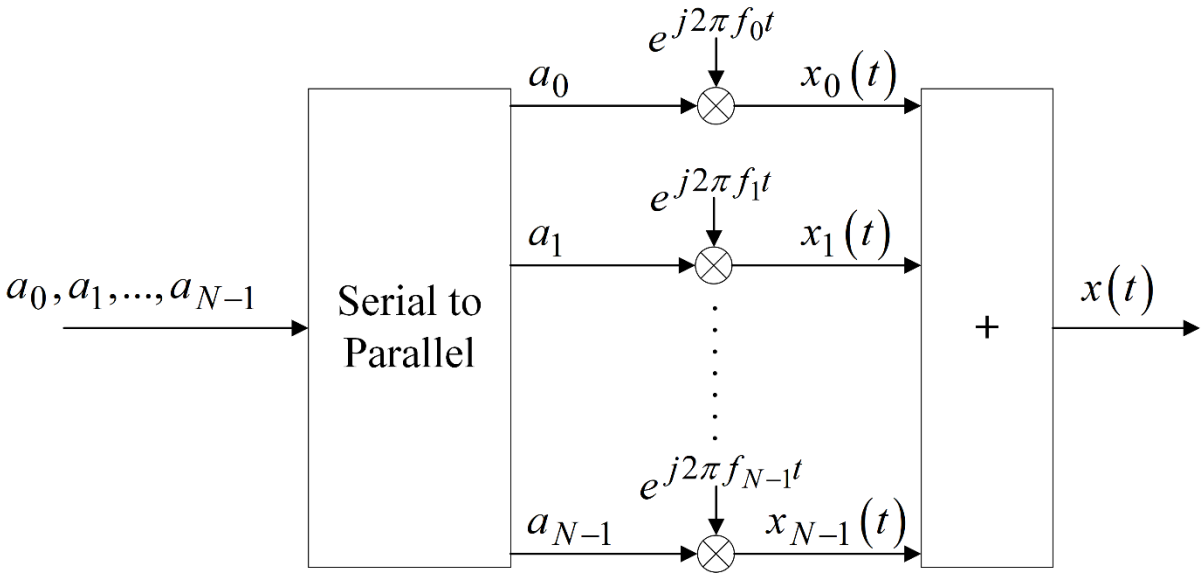

Figure 3.5: OFDM modulator (adapted from Dahlman et al., 2011)

In discreet time, the output of the OFDM modulator is given by equation (3.3) where the sample rate and sample time of the channel are assumed to be Fs and $Ts = 1/Fs$, respectively.

$$x[n] = \sum_{k=1}^{N} a_k e^{j2\pi k \Delta f n / N} \tag{3.3}$$

The downlink operation of the transmitter and receiver in OFDM is given in Figure 3.6. At the transmitter, the data bits of each user undergoes modulation, such as quadrature phase-shift keying (QPSK) or quadrature amplitude modulation (QAM) after which, the modulated symbols are converted from a serial data stream to parallel data sub-streams. The mapping of a symbol to a sub-carrier occurs within the resource element mapping block, where each symbol corresponds to a sub-carrier. The output of the resource element mapper gives the data in the frequency domain, providing the amplitude and phase of the subcarriers. Then, the inverse fast Fourier transform (FFT) computes the data in the time domain by adding the subcarriers and dividing them by N , thus producing a single waveform.

The parallel to serial converter uses the time domain components to arrange the data correctly, after which a cyclic prefix is added to prevent intersymbol interference and ensure orthogonality. The final transmitter step is to mix up the signal to the carrier frequency and convert it to analog form before transmission.

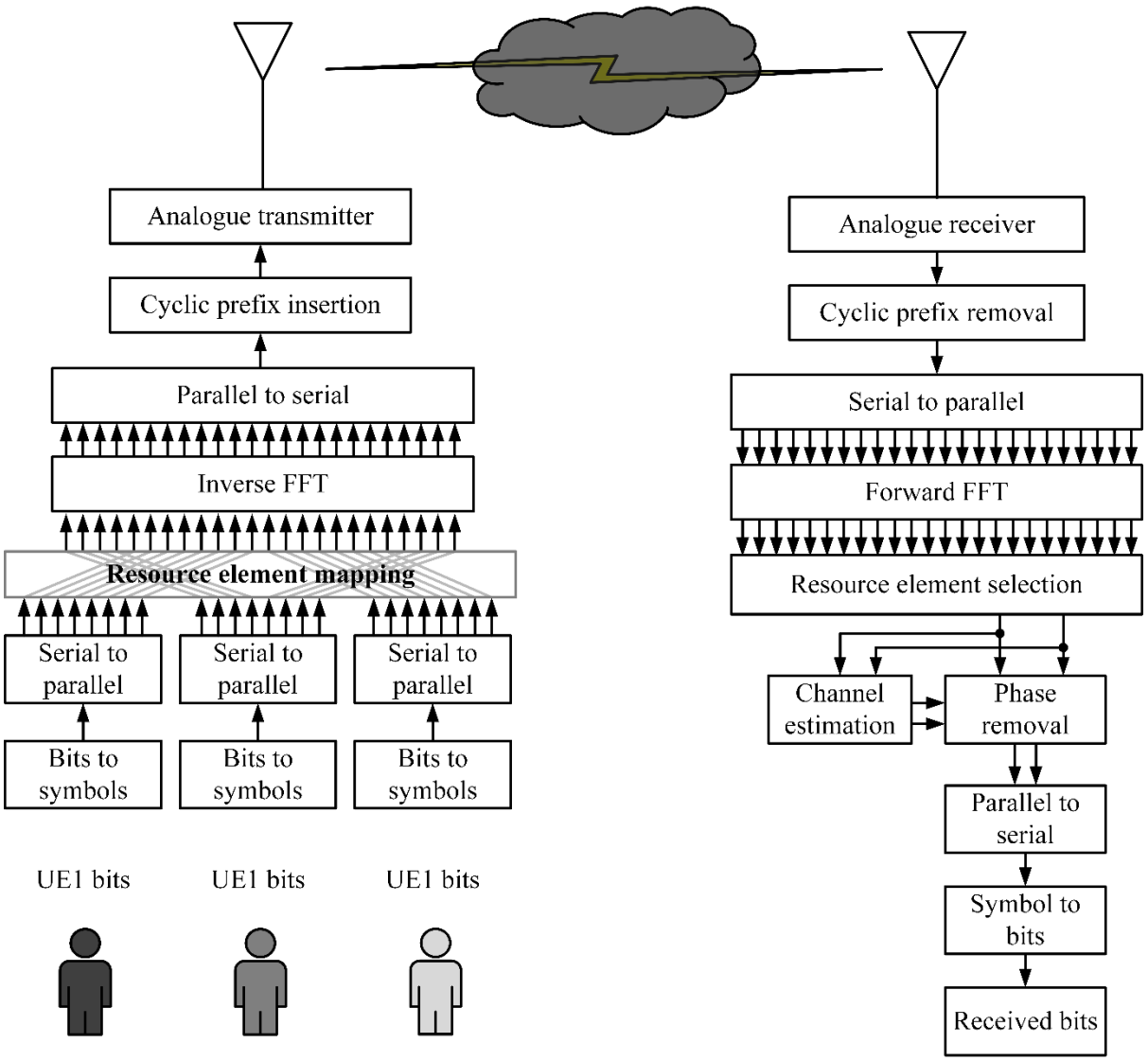

Figure 3.6: Block diagram of OFDM transmitter and receiver (adapted from Cox, 2014)

The receiver process is the transmitter process in reverse, starting with the sampling, converting, and filtering of the received signal. The receiver utilises the channel information given by the base station to recover its transmitted information. The benefits and features of OFDMA are given in Table 3.7 and make OFDM a superb technique for LTE (Cox, 2014) and (Zarrinkoub, 2014).

Table 3.7: Benefits and features of OFDMA

Feature	Benefit
Orthogonal Sub-carriers	Greater Spectral efficiency due to tightly packed sub-carriers
Sub-carrier Spacing Choice	Choosing a sub-carrier spacing greater than the Doppler shift reduces degradations
Resource Block Size	Resource block size of 180 kHz or 12 sub-carriers ensures low latency and efficient small packet data support
Cyclic Prefix	Prevents inter-symbol interference
Frequency Domain Scheduling	Multiple bandwidths utilise the same equalisation methods due to the constant symbol duration of $66.7\mu s$

3.4.5. Single-Carrier Frequency Division Multiplexing (SC-FDM)

In LTE, the uplink transmission utilises the SC-FDM scheme to reduce the fluctuations in the instantaneous power which occurred in OFDM. In order to combat the power issue, a modified OFDM technique known as discrete Fourier transform-spread orthogonal frequency division multiplexing (DFTS-OFDM) is utilised. This technique implements a DFT precoder placed before the OFDM modulator. Unlike OFDM, SC-OFDM reduces the power fluctuations by mixing the symbols and transmitting them over the whole bandwidth (Zarrinkoub, 2014; Das, 2017).

3.4.6. MIMO

As previously mentioned, MIMO is one of LTE's technologies, which results in superior system performance. There are different MIMO antenna configurations, and the utilisation of each depends on the system's requirement. The most common antenna configurations are: receive diversity, transmit diversity, and spatial multiplexing, shown in Figure 3.7. Receive diversity, known as single-input multiple-output (SIMO), utilises a single transmit antenna and multiple receive antennas. Transmit diversity, known as multiple-input single-output (MISO), utilises multiple transmit antennas and a single receive antenna. Spatial multiplexing combines SIMO and MISO to produce MIMO, utilising multiple antennas at the transmitter and receiver (Brown et al., 2012).

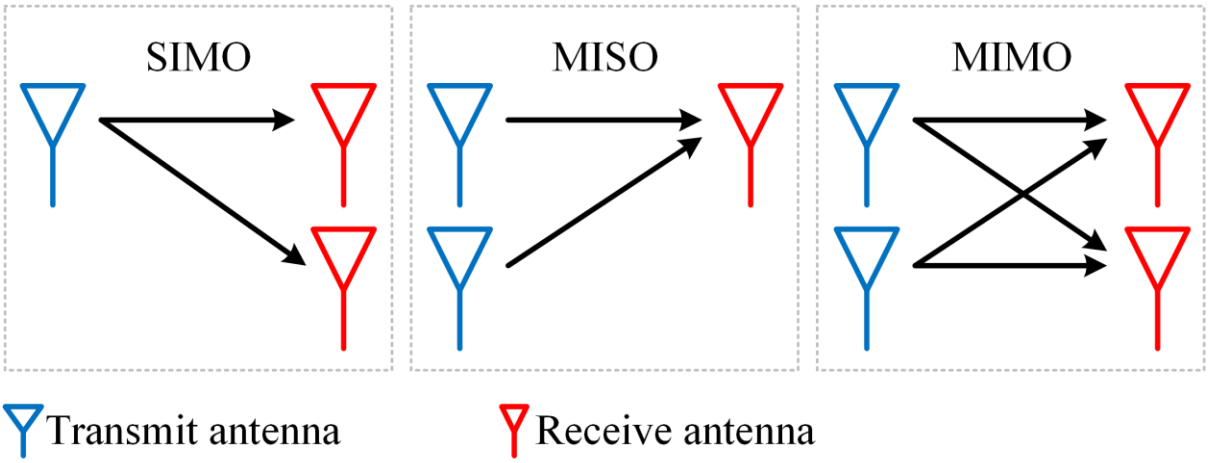

Figure 3.7: Antenna configuration

3.4.6.1. MIMO Channel Model

This section gives the details of the MIMO channel model with the transmitter and receiver models shown in Figure 3.8 and Figure 3.9, respectively.

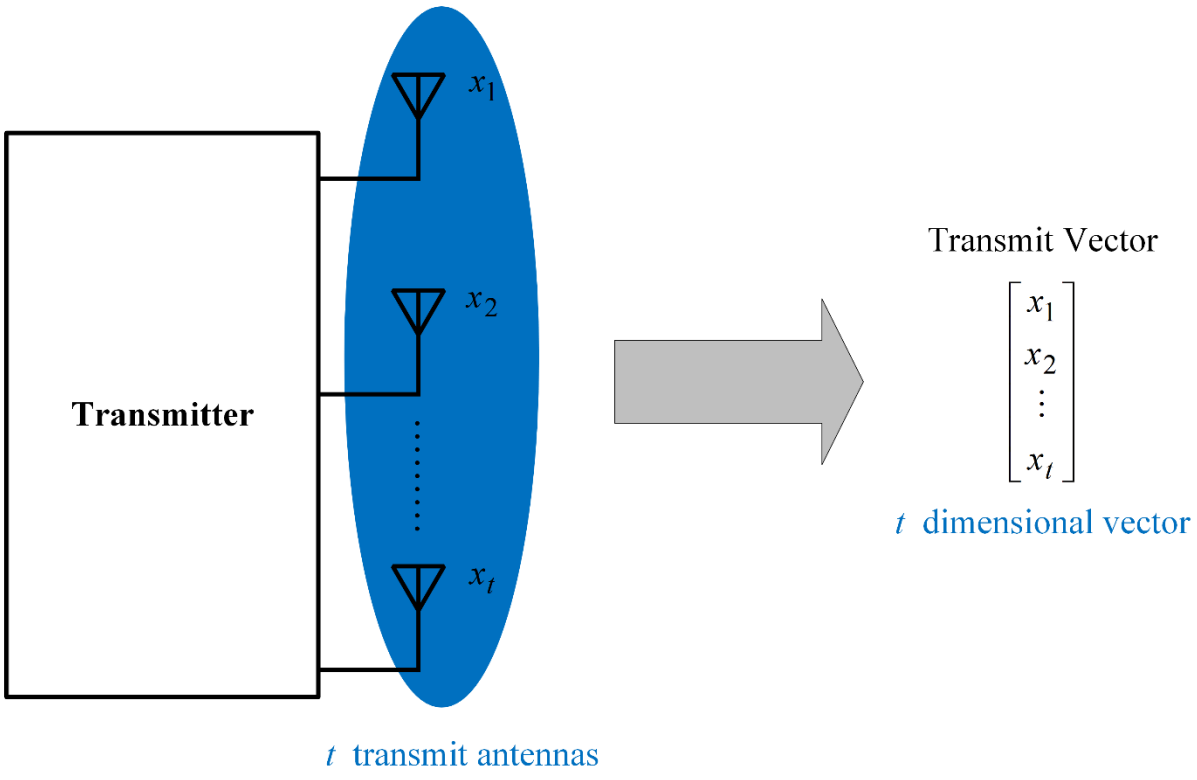

Figure 3.8: Transmitter model

The transmitter consists of t transmit antennas, where $x_1, x_2, ..., x_t$ are the data symbols from the t antennas; thus, t antennas can transmit t data symbols. The transmit vector with t dimensions displays the data symbols in vector form.

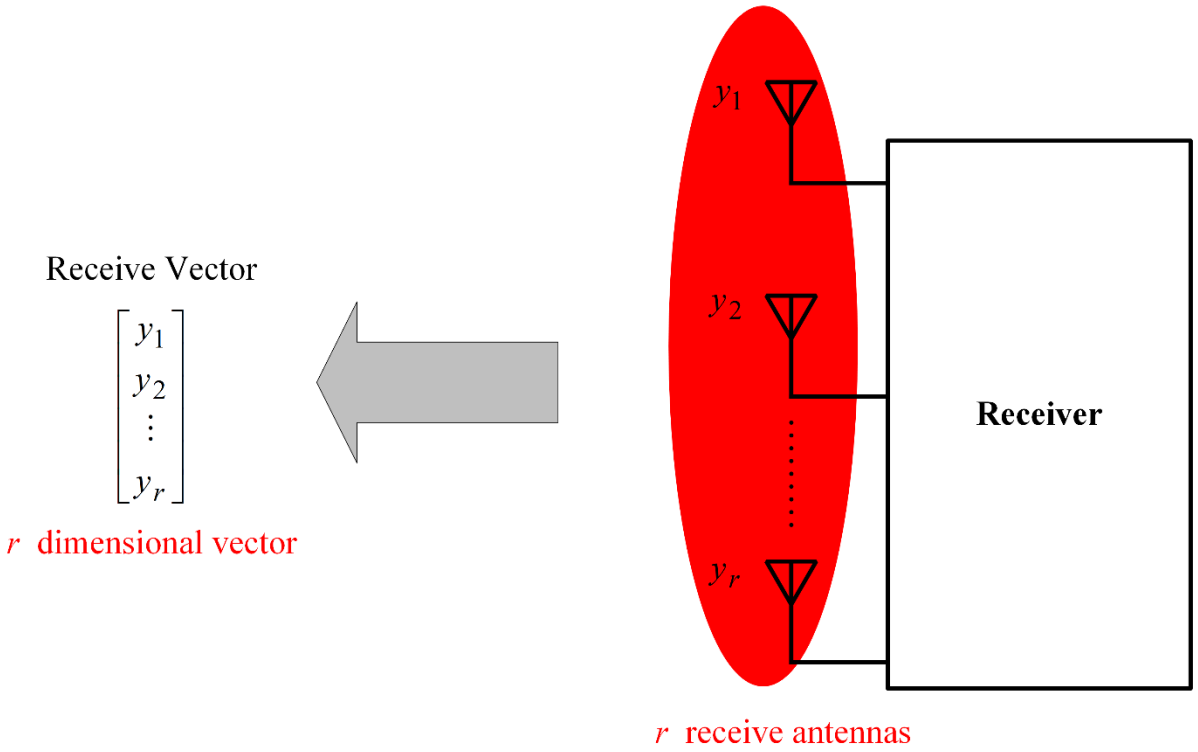

Figure 3.9: Receiver model

The receiver consists of r receive antennas, where $y_1, y_2, ..., y_r$ are the received samples from the r receive antennas. The receive vector with r dimensions displays the received samples in vector form. Figure 3.10 shows the transformation by the MIMO channel of the input transmit vector into the output receive vector, where the MIMO channel is given by $\bar{y}_{r\times 1}$. The channel matrix H, a $r \times t$ matrix, is responsible for transforming the transmit vector into the receive vector (Huang et al., 2011).

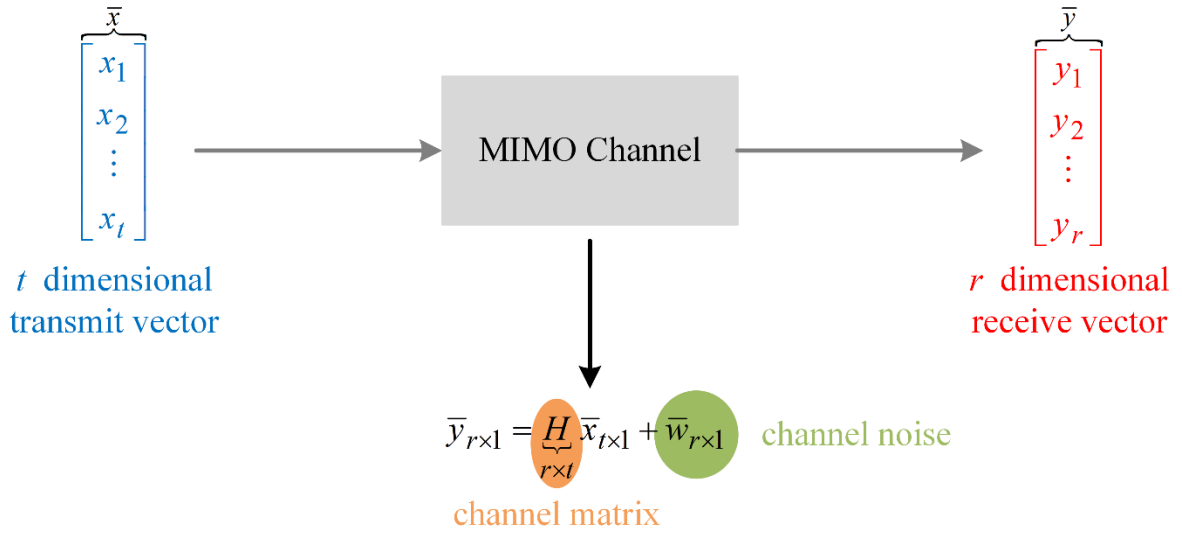

Figure 3.10: MIMO channel transform

The MIMO channel is given by equation (3.4) with the channel matrix given in expanded vector form in Figure 3.11.

$$\bar{y} = H\,\bar{x} + \bar{w} \tag{3.4}$$

The channel matrix dimensions depend on the number of antennas at the transmitter and receiver. The channel coefficient h_{ij} corresponds to the i^{th} row and j^{th} column of the matrix, representing the channel conditions between the i^{th} and j^{th} antenna.

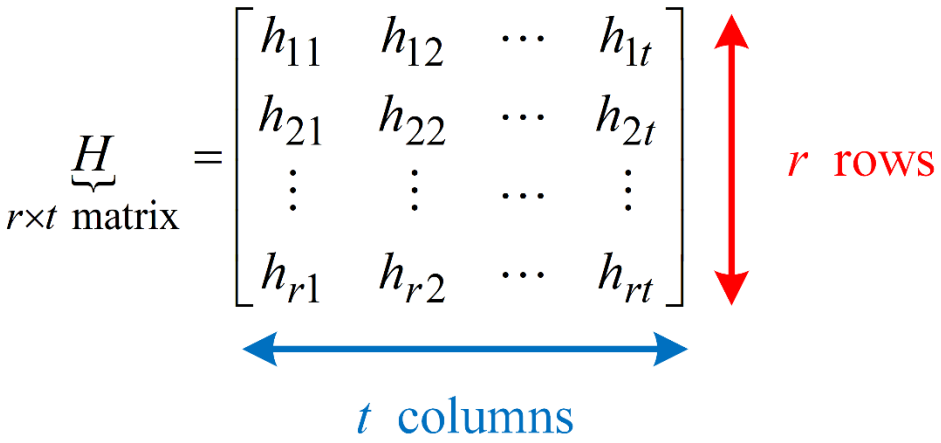

Figure 3.11: Channel matrix

Figure 3.12 shows an example of a 2x3 MIMO channel with 2 receive antennas and 3 transmit antennas; the channel matrix is a 2x3 dimensional vector composed of 2 rows and 3 columns.

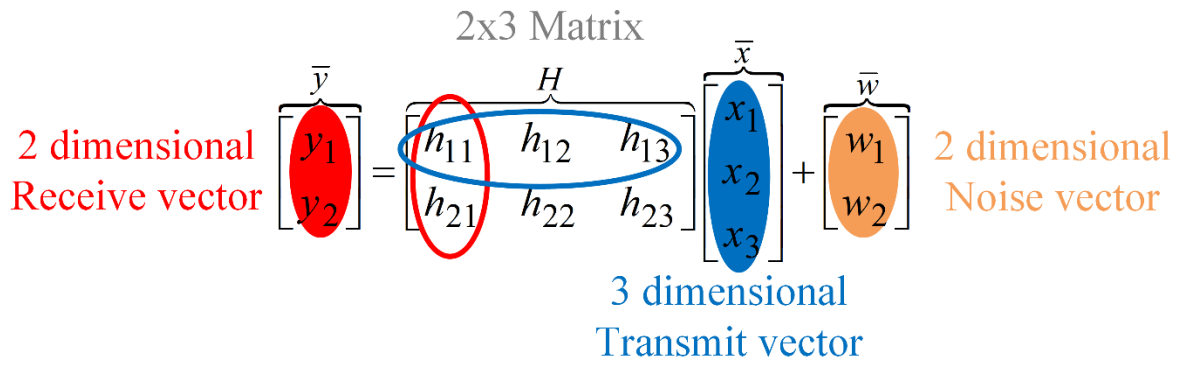

Figure 3.12: 2x3 MIMO channel

The received vector equals the channel matrix multiplied by the transmit vector plus the noise vector, and equation (3.5) gives the mathematical expression of the signal received by the two receive antennas. The equation shows the sum of the data symbols multiplied by the channel coefficient and the noise over each antenna.

$$\begin{aligned} y_1 &= h_{11}x_1 + h_{12}x_2 + h_{13}x_3 + w_1 \\ y_2 &= h_{21}x_1 + h_{22}x_2 + h_{23}x_3 + w_2 \end{aligned} \tag{3.5}$$

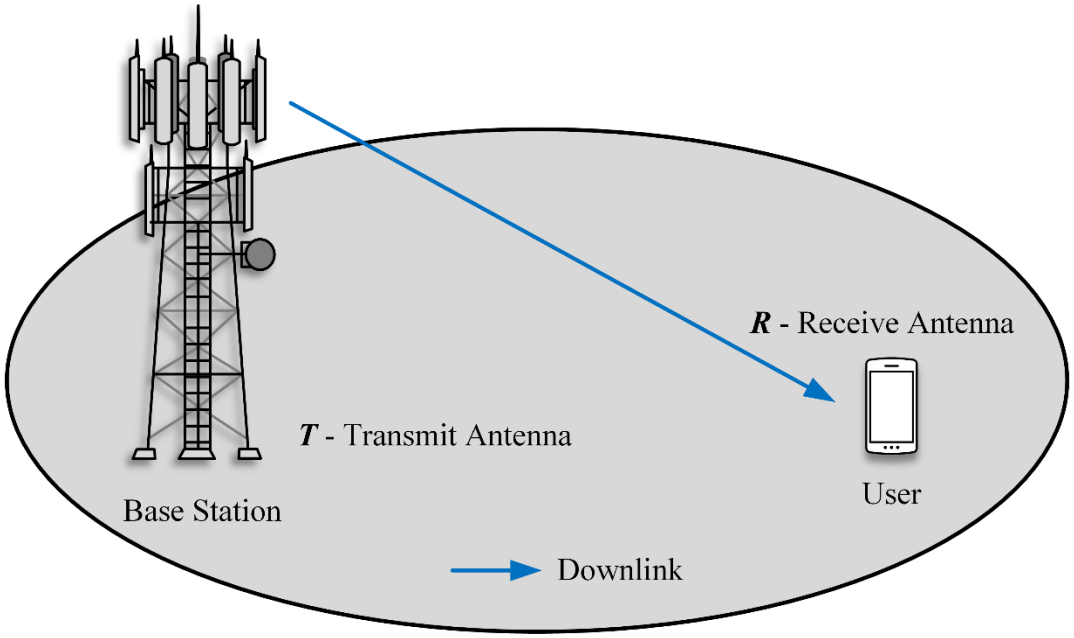

Figure 3.13: Single-user MIMO

Particular MIMO channels are considered unique because it is composed of either one transmitter or receiver, i.e., single-input single-output (SISO), MISO, and SIMO. There are two categories of MIMO channels known as single-user channels and multi-user channels. Figure 3.13 shows a single user MIMO channel where a single base station communicates on the downlink with a single user, also called a SISO channel.

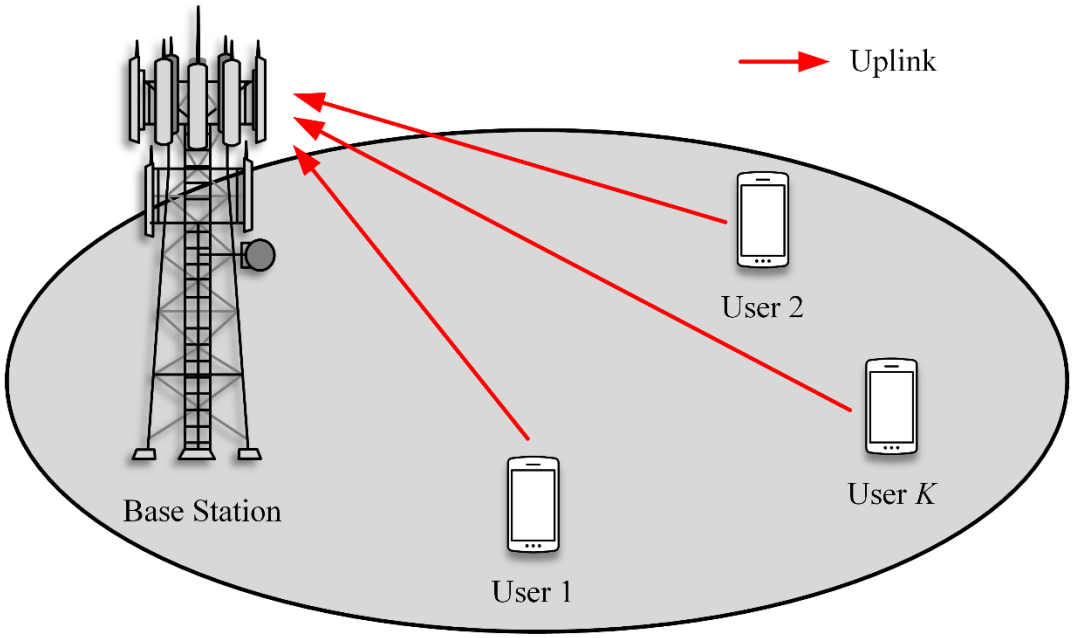

Figure 3.14: Multiple access channel

Multi-user channels have two categories known as a multiple access channel (MAC) and broadcast channel (BC). Figure 3.14 is an example of a multiple access channel where a single base station and multiple users communicate on the uplink, and Figure 3.15 is an example of a broadcast MIMO channel where a single base station communicates on the downlink with multiple users (Huang et al., 2011; Oestges & Clerckx, 2007).

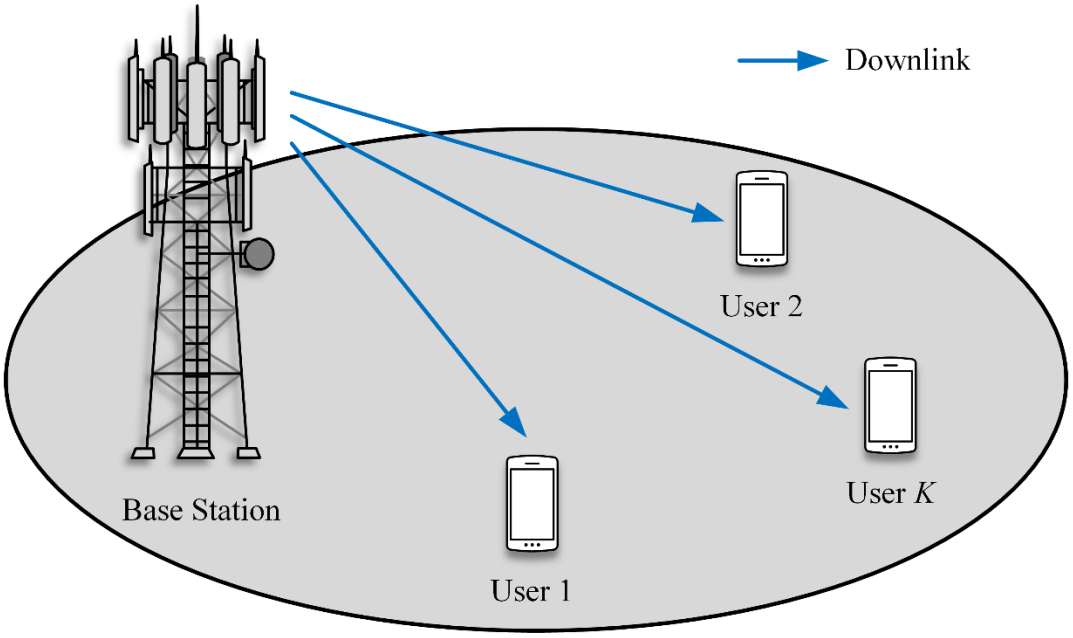

Figure 3.15: Broadcast channel

MIMO allowed an increase in capacity, signal strength, and data rates. Although the complexity of this multiple antenna scheme increased, the pros still outweigh the cons thus, making it an excellent technique (McDonough, 2009; Zarrinkoub, 2014).

As previously stated, each technique has its limitations, and LTE is no different. Thus, we move on to the following mobile generation, the fifth generation (5G).

3.5. Fifth Generation (5G)

5G expects to address the limitations of its predecessors as well as introduce new capabilities. However, 5G must have an incredible performance increase and significant capabilities compared to LTE to be considered the next mobile generation. This section discusses the drivers, technologies, and capabilities of 5G.

3.5.1. 5G Drivers

Mobile communications have become essential to our modern lives; it is intrinsically entwined in our daily activities like work pleasure and health-related activities. This constant utilisation of mobile communications caused an increase in mobile data traffic resulting in the demand for increased performance and features. These demands gave rise to the Internet of Things (IoT) and mobile internet, the drivers for 5G.

The requirements for these drivers are listed below (Vaezi et al., 2018):

- An increase in the system capacity
- The flexibility of the network
- An increase in the data rates of the user
- An increase in the number of connections
- An increase in the energy efficiency
- The heterogeneous mixing of services
- A decrease in the latency
- Deployments of flexible bandwidth

Virtual Reality (VR), electronic health services, Cyber-Physical System (CPS), cloud-based computing, and automotive driving are some of 5G's applications which are divided into three usage categories, namely, Enhanced Mobile Broadband (eMBB), Ultra-Reliable and Low Latency Communications (URLLC), and Massive Machine Type Communications (mMTC). Figure 3.16 shows the three categories and their expected future usages presented in pyramid form, with each category at a pyramid point. A key factor in 5G development is to provide support for legacy LTE systems and emerging systems.

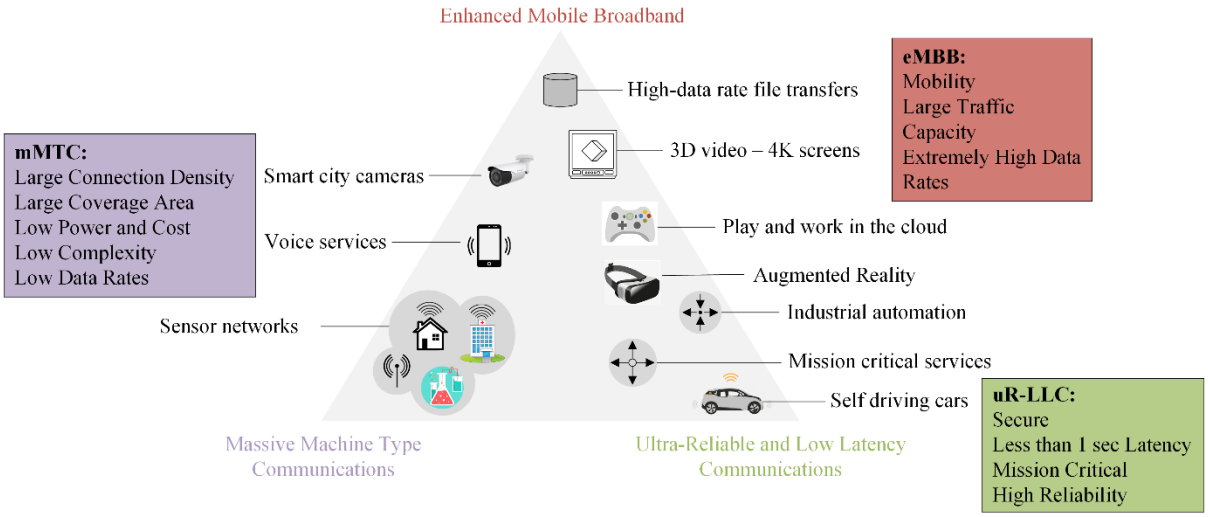

Figure 3.16: Usage categories (adapted from Ahmadi, 2019)

The utilisation of the technologies listed below enables 5G to support the use cases given in the pyramid. Figure 3.17 gives a graphical mapping of these technologies with their leading performance indicators (Ahmadi, 2019), (Vaezi et al., 2018), and (Zhao et al., 2017).

- The utilisation of multiple access schemes such as NOMA and OFDM to support spectral shaping and full-duplexing.
- The implementation of flexible numerology enables the flexibility of time slots and bandwidths for transmission—also, the utilisation of higher frequency bands above 6 GHz.

- The utilisation of QAM as a modulation scheme and the use of forward error-correcting and polar coding.
- Network behaviour management through software-defined networking.
- The improvement of network architecture to support 5G, such as network function virtualisation (NFV), core network architecture, and cloud-based radio access.
- The efficient utilisation of the spectrum such as spectrum sharing, multi-RAT, licensed, and unlicensed spectrum usage.
- Implementing multi-connectivity whereby the uplink and downlink control paths are decoupled, thus enabling macro-cell level control of devices.
- The implementation of MIMO on a much larger scale is called, Massive MIMO.

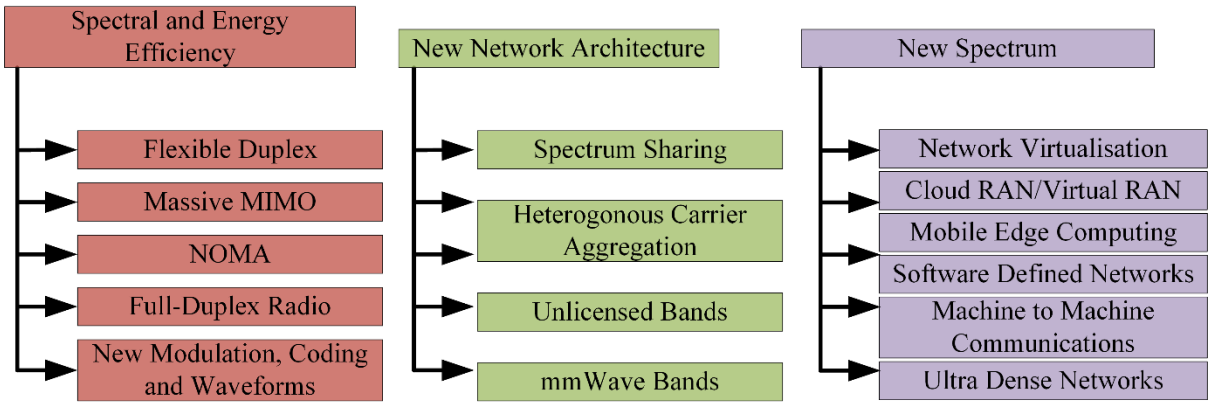

Figure 3.17: Technology mapping (adapted from Ahmadi, 2019)

3.5.2. 5G Technologies

The development of 5G is underway, and the performance expectation is rather significant. This section gives a brief description of the technologies considered in 5G to meet the requirements set out by ITU.

3.5.2.1. Multi-Access Edge Computing

A new method of providing cloud-based core network functions and services, such as management, processing, routing, and networking, at the network's edge is called Multi-access Edge Computing (MEC). The network's edge refers to the base station or antenna situated within the user's proximity inside the radio access network (RAN). The main reason for the utilisation of MEC is to reduce latency; however, there are more benefits, such as the decrease in network congestion and increase in service quality because the functions are performed at the MEC server instead of the core network (Vaezi et al., 2018) and (Ahmadi, 2019).

3.5.2.2. Software-Defined Networking

In order to facilitate the move toward the software-based network requirement for 5G, the utlisation of Software-defined Networking (SDN) and NFV are required. SDN and NFV are used to create virtual networks or slices, known as network slicing. Network slicing allows the separation of services or functions and creates virtual networks of the functions, namely, user and control functions. The benefits of the software-based networks include (Vaezi et al., 2018), (Rodriguez, 2015), (Ahmadi, 2019) and (Asif, 2018):

- Customisation: Each slice can provide different services and requirements
- Cost-effective: Slices operate on the same infrastructure, thus saving money on upgrades of new physical infrastructures.
- Improved operator control: Better network monitorisation and support.
- Network flexibility: Improved implementation of new services or features

3.5.2.3. Massive MIMO

Massive MIMO increases the data rate and energy efficiency and reduces bit error by servicing users using many antennas simultaneously. The use of multiple antennas provides array and spatial gains, achieved by beamforming and independent antenna data streams, respectively. Transmission imperfections such as multipath fading and noise are mitigated due to the number of antennas used (Vaezi et al., 2018), (Rodriguez, 2015), (Ahmadi, 2019), and (Asif, 2018).

3.5.2.4. RAN Split

Another proposed 5G technology delves into the radio access network architecture known as RAN splitting. There are different RAN splits which transport modulated symbols and user packet data. The benefits of utilising RAN splits are reduced latency and supports increased antenna configurations (Vaezi et al., 2018).

3.5.3. 5G Spectrum

Due to the increasing congestion of the current mobile spectrum, research into new frequency bands such as cm and mmWave bands for 5G are already underway. Mobile communications in the mmWave band have three significant disadvantages: high penetration loss, high path-loss, and propagation of electromagnetic waves in the line-of-sight (LOS). However, the multitude of advantages outweighs the disadvantages. The large spectrum availability provides ultra-broadband infrastructure for seamless wired and wireless networks. The mmWave band supports small antenna configurations with antenna sizes and spacings as small as $\lambda/2$; this allows the tight compaction of antennas in a small area, resulting in improved system capacity (Vaezi et al., 2018; Rodriguez, 2015).

3.5.4. Waveform and Multiple Access Design for 5G

The OFDM waveform design was able to satisfy the requirements of 4G; however, that is not the case for 5G due to the significantly greater demands such as decreased band transmissions, increased spectral efficiency, greater energy efficiency, and reduced latency. Thus, the proposals for new waveform designs to support 5Gs applications are underway. Despite certain drawbacks of OFDM in terms of 5G requirement satisfaction, it is still considered for 5G waveform design due to its flexibility. However, OFDM requires appropriate and necessary adjustments for 5G implementation. Proposals for 5G waveform design considerations are OFDM-based waveform design, filter-based waveform design, multiple-access, and non-orthogonal multi-carrier waveform design, namely Filtered OFDM (F-OFDM), Filter Bank based Multi-Carrier (FBMC), Universal Filtered Multi-Carrier (UFMC), Generalised Frequency Division Multiplexing (GFDM), NOMA, and Sparse Code Multiple Access (SCMA) (Osseiran et al., 2016; Xiang et al., 2016; Alexiou, 2017; Ahmadi, 2019)

3.6. Summary

The history of mobile technology discusses the evolution of mobile communications, specifically the multiple access techniques such as FDMA, TDMA, CDMA, and OFDMA. Brief definitions and application of the multiple access techniques highlight the utilisation of each technique in the various mobile system generations. The constant increase in data traffic and the requirement for better system performance led to the evolution of a new mobile generation, with the subsequent implementation of new multiple access techniques. The physical layer introduction and the OFDMA implementation show the technique's benefits and features, such as orthogonal subcarriers, resource block size, and frequency domain scheduling. An introduction to MIMO shows the benefits, antenna configurations, and channel models of this technique. A discussion of 5G drivers, possible technologies and applications gives the current mobile technology requirements and proposed technological solutions.

Chapter 4

NON-ORTHOGONAL MULTIPLE ACCESS

4.1. Introduction

Multiple access is the core of mobile communication systems and has evolved with each new mobile generation, which is undoubtedly necessary to keep up with the constant increase in network demands. Multiple access schemes allow multiple users to share network resources, where each generation adopted a different multiple access technique from 1G FDMA to 4G OFDMA. The utilisation of OFDMA in 4G is exceptionally beneficial by mitigating mutual interference between users and providing excellent performance with simple receiver designs. However, OFDMA cannot meet the current 5G demands; therefore, research has led to NOMA as a candidate technique for 5G. NOMA uses power and code domain based on user's channel conditions and detection schemes of multiple users with low complexity. Some code domain techniques are sparse code multiple access (SCMA), low-density spreading (LDS) CDMA, and interleave division multiple access (IDMA).

NOMA performs multiplexing in the power domain, increases spectrum efficiency by capiltalising on the user's channel conditions, and utilises more complex receiver designs to separate multiple user's signals. Previous multiple access schemes provide orthogonal user access in frequency, time, space, or code, whereas NOMA utilises the power domain to service multiple users simultaneously by multiplexing them over the same resource; however, with varying power levels (Choi, 2017a), (Yang et al., 2016). Instead of mitigating interference like OFDMA, NOMA intentionally implements inter-cell interference. NOMA utilises superposition coding and successive interference cancellation at the transmitter and receiver, respectively, thus enabling users to utilise the same spectrum (Luo & Zhang, 2016; Bizaki, 2016).

4.2. NOMA Concept

OFDMA allocates sets of subcarriers to users, as explained in section 3.4.4, whereas NOMA enables users to utilise the entire allocated spectrum. Figure 4.1 shows the OFDMA and NOMA spectrum allocation of two users. For OFDMA, user 1 and user 2 each occupy parts of the spectrum, whereas the NOMA users occupy the whole spectrum with different power levels.

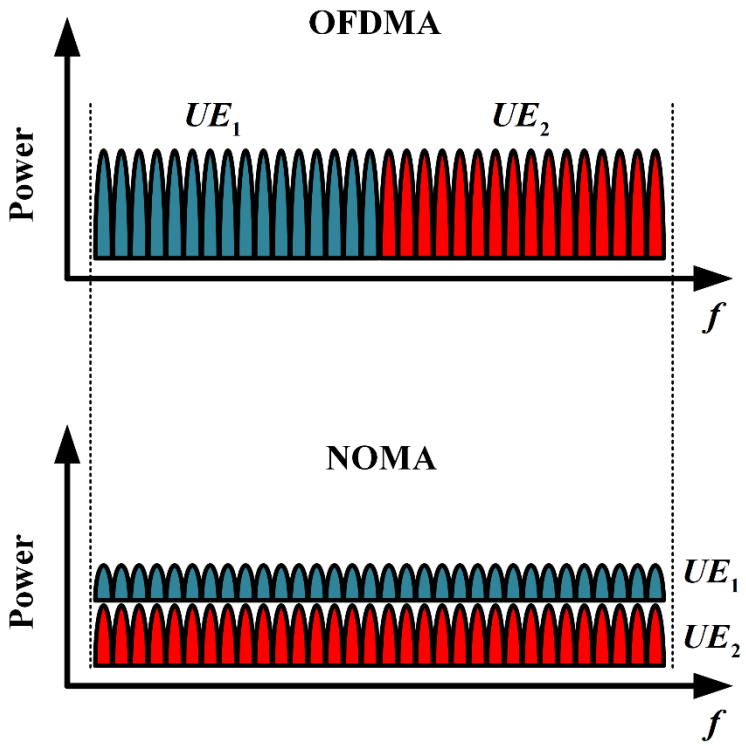

Figure 4.1: OFDMA vs. NOMA spectrum allocation

4.3. Successive Interference Cancellation

The superimposed information signal at the transmitter consists of all user's information signals, while the receiver performs SIC to decode the superimposed signal and retrieve the signals of interest. In this case, we have the superimposed information signals of three users demonstrated by Figure 4.2. It shows that each user has a different power allocation and the order of power allocation is as follows; the most power allocated to user 3, then user 2, and finally user 1 with the least allocated power.

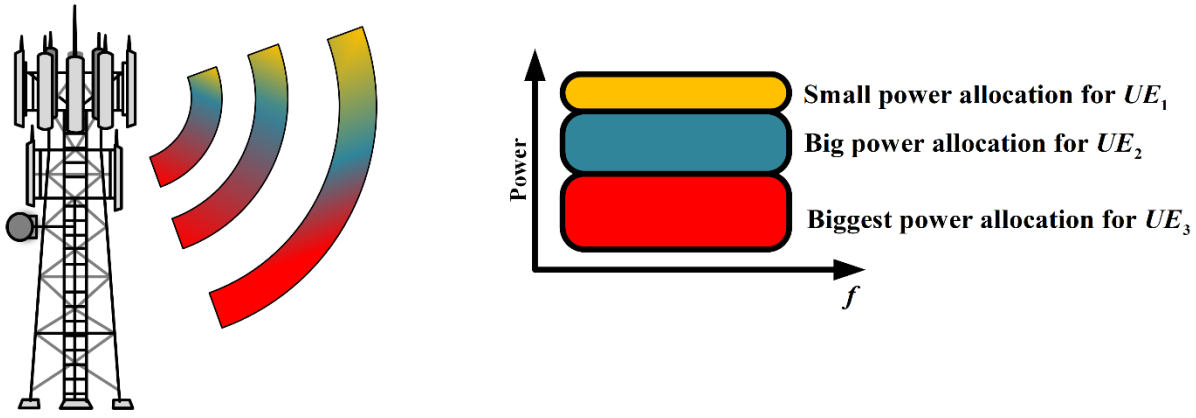

Figure 4.2: Power allocation of three users

To extract its signal of interest, each user must decode and subtract the signals stronger than itself from the received superimposed. SIC is an iterative process and assumes perfect decoding and signal cancellation.

Firstly, user 1 decodes the signals of users 3 and 2, and after subtracting the decoded signals, user 1 obtains its signal of interest, as shown by Figure 4.3.

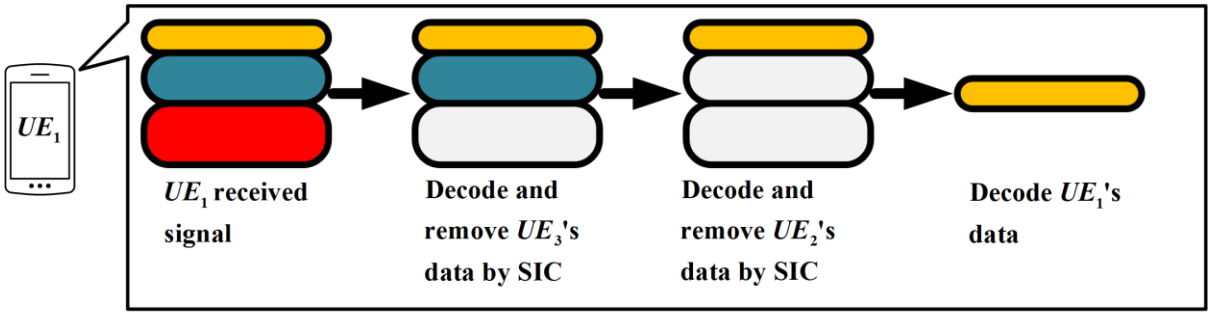

Figure 4.3: SIC at user 1

Then user 2 decodes the signal of user 3, and after subtracting the decoded signal, user 2 obtains its signal of interest with interference from user 1 still present, as shown by Figure 4.4.

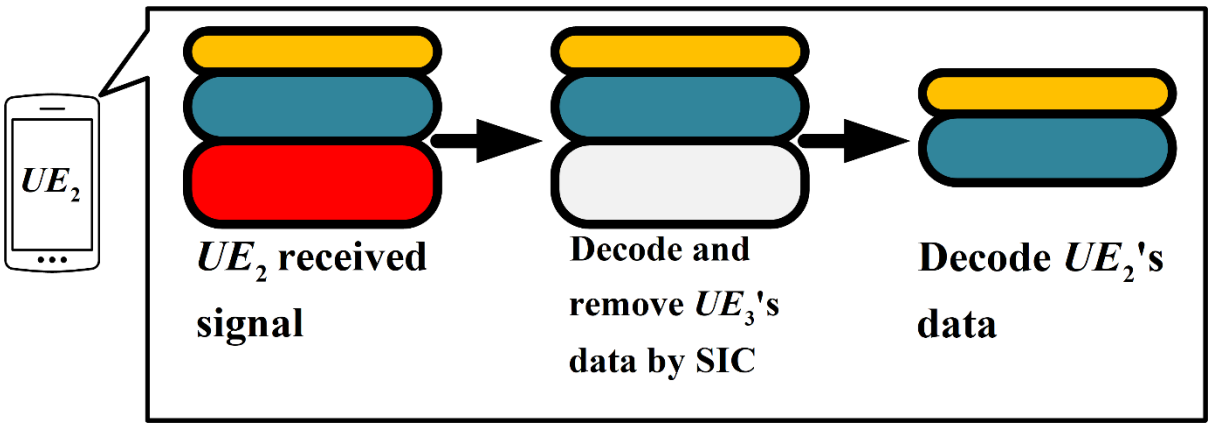

Figure 4.4: SIC at user 2

Finally, user 3 directly decodes its signal of interest with interference from users 1 and 2 still present, as shown by Figure 4.5.

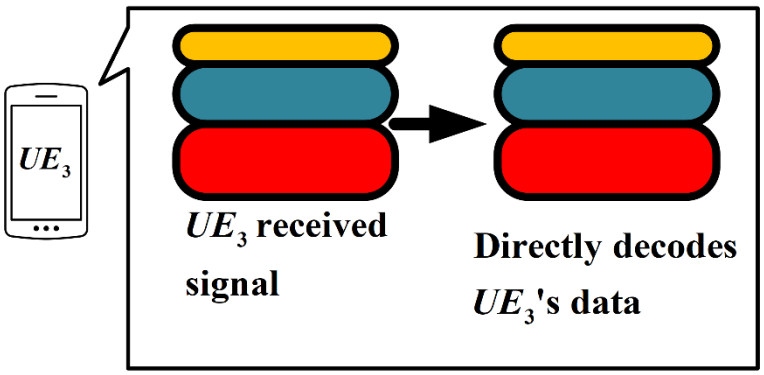

Figure 4.5: SIC at user 3

4.4. NOMA Downlink

This section briefly describes a two-user NOMA system's downlink communication and the SIC procedure at the receiver, as illustrated by Figure 4.6. The system model consists of a base station servicing two user equipment (UE), with UE_1 as the near user and UE_2 as the far user. Power allocation in NOMA works by allocating more power to the user with the worst channel conditions, .i.e. the far user, and allocates the least power to the user with the best channel conditions, .i.e. the near user. The base station transmits the superimposed signal of the connected UEs $\left(UE_j, j=1,2\right)$, given by equation (4.1)

$$x(t)=\sqrt{P_1P_s}x_1(t)+\sqrt{P_2P_s}x_2(t) \tag{4.1}$$

Where $x_1(t)$ and $x_2(t)$ and P_1 and P_2 are the data symbols and power allocation coefficients for UE_1 and UE_2, respectively. Also, P_s is the power allocation of the base station with $P_1+P_2=P_s$, $P_1<P_2$, and $E\left[\left|x_j\right|^2\right]=1$.

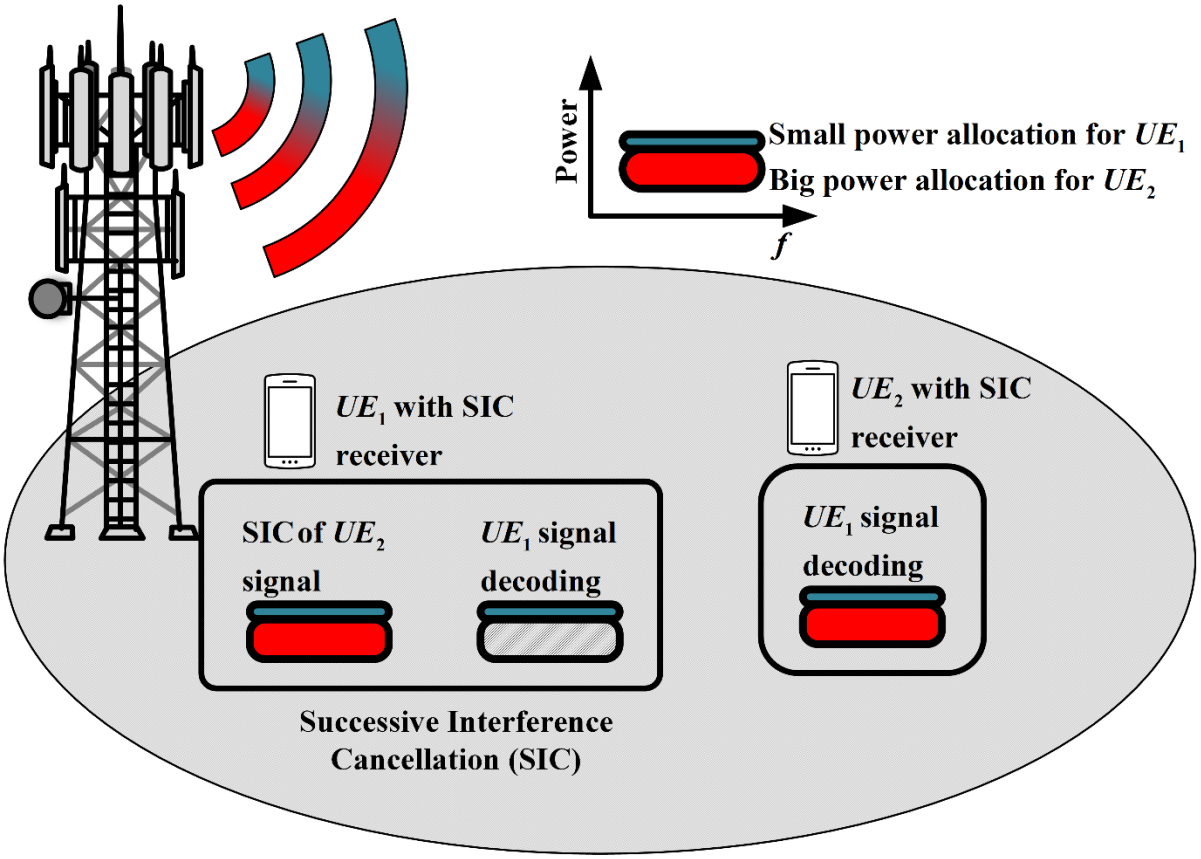

Figure 4.6: Downlink NOMA with SIC

The signals received at UE_1 and UE_2 are given by equations (4.2) and (4.3)

$$y_1(t) = h_1 x(t) + w_1 \tag{4.2}$$

$$y_2(t) = h_2 x(t) + w_2 \tag{4.3}$$

Where h_j is the channel coefficient between the UE and the base station and w_j is the additive white Gaussian noise with zero mean and power spectral density $N_{0,j}$.

The equation (4.4) gives the generalised decoded SINR for UE $\left(UE_j\right)$, where B is the bandwidth and is assumed to be 1 Hz.

$$SINR_j = \frac{P_j P_s \left|h_j\right|^2}{\sum_{i=1}^{j-1} P_i \left|h_j\right|^2 + N_{0,j} B} \tag{4.4}$$

The least power is allocated to the near user; in this case UE_1. To obtain its signal of interest, UE_1 must decode and subtract the signal of UE_2. The signal to interference plus noise ratio (SINR) of the decoded signal for UE_2 is given by equation (4.5), with the signal for UE_1 considered as interference.

$$SINR_{2-1} = \frac{P_2 P_s |h_1|^2}{P_1 P_s |h_1|^2 + N_{0,1} B} \tag{4.5}$$

After subtracting the decoded signal of UE_2, UE_1 decodes its signal of interest as shown by equation (4.6)

$$SINR_{1-1} = \frac{P_1 P_s |h_1|^2}{N_{0,1} B} \tag{4.6}$$

With the most power allocated to UE_2, it can directly decode its signal of interest with interference from UE_1 still present, as shown by equation (4.7)

$$SINR_{2-2} = \frac{P_2 P_s |h_2|^2}{P_1 P_s |h_2|^2 + N_{0,2} B} \tag{4.7}$$

The generalised throughput of each UE is given by equation (4.8)

$$R_j = B \log_2 \left(1 + \frac{P_j P_s |h_j|^2}{\sum_{i=1}^{j-1} P_i |h_j|^2 + N_{0,j} B} \right) \tag{4.8}$$

The throughput of UE_1 and UE_2 are given by equations

$$R_1 = B \log_2 \left(1 + SINR_{1-1}\right) = B \log_2 \left(1 + \frac{P_1 P_s |h_1|^2}{N_{0,1} B} \right) \tag{4.9}$$

$$R_2 = B \log_2 \left(1 + SINR_{2-2}\right) = B \log_2 \left(1 + \frac{P_2 P_s |h_2|^2}{P_1 P_s |h_2|^2 + N_{0,2} B} \right) \tag{4.10}$$

The user power allocation directly impacts the user's throughput; thus, coding and modulation techniques are essential for data transmissions. Also, user fairness in a NOMA system is fundamental where it measures the fairness of the shared capacity between the users and is given by equation (4.11)

$$F = \frac{\left(\sum_{i=1}^{j} R_j\right)^2}{j\sum_{i=1}^{j} R_j} \tag{4.11}$$

As mentioned in the literature review section, many researchers focus on user fairness and power allocation. They do this to increase the sum capacity of the system while considering user fairness.

4.5. NOMA Uplink

This section briefly describes a two-user NOMA system's uplink communication and the SIC procedure performed by the base station, as illustrated by Figure 4.7. The UEs simultaneously transmit their signals to the base station utilising one frequency resource.

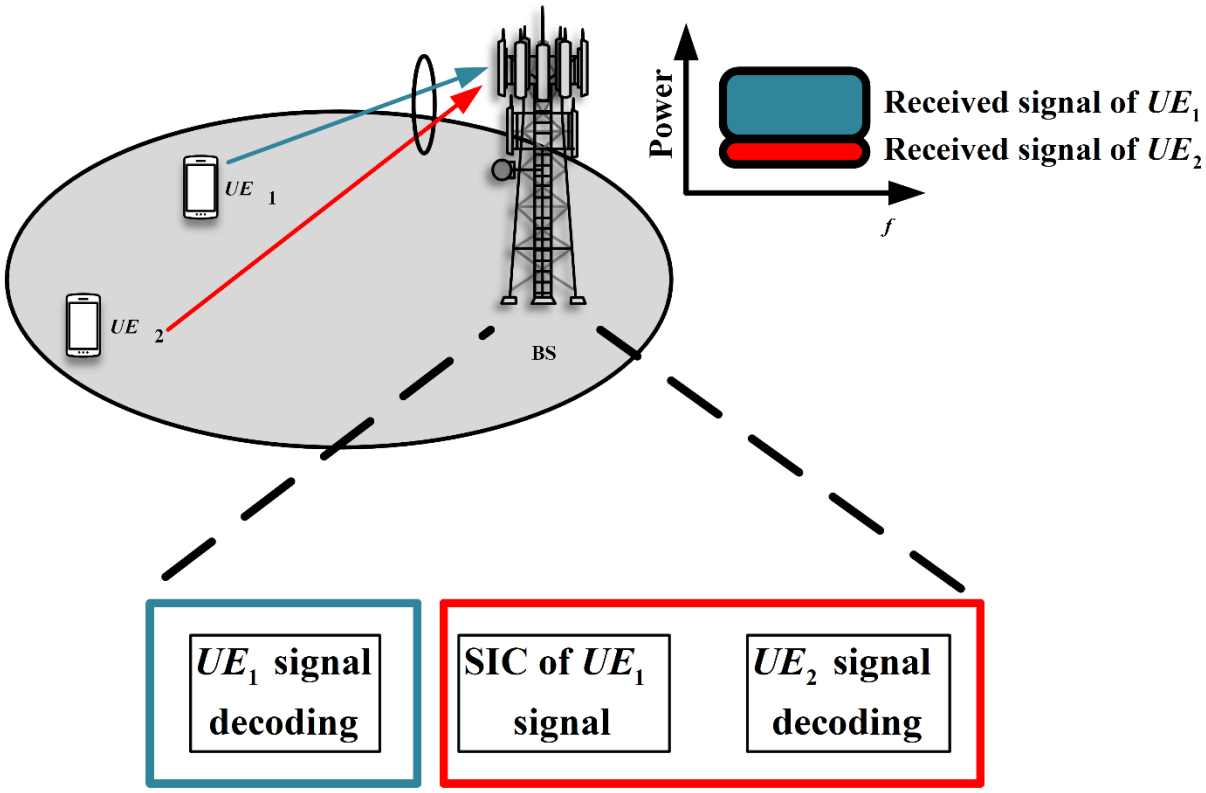

Figure 4.7: Uplink NOMA with SIC

The received superimposed signal at the base station is given by equation

$$y(t) = h_1\sqrt{P_1}x_1(t) + h_2\sqrt{P_2}x_2(t) + w \tag{4.12}$$

Where x_1 and x_2 and P_1 and P_2 are the data symbols and power allocation coefficients for UE_1 and UE_2, respectively. Where h_j is the channel coefficient between the UE and the base station and w is the additive white Gaussian noise with zero mean and power spectral density N_0. Also, the expectation is denoted by $E\left[\left|x_j\right|^2\right] = 1$. The channel conditions of UE_1 are better than UE_2 because UE_1 is closer to the base station. Therefore, the base station first performs SIC and decodes the signal of UE_1 followed by UE_2. Equations (4.13) to (4.16) give the decoded SINRs and user's throughput (Luo & Zhang, 2016; Bizaki, 2016).

$$SINR_1 = \frac{P_1\left|h_1\right|^2}{P_2\left|h_2\right|^2 + N_0B} \tag{4.13}$$

$$SINR_2 = \frac{P_2\left|h_2\right|^2}{N_0B} \tag{4.14}$$

$$R_1 = B\log_2\left(1 + SINR_1\right) = B\log_2\left(1 + \frac{P_1\left|h_1\right|^2}{P_2\left|h_2\right|^2 + N_0B}\right) \tag{4.15}$$

$$R_2 = B\log_2\left(1 + SINR_2\right) = B\log_2\left(1 + \frac{P_2\left|h_2\right|^2}{N_0B}\right) \tag{4.16}$$

An interesting observation of the SIC order at the base station shows that the order of decoding does not affect the total throughput of the users, as shown by equations (4.17) to (4.19). However, the norm is to perform SIC in descending order, and SIC decoding and signal cancellation for the downlink and uplink system is assumed to be perfect.

$$R_1 = B\log_2\left(1 + \frac{P_1\left|h_1\right|^2}{N_0B}\right) \tag{4.17}$$

$$R_2 = B\log_2\left(1 + \frac{P_2\left|h_2\right|^2}{P_1\left|h_1\right|^2 N_0B}\right) \tag{4.18}$$

$$R_1 + R_2 = B\log_2\left(1+\frac{P_1|h_1|^2 + P_2|h_2|^2}{N_0 B}\right) \tag{4.19}$$

4.6. NOMA vs. OMA Comparison

A comparison between NOMA and OMA is the best way to convey the benefits of NOMA. The comparison illustrates the previously discussed downlink and uplink NOMA systems, with the values taken from (Luo & Zhang, 2016).

The bandwidth $\beta\,(0<\beta<1)$ allocations for users in the OMA system is as follows:

- UE_1 - bandwidth of β Hz
- UE_2 - remaining bandwidth of $(1-\beta)$ Hz

Equations (4.20) and (4.21) give the throughput for the users (UE_1, UE_2) in the downlink OMA system

$$R_1 = \beta\log_2\left(1+\frac{P_1|h_1|^2}{\beta N_{0,1}}\right) \tag{4.20}$$

$$R_2 = (1-\beta)\log_2\left(1+\frac{P_2|h_2|^2}{(1-\beta)N_{0,2}}\right) \tag{4.21}$$

Table 4.1 gives the downlink OMA and NOMA parameters for a two-user system. The user rates for the NOMA system are calculated using equations (4.9) and (4.10), and equations (4.20) and (4.21) for the OMA users.

Table 4.1: Downlink system parameters

Parameter	OMA	NOMA
SNR	$UE_1 = \lvert h_1\rvert^2 / N_{0,1} = 20$ dB $UE_2 = \lvert h_2\rvert^2 / N_{0,2} = 0$ dB	
Bandwidth	$\beta = 0.5$	$\beta = 1$
Power Allocation	$P_1 = P_2 = 0.5P_s$	$P_1 = 1/5P_s$ $P_2 = 4/5P_s$

User Rates	$R_1 = 3.33$ bps $R_2 = 0.5$ bps	$R_1 = 4.39$ bps $R_2 = 0.74$ bps

The NOMA gain of user 1 is 32%, and user 2 is 48% over OMA, as seen in Figure 4.8. NOMA excels when the channel gain difference between users is significant and achieves higher sum rates than OMA. The UEs benefit from the transmit bandwidth of NOMA, even though they have power limitations.

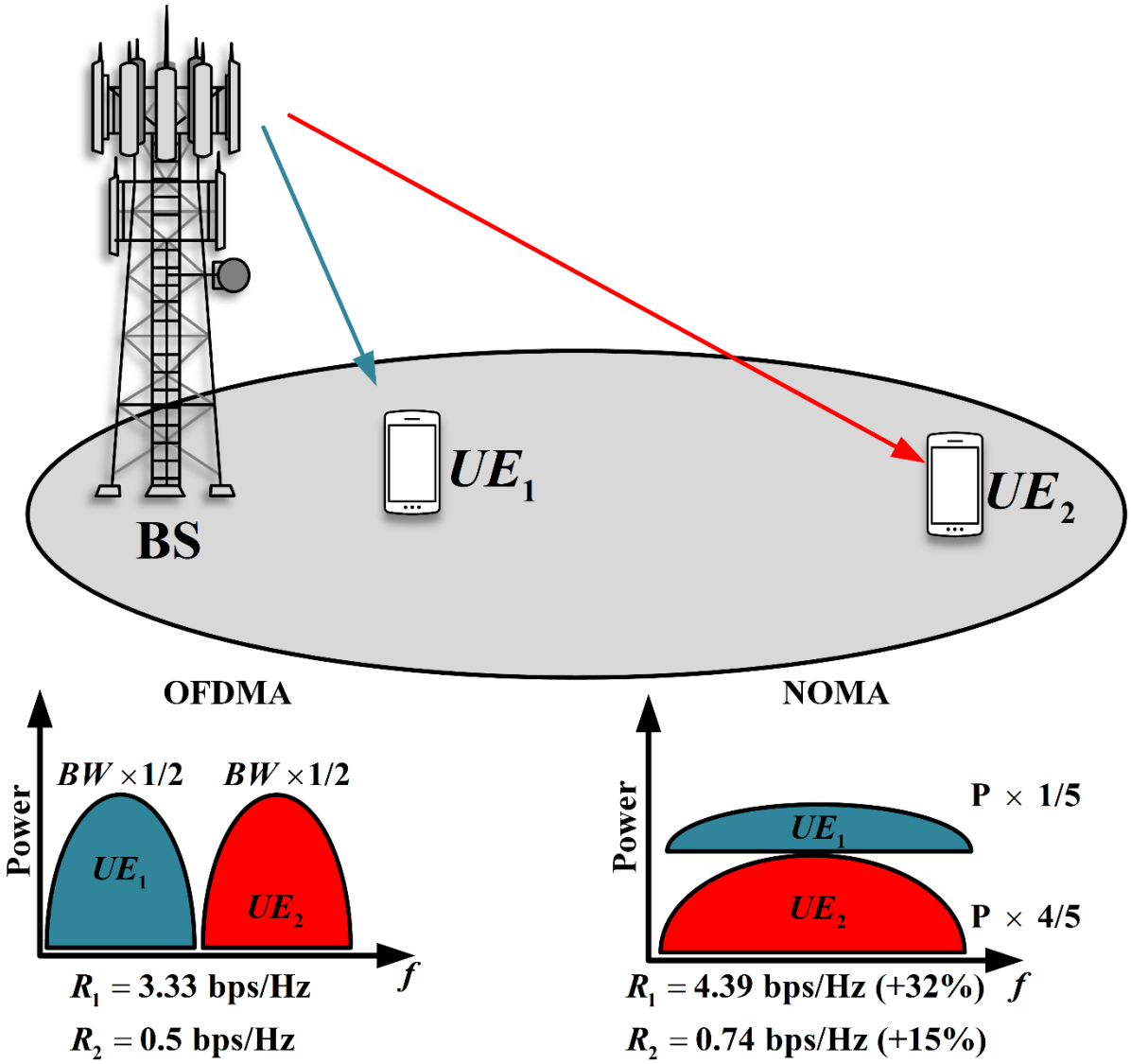

Figure 4.8: Downlink OMA vs. NOMA

Equations (4.20) and (4.21) give the throughput for the users (UE_1, UE_2) in the uplink OMA system

$$R_1 = \beta \log_2 \left(1 + \frac{P_1 |h_1|^2}{\beta N_0} \right) \tag{4.22}$$

$$R_2 = (1-\beta) \log_2 \left(1 + \frac{P_2 |h_2|^2}{(1-\beta) N_0} \right) \tag{4.23}$$

Figure 4.9 illustrates the uplink comparison of OMA and NOMA. Thus, utilising the same system parameters of Table 4.1 for the uplink, the total NOMA UE throughput outperforms OMA by 46%. The user rates for the NOMA system are calculated using equations (4.15) and (4.16), and equations (4.22) and (4.23) for the OMA users.

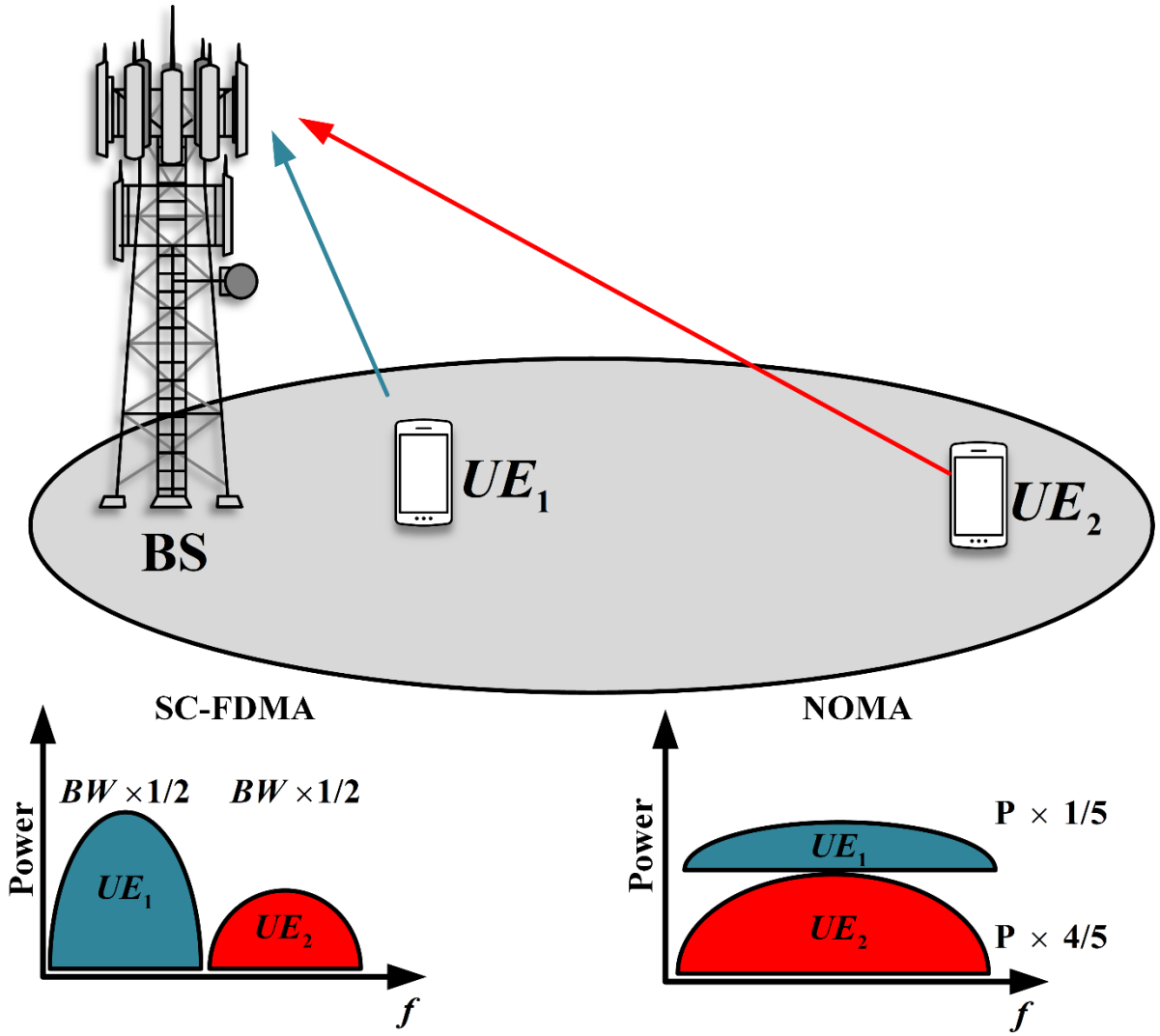

Figure 4.9: Uplink OMA vs. NOMA

As illustrated, NOMA utilises the power domain to improve the system's spectral efficiency, resulting in increased throughput. Additionally, the high-powered user performs successful decoding for the lower-powered user. In conclusion, NOMA is a front runner for 5G applications and can be utilised by other diversity and coding schemes (Luo & Zhang, 2016; Bizaki, 2016).

4.7. Summary

A detailed discussion of NOMA shows the benefits of utilising this technique as a candidate for 5G communications, whereby NOMA utilises the power domain to increase the system's spectral efficiency. A comparison shows the superiority of NOMA over the previous multiple access technique, OFDMA. A detailed succession of figures explains the NOMA concept and the utilisation of SIC by exploring the uplink and downlink communications of a NOMA based system. Lastly, a comparison of the up and downlink communications of NOMA and OMA highlights the effectiveness of NOMA.

Chapter 5

RESOURCE ALLOCATION FOR NOMA BASED NETWORKS USING RELAYS: CELL CENTRE AND CELL EDGE USERS

5.1. Introduction

The previous chapter discusses NOMA and its applications in the communication system, resulting in the clear superiority of NOMA over OMA. This chapter explores a four-user downlink NOMA-based MIMO system equipped with relays to aid users in communicating with the base station and the SIC process at each UE. It also derives the UE's outage probability and ergodic rate and a power allocation algorithm that allocates power to the UEs considering user fairness. The MIMO channel implemented in this system model is a multi-user channel, specifically the broadcast channel explained in section 3.4.6, where the base station communicates on the downlink with the connected equipment. This chapter utilises the research paper published by (Balyan & Daniels, 2020).

5.2. System Model

Extensive evaluation of the papers presented by authors (Zhao et al., 2019; Balyan & Daniels, 2020) led to the chosen system models. It provides more system variables and better showcases the effectiveness of NOMA in a multi-user system. The system model configuration allows the mobility of users, thus showing the evaluation of cell center and cell-edge users.

The proposed system model consists of a base station (BS), three relays, and four random users, as seen in Figure 5.1. The time slot is divided into four sub-slots, with all sub-slots equal and the channel conditions in a time sub-slot remain constant. There are cell center and cell edge users who change their positions in different time slots, as seen in Figure 5.2. The cell centre users communicate directly with the BS, while the cell edge users use the relays for communication with the BS as they operate in half-duplex mode, with communication in the downlink direction. The channels are independent and are under the influence of Rayleigh fading. The cell centre user's channel conditions are better than cell edge users. For cell edge users, a selected relay is used to forward signals from the BS using NOMA. As shown in Figure 5.1, a user equipment can be in the coverage area of one or more relays. A cell edge UE is connected to the BS in two hops, the communication link between the BS and relay is the *relay link*, and the link between a relay and UE is the *access link*. Table 5.1 gives the denotations used in the paper (Balyan & Daniels, 2020).

Table 5.1: Denotations

$r_i, i = 1,2,3$	Relays 1 to 3
$UE_j, j = 1,2,...4$	Users 1 to 4
h_j^{BS}	Channel coefficient from the BS to user *j*
h_j^r	Channel coefficient from a relay to user *j*
$h_j^{BS} \sim CN\left(0, \lambda_j^{BS}\right)$	Channel model
$t_{s_k}, k = 1,2,...4$ $t = \sum_{k=1}^{4} t_{s_k}$	Time sub-slots 1 to 4
$t_{s_1} = t_{s_2} = t_{s_3} = t_{s_4}$	All the sub-slots are equal
$E\left[x_j\right] = 1$	Expected value
P_s	Power allocation of the base station
P_{r_1}, P_{r_2}	Power allocation of the relays

The UE selects the relay with the best channel coefficient in a particular time slot. The smartly equipped relays used in this paper can perform successive interference cancellation by removing information signals of UEs not connected to it. In doing so, the relay avoids the unnecessary regeneration of signals for higher transmission power UEs. Thus, the relays can provide better service to the UEs connected to it without this regeneration of other UE signals.

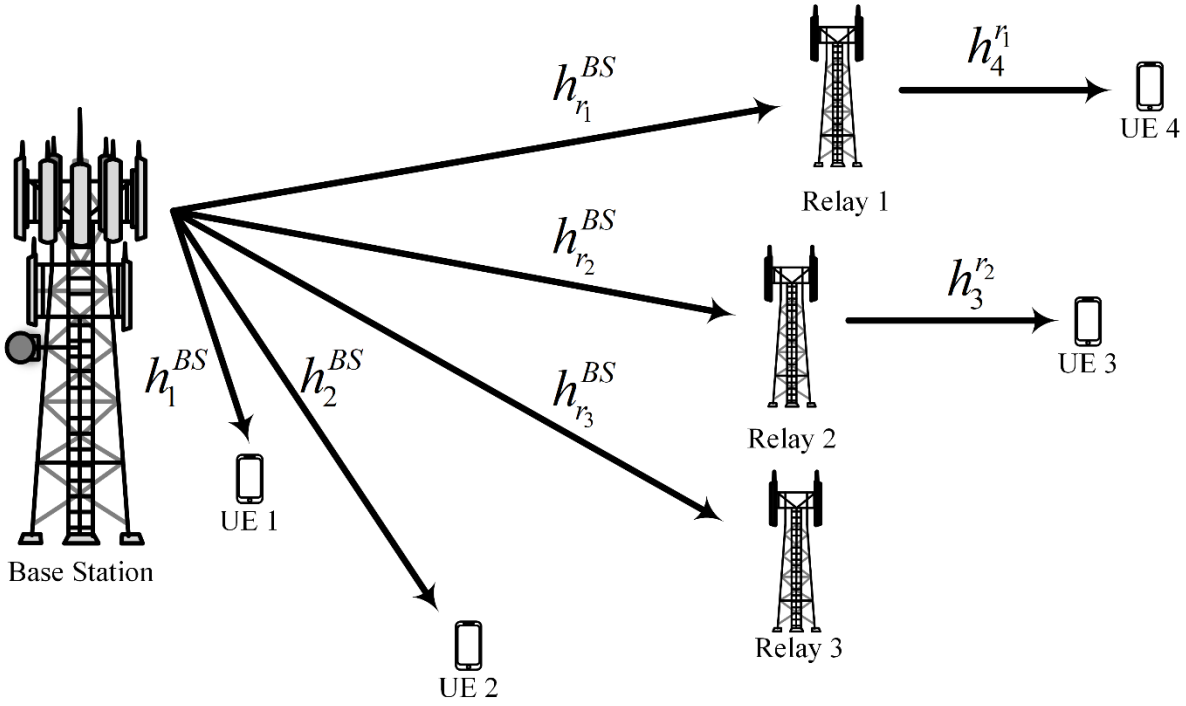

Figure 5.1: System model in time sub-slot 1 and 2

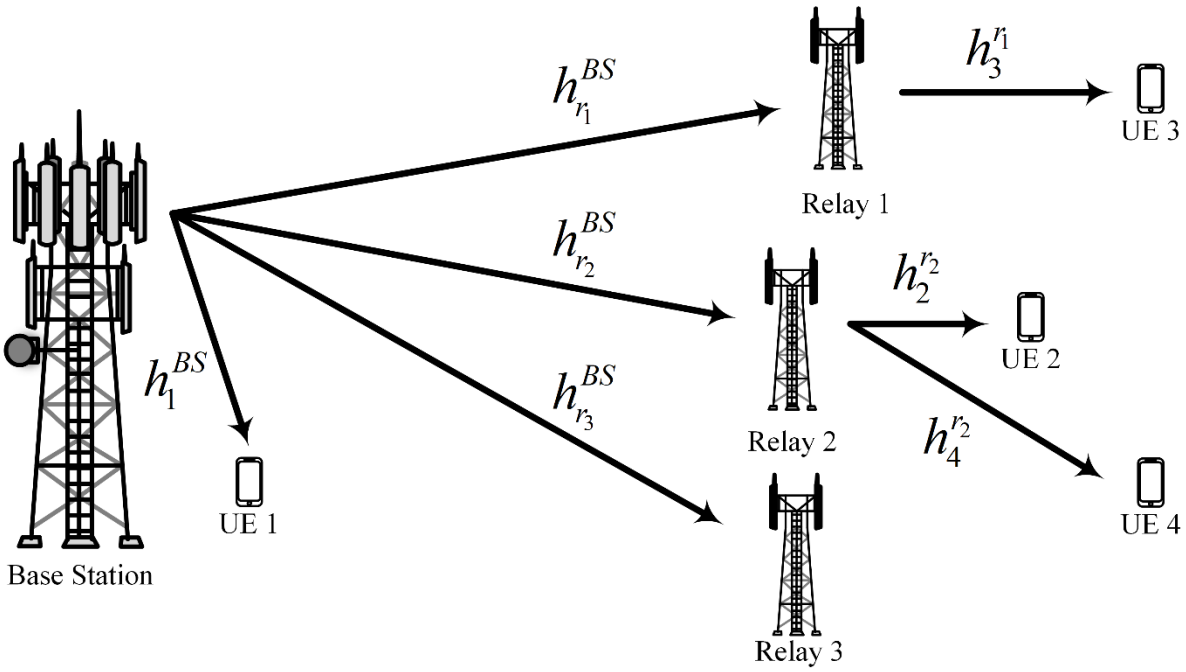

Figure 5.2: System model in time sub-slot 3 and 4

5.2.1. Time Sub-slot t_{s_1} :

The active users in the network are $UE_1, UE_2, UE_3,$ and UE_4. The status of these users in time sub-slot 1 is according to their locations, as seen in Figure 5.1:

a) UE_1 and UE_2 are cell center users
b) UE_3 and UE_4 are cell edge users

The channel conditions of the access link between UE_4 and relays are better, worse, and worst for $r_1, r_2,$ and r_3, respectively. UE_4 chooses r_1 as its access link to the base station. The channel conditions of the access link between UE_3 and relays are worse, better, and worst for $r_1, r_2,$ and r_3, respectively. UE_3 chooses r_2 as its access link to the base station.

The base station transmits the superimposed signal to the user equipment connected to it $UE_1, UE_2,$ relays $r_1,$ and r_2, given by equation (5.1)

$$x_s(t_{s_1}) = \sqrt{P_1^{t_{s_1}} P_s}\, x_1\left(t_{s_1}\right) + \sqrt{P_2^{t_{s_1}} P_s}\, x_2\left(t_{s_1}\right) + \sqrt{P_3^{t_{s_1}} P_s}\, x_3\left(t_{s_1}\right) + \sqrt{P_4^{t_{s_1}} P_s}\, x_4\left(t_{s_1}\right) \qquad (5.1)$$

Table 5.2 gives the system parameters and denotations for the time sub-slots, such as the data symbols and power allocation coefficient for each user and the base station. As seen in the table, the sum of the power allocations for users 1 to 4 equals 1.

Table 5.2: Denotations in time sub-slots

$x_1\left(t_{s_1}\right), x_2\left(t_{s_1}\right), x_3\left(t_{s_1}\right),\ x_4\left(t_{s_1}\right)$ $x_1\left(t_{s_3}\right), x_2\left(t_{s_3}\right), x_3\left(t_{s_3}\right),\ x_4\left(t_{s_3}\right)$	Data symbols of UEs in t_{s_1} and t_{s_3}
$P_1^{t_{s_1}}, P_2^{t_{s_1}}, P_3^{t_{s_1}}, P_4^{t_{s_1}}$ $P_3^{t_{s_2}}, P_4^{t_{s_2}}$ $P_1^{t_{s_3}}, P_2^{t_{s_3}}, P_3^{t_{s_3}}, P_4^{t_{s_3}}$ $P_2^{t_{s_4}}, P_3^{t_{s_4}}, P_4^{t_{s_4}}$	Power allocation coefficients of UEs in time sub-slots
$P_1^{t_{s_1}} + P_2^{t_{s_1}} + P_3^{t_{s_1}} + P_4^{t_{s_1}} = 1$ $P_3^{t_{s_2}} + P_4^{t_{s_2}} = 1$ $P_1^{t_{s_3}} + P_2^{t_{s_3}} + P_3^{t_{s_3}} + P_4^{t_{s_3}} = 1$ $P_2^{t_{s_4}} + P_3^{t_{s_4}} + P_4^{t_{s_4}} = 1$	Sum powers in time sub-slots

$P_1^{t_{s1}} < P_2^{t_{s1}} < P_3^{t_{s1}} < P_4^{t_{s1}}$ $P_3^{t_{s2}} < P_4^{t_{s2}}$ $P_1^{t_{s3}} < P_2^{t_{s3}} < P_4^{t_{s3}} < P_3^{t_{s3}}$ $P_2^{t_{s4}} < P_4^{t_{s4}}$	Power allocation in time sub-slots

5.2.1.1. Received Signal

The received superimposed signals at UE_1, UE_2, r_1, and r_2 are given by equations (5.2) to (5.5) .

$$y_1\left(t_{s_1}\right) = h_1^{BS} x_s\left(t_{s_1}\right) + N_1 \tag{5.2}$$

$$y_2\left(t_{s_1}\right) = h_2^{BS} x_s\left(t_{s_1}\right) + N_2 \tag{5.3}$$

$$y_{r_1}\left(t_{s_1}\right) = h_{r_1}^{BS} x_s\left(t_{s_1}\right) + N_{r_1} \tag{5.4}$$

$$y_{r_2}\left(t_{s_1}\right) = h_{r_2}^{BS} x_s\left(t_{s_1}\right) + N_{r_2} \tag{5.5}$$

The received signal consists of a channel coefficient $\left(h_j^{BS}\right)$, data symbol $\left(x_j\right)$, and additive white Gaussian noise $\left(N_j\right)$ at the respective user or relay.

5.2.1.2. SINR

Each UE must perform SIC on the received superimposed signal and decode the signals stronger than itself to extract its signal of interest. The power allocation in this time sub-slot is descending from UE_4 to UE_1, with UE_4 allocated the most power and UE_1 the least power. Table 5.3 and Table 5.4 gives the SINR of UE_1, UE_2, r_1, and r_2. The order of decoding is as follows:

i. UE_1 first decodes the signals of $UE_4, UE_3,$ and then UE_2. After removing the decoded signals, UE_1 obtains its signal of interest. The decoded SINRs are given by equations (5.6) to (5.9).

ii. UE_2 first decodes the signals of UE_4 and then UE_3. After removing the decoded signals, UE_2 obtains its signal of interest with interference from UE_1 still present. The decoded SINRs are given by equations (5.10) to (5.12).

iii. Relay r_1 decodes the signal of UE_4 directly with interference from $UE_1, UE_2,$ and UE_3 still present. The decoded SINR is given by equation (5.14).

iv. Relay r_2 decodes the signal of UE_4 and then removes the decoded signal to obtain the signal of interest for UE_3 with interference from UE_1 and UE_2 still present. The decoded SINRs are given by equations (5.15) and (5.16).

Table 5.3: SINR of UE_1 and UE_2 for time sub-slot t_{s_1}

UE_1	UE_2
$SINR_{t_{s_1}}^{4-1} = \frac{P_4^{t_{s_1}} P_s \left\lvert h_1^{BS} \right\rvert^2}{\sum_{j=1}^{3} P_j^{t_{s_1}} P_s \left\lvert h_1^{BS} \right\rvert^2 + {\sigma_1}^2}$ (5.6)	$SINR_{t_{s_1}}^{4-2} = \frac{P_4^{t_{s_1}} P_s \left\lvert h_2^{BS} \right\rvert^2}{\sum_{j=1}^{3} P_j^{t_{s_1}} P_s \left\lvert h_2^{BS} \right\rvert^2 + {\sigma_2}^2}$ (5.10)
$SINR_{t_{s_1}}^{3-1} = \frac{P_3^{t_{s_1}} P_s \left\lvert h_1^{BS} \right\rvert^2}{\sum_{j=1}^{2} P_j^{t_{s_1}} P_s \left\lvert h_1^{BS} \right\rvert^2 + {\sigma_1}^2}$ (5.7)	$SINR_{t_{s_1}}^{3-2} = \frac{P_3^{t_{s_1}} P_s \left\lvert h_2^{BS} \right\rvert^2}{\sum_{j=1}^{2} P_j^{t_{s_1}} P_s \left\lvert h_2^{BS} \right\rvert^2 + {\sigma_2}^2}$ (5.11)
$SINR_{t_{s_1}}^{2-1} = \frac{P_2^{t_{s_1}} P_s \left\lvert h_1^{BS} \right\rvert^2}{P_1^{t_{s_1}} P_s \left\lvert h_1^{BS} \right\rvert^2 + {\sigma_1}^2}$ (5.8)	$SINR_{t_{s_1}}^{2-2} = \frac{P_2^{t_{s_1}} P_s \left\lvert h_2^{BS} \right\rvert^2}{P_1^{t_{s_1}} P_s \left\lvert h_2^{BS} \right\rvert^2 + {\sigma_2}^2}$ (5.12)
$SINR_{t_{s_1}}^{1-1} = \frac{P_1^{t_{s_1}} P_s \left\lvert h_1^{BS} \right\rvert^2}{{\sigma_1}^2}$ (5.9)	Minimum SINR of UE_2 $a_2^{t_{s_1}} = \min\left(SINR_{t_{s_1}}^{2-2}, SINR_{t_{s_1}}^{2-1}\right)$ (5.13)

Table 5.4: SINR at relays r_1 and r_2 for time sub-slot t_{s_1}

r_1	r_2
$SINR_{t_{s_1}}^{4-r_1} = \frac{P_4^{t_{s_1}} P_s \left\| h_{r_1}^{BS} \right\|^2}{\sum_{j=1}^{3} P_j^{t_{s_1}} P_s \left\| h_{r_1}^{BS} \right\|^2 + {\sigma_{r_1}}^2}$ (5.14)	$SINR_{t_{s_1}}^{4-r_2} = \frac{P_4^{t_{s_1}} P_s \left\| h_{r_2}^{BS} \right\|^2}{\sum_{j=1}^{3} P_j^{t_{s_1}} P_s \left\| h_{r_2}^{BS} \right\|^2 + {\sigma_{r_2}}^2}$ (5.15) $SINR_{t_{s_1}}^{3-r_2} = \frac{P_3^{t_{s_1}} P_s \left\| h_{r_2}^{BS} \right\|^2}{\sum_{j=1}^{2} P_j^{t_{s_1}} P_s \left\| h_{r_2}^{BS} \right\|^2 + {\sigma_{r_2}}^2}$ (5.16)

5.2.2. Time Sub-slot t_{s_2} :

In this time sub-slot, the relays regenerate the new signals for the users connected to it. UE_4 is connected to relay r_1, and UE_3 is connected to relay r_2. Equations (5.17) and (5.18) give the signals generated by relays 1 and 2; it shows that only the signals of UE_3 and UE_4 are regenerated as they are connected to the relays.

$$x_{s_{r_1}}(t_{s_2}) = \sqrt{P_4^{t_{s_2}} P_{r_1}}\, x_4(t_{s_1}) \tag{5.17}$$

$$x_{s_{r_2}}(t_{s_2}) = \sqrt{P_3^{t_{s_2}} P_{r_2}}\, x_3(t_{s_1}) \tag{5.18}$$

5.2.2.1. Received Signal

The received signals of UE_3 and UE_4 are given by equations (5.19) and (5.20).

$$y_3(t_{s_2}) = h_3^{r_2} x_{s_{r_2}}(t_{s_2}) + N_3 \tag{5.19}$$

$$y_4(t_{s_2}) = h_4^{r_1} x_{s_{r_1}}(t_{s_2}) + N_4 \tag{5.20}$$

5.2.2.2. SINR

There is no need to perform SIC at UE_3 and UE_4 as the received signal of each user is not superimposed with the signals of the other users; they can directly decode their signals as shown by equations (5.21) and (5.23) from Table 5.5. The minimum SINR for UE_3 and UE_4 can be seen by equations (5.22) and (5.24); it shows the previously decoded signals of UE_3 and UE_4.

Table 5.5: SINR of UE_3 and UE_4 and *UE4* for t_{s_2}

UE	SINR
UE_3	$$SINR_{t_{s_2}}^{3-3} = \frac{P_3^{t_{s_2}} P_{r_2} \left\| h_3^{r_2} \right\|^2}{{\sigma_3}^2} \quad (5.21)$$ Minimum SINR of UE_3 $$a_3^{t_{s_2}} = \min\left(SINR_{t_{s_1}}^{3-1}, SINR_{t_{s_1}}^{3-2}, SINR_{t_{s_1}}^{3-r_2}, SINR_{t_{s_2}}^{3-3} \right) \quad (5.22)$$
UE_4	$$SINR_{t_{s_2}}^{4-4} = \frac{P_4^{t_{s_2}} P_{r_1} \left\| h_4^{r_1} \right\|^2}{{\sigma_4}^2} \quad (5.23)$$ Minimum SINR of UE_4 $$a_4^{t_{s_2}} = \min\left(SINR_{t_{s_1}}^{4-1}, SINR_{t_{s_1}}^{4-2}, SINR_{t_{s_1}}^{4-r_1}, SINR_{t_{s_1}}^{4-r_2}, SINR_{t_{s_2}}^{4-4} \right) \quad (5.24)$$

5.2.2.3. Data Rate and Throughput

The data rate and throughput of UE_1, UE_2, UE_3, and UE_4 in t_{s_1} and t_{s_2} is given in Table 5.6, where n_{rb1} denotes the number of resource blocks assigned of bandwidth *B*, and σ^2 is the AWGN variance. The data rate of UE_2, UE_3, and UE_4 depends on the minimum SINR achieved.

Table 5.6: Data rate and throughput of users in time sub-slot 1 and 2

UE	Data Rate	Throughput
UE_1	$t_{s_1}\log_2\left(1+SINR_{t_{s_1}}^{1-1}\right)$ (5.25)	$Th_1 = n_{rb1}B\log_2\left(1+SINR_{t_{s_1}}^{1-1}\right)$ (5.26)
UE_2	$t_{s_1}\log_2\left(1+a_2^{t_{s_1}}\right)$ (5.27)	$Th_2 = n_{rb2}B\log_2\left(1+a_2^{t_{s_1}}\right)$ (5.28)
UE_3	$t_{s_2}\log_2\left(1+a_3^{t_{s_2}}\right)$ (5.29)	$Th_3 = n_{rb3}B\log_2\left(1+a_3^{t_{s_2}}\right)$ (5.30)
UE_4	$t_{s_2}\log_2\left(1+a_4^{t_{s_2}}\right)$ (5.31)	$Th_4 = n_{rb4}B\log_2\left(1+a_4^{t_{s_2}}\right)$ (5.32)

5.2.3. Time Sub-slot t_{s_3} :

In this time slot, the status of the user's changes according to their locations, as shown in Figure 5.2:

a) UE_1 is a cell centre user
b) UE_2,UE_3, and UE_4 are cell edge users

UE_2 changes its position and uses relay r_2 as an access link to connect with the base station, and UE_3 and UE_4 also change their positions and uses relays r_1 and r_2 as an access link, respectively. Two users are connected to relay r_2 in this time slot, UE_2 and UE_4.UE_1 maintained its position from time sub-slot t_{s_1}, nearest to the base station.

The base station transmits the superimposed signals of UE_1,UE_2,UE_3, and UE_4 to the connected user equipment UE_1, relays r_1 and r_2 given by equation (5.33)

$$x_s(t_{s_3}) = \sqrt{P_1^{t_{s_3}}P_s}\,x_1(t_{s_3}) + \sqrt{P_2^{t_{s_3}}P_s}\,x_2(t_{s_3}) + \sqrt{P_3^{t_{s_3}}P_s}\,x_3(t_{s_3}) + \sqrt{P_4^{t_{s_3}}P_s}\,x_4(t_{s_3}) \quad (5.33)$$

5.2.3.1. Received Signal

The received signals at UE_1, r_1, and r_2 are given by equations (5.34) to (5.36).

$$y_1(t_{s_3}) = h_1^{BS} x_s(t_{s_3}) + N_1 \tag{5.34}$$

$$y_{r_1}(t_{s_3}) = h_{r_1}^{BS} x_s(t_{s_3}) + N_{r_1} \tag{5.35}$$

$$y_{r_2}(t_{s_3}) = h_{r_2}^{BS} x_s(t_{s_3}) + N_{r_2} \tag{5.36}$$

5.2.3.2. SINR

UE_1, r_1, and r_2 must perform SIC on the received superimposed signals to decode the signals of interest. In this time slot, UE_3 has the most power; thus, it is decoded first, followed by UE_4,UE_2, and then UE_1. Table 5.7 and Table 5.8 gives the SINR of UE_1, r_1, and r_2. The order of decoding is as follows:

i. UE_1 first decodes the signals of UE_3,UE_4, and then UE_2. After removing the decoded signals, UE_1 obtains its signal of interest. The decoded SINRs are given by equations (5.37) to (5.40)
ii. Relay r_1 decodes the signal of UE_3 directly with interference from UE_1,UE_2, and UE_4 still present. The decoded SINR is given by equation (5.41).
iii. Relay r_2 decodes the signal of UE_3 and then removes the decoded signal. It then decodes the signal of UE_4 with interference from UE_1 and UE_2 still present. Finally, relay r_2 decodes the signal of UE_2 with interference from UE_1 still present. The decoded SINRs are given by equations (5.42) to (5.44).

Table 5.7: SINR of UE_1 in t_{s_3}

UE_1	
$$SINR_{t_{s3}}^{3-1} = \frac{P_3^{t_{s3}} P_s \left\lvert h_1^{BS} \right\rvert^2}{\sum_{j=1}^{2} P_j^{t_{s3}} P_s \left\lvert h_1^{BS} \right\rvert^2 + P_4^{t_{s3}} P_s \left\lvert h_1^{BS} \right\rvert^2 + {\sigma_1}^2}$$	(5.37)
$$SINR_{t_{s3}}^{4-1} = \frac{P_4^{t_{s3}} P_s \left\lvert h_1^{BS} \right\rvert^2}{\sum_{j=1}^{2} P_j^{t_{s3}} P_s \left\lvert h_1^{BS} \right\rvert^2 + {\sigma_1}^2}$$	(5.38)
$$SINR_{t_{s3}}^{2-1} = \frac{P_2^{t_{s3}} P_s \left\lvert h_1^{BS} \right\rvert^2}{P_1^{t_{s3}} P_s \left\lvert h_1^{BS} \right\rvert^2 + {\sigma_1}^2}$$	(5.39)
$$SINR_{t_{s3}}^{1-1} = \frac{P_1^{t_{s3}} P_s \left\lvert h_1^{BS} \right\rvert^2}{{\sigma_1}^2}$$	(5.40)

Table 5.8: SINR at relays 1 and 2

Relay r_1 and r_2	
$$SINR_{t_{s3}}^{3-r_1} = \frac{P_3^{t_{s3}} P_s \left\lvert h_{r_1}^{BS} \right\rvert^2}{\sum_{j=1}^{2} P_j^{t_{s3}} P_s \left\lvert h_{r_1}^{BS} \right\rvert^2 + P_4^{t_{s3}} P_s \left\lvert h_{r_1}^{BS} \right\rvert^2 + {\sigma_{r_1}}^2}$$	(5.41)
$$SINR_{t_{s3}}^{3-r_2} = \frac{P_3^{t_{s3}} P_s \left\lvert h_{r_2}^{BS} \right\rvert^2}{\sum_{j=1}^{2} P_j^{t_{s3}} P_s \left\lvert h_{r_2}^{BS} \right\rvert^2 + P_4^{t_{s3}} P_s \left\lvert h_{r_2}^{BS} \right\rvert^2 + {\sigma_{r_2}}^2}$$	(5.42)
$$SINR_{t_{s3}}^{4-r_2} = \frac{P_4^{t_{s3}} P_s \left\lvert h_{r_2}^{BS} \right\rvert^2}{\sum_{j=1}^{2} P_j^{t_{s3}} P_s \left\lvert h_{r_2}^{BS} \right\rvert^2 + {\sigma_{r_2}}^2}$$	(5.43)
$$SINR_{t_{s3}}^{2-r_2} = \frac{P_2^{t_{s3}} P_s \left\lvert h_{r_2}^{BS} \right\rvert^2}{P_1^{t_{s3}} P_s \left\lvert h_{r_2}^{BS} \right\rvert^2 + {\sigma_{r_2}}^2}$$	(5.44)

5.2.4. Time sub-slot t_{s_4} :

The relays regenerate the new signals as previously mentioned in time sub-slot t_{s_2}. However, in this time slot, relay r_1 regenerates the signal for UE_3, given by equation (5.45) and relay r_2 regenerates the signals for UE_2 and UE_4 as they are connected to relay r_2, given by equation (5.46).

$$x_{s_{r_1}}(t_{s_4}) = \sqrt{P_3^{t_{s_4}} P_{r_1}}\, x_3(t_{s_3}) \tag{5.45}$$

$$x_{s_{r_2}}(t_{s_4}) = \sqrt{P_2^{t_{s_4}} P_{r_2}}\, x_2(t_{s_3}) + \sqrt{P_4^{t_{s_4}} P_{r_2}}\, x_4(t_{s_3}) \tag{5.46}$$

5.2.4.1. Received Signal

The received signals of users $UE_2, UE_3,$ and UE_4 are given by equations (5.47) to (5.49).

$$y_2(t_{s_4}) = h_2^{r_2} x_{s_{r_2}}(t_{s_4}) + N_2 \tag{5.47}$$

$$y_3(t_{s_4}) = h_3^{r_1} x_{s_{r_1}}(t_{s_4}) + N_3 \tag{5.48}$$

$$y_4(t_{s_4}) = h_4^{r_2} x_{s_{r_2}}(t_{s_4}) + N_4 \tag{5.49}$$

5.2.4.2. SINR

UE_2 must perform SIC on the received superimposed signal and extract its signal of interest after decoding the signal for UE_4. UE_3 and UE_4 can directly decode their signals of interest. However, UE_4 has interference from UE_2, whereas UE_3 has no interfering signals present. The decoded SINR for $UE_2, UE_3,$ and UE_4 can be seen in Table 5.9.

Table 5.9: SINR of UE_2, UE_3, and UE_4

UE	SINR
UE_2	$SINR_{t_{s_4}}^{4-2} = \frac{P_4^{t_{s_4}} P_{r_2} \left\| h_2^{r_2} \right\|^2}{P_2^{t_{s_4}} P_{r_2} \left\| h_2^{r_2} \right\|^2 + {\sigma_2}^2}$ (5.50)
	$SINR_{t_{s_4}}^{2-2} = \frac{P_2^{t_{s_4}} P_{r_2} \left\| h_2^{r_2} \right\|^2}{{\sigma_2}^2}$ (5.51)
	$a_2^{t_{s_4}} = \min\left(SINR_{t_{s_3}}^{2-1}, SINR_{t_{s_3}}^{2-r_2}, SINR_{t_{s_4}}^{2-2} \right)$ (5.52)
UE_3	$SINR_{t_{s_4}}^{3-3} = \frac{P_3^{t_{s_4}} P_{r_1} \left\| h_3^{r_1} \right\|^2}{{\sigma_3}^2}$ (5.53)
	$a_3^{t_{s_4}} = \min\left(SINR_{t_{s_3}}^{3-1}, SINR_{t_{s_3}}^{3-r_1}, SINR_{t_{s_3}}^{3-r_2}, SINR_{t_{s_4}}^{3-3} \right)$ (5.54)
UE_4	$SINR_{t_{s_4}}^{4-4} = \frac{P_4^{t_{s_4}} P_{r_2} \left\| h_4^{r_2} \right\|^2}{P_2^{t_{s_4}} P_{r_2} \left\| h_4^{r_2} \right\|^2 + {\sigma_4}^2}$ (5.55)
	$a_4^{t_{s_4}} = \min\left(SINR_{t_{s_3}}^{4-1}, SINR_{t_{s_3}}^{4-r_2}, SINR_{t_{s_4}}^{4-2}, SINR_{t_{s_4}}^{4-4} \right)$ (5.56)

5.2.4.3. Data Rate and Throughput

The data rate and throughput of UE_1,UE_2,UE_3, and UE_4 in t_{s_3} and t_{s_4} are given in Table 5.10. UE_1 achieves its throughput in t_{s_3} whereas UE_2,UE_3, and UE_4 achieve their throughput in t_{s_4}.

Table 5.10: Data rate and throughput

UE	Data Rate	Throughput
UE_1	$t_{s_3}\log_2\left(1+SINR_{t_{s_3}}^{1-1}\right)$ (5.57)	$Th_1 = n_{rb1}B\log_2\left(1+SINR_{t_{s_3}}^{1-1}\right)$ (5.58)
UE_2	$t_{s_4}\log_2\left(1+a_2^{t_{s_4}}\right)$ (5.59)	$Th_2 = n_{rb2}B\log_2\left(1+a_2^{t_{s_4}}\right)$ (5.60)
UE_3	$t_{s_4}\log_2\left(1+a_3^{t_{s_4}}\right)$ (5.61)	$Th_3 = n_{rb3}B\log_2\left(1+a_3^{t_{s_4}}\right)$ (5.62)
UE_4	$t_{s_4}\log_2\left(1+a_4^{t_{s_4}}\right)$ (5.63)	$Th_4 = n_{rb4}B\log_2\left(1+a_4^{t_{s_4}}\right)$ (5.64)

5.3. Outage Probability

The outage probability (*OP*) is used to define the probability of occurrence of an outage event in the communication system. The outage event is when a UE achieved rates (*R*) are less than the required rates. The outage probability of a cell center user depends upon the direct link between UE and BS, while for a cell edge user, it depends upon both access and relay link.

The expressions for the outage event $\left(OE_{j,t_{s_j}}, j=1,2,...4\right)$ and outage probability $\left(P_{j,t_{s_j}}, j=1,2,...4\right)$ of the users in the various time sub-slots are given in Table 5.11. The outage probability is a combination of the outage events of the user in a specific time sub-slot.

Table 5.11: Outage probability expressions

UE	Sub-Slot	Outage Event	Outage Probability
UE_1	t_{s_1}	$P_r\left[OE_{1,t_{s_1}}\right]$	$P_r\left[OE_{r_{4-1}}^{t_{s1}} \cup OE_{r_{3-1}}^{t_{s1}} \cup OE_{r_{2-1}}^{t_{s1}} \cup OE_{r_{1-1}}^{t_{s1}}\right]$
	t_{s_3}	$P_r\left[OE_{1,t_{s_3}}\right]$	$P_r\left[OE_{r_{3-1}}^{t_{s3}} \cup OE_{r_{4-1}}^{t_{s3}} \cup OE_{r_{2-1}}^{t_{s3}} \cup OE_{r_{1-1}}^{t_{s3}}\right]$
UE_2	t_{s_1}	$P_r\left[OE_{2,t_{s_1}}\right]$	$P_r\left[OE_{r_{4-2}}^{t_{s1}} \cup OE_{r_{3-2}}^{t_{s1}} \cup OE_{r_{2-2}}^{t_{s1}}\right]$
	t_{s_3} and t_{s_4}	$P_r\left[OE_{2,t_{s_4}}\right]$	$P_r\left[OE_{r_{3-r_2}}^{t_{s3}} \cup OE_{r_{4-r_2}}^{t_{s3}} \cup OE_{r_{2-r_2}}^{t_{s3}} \cup OE_{r_{4-2}}^{t_{s4}} \cup OE_{r_{2-2}}^{t_{s4}}\right]$

UE_3	t_{s_1} and t_{s_2}	$P_r\left[OE_{3,t_{s_2}}\right]$	$P_r\left[OE_{r_{4-r_2}}^{t_{s_1}} \cup OE_{r_{3-r_2}}^{t_{s_1}} \cup OE_{r_{3-3}}^{t_{s_2}}\right]$
	t_{s_3} and t_{s_4}	$P_r\left[OE_{3,t_{s_4}}\right]$	$P_r\left[OE_{r_{3-r_1}}^{t_{s_3}} \cup OE_{r_{3-3}}^{t_{s_4}}\right]$
UE_4	t_{s_1} and t_{s_2}	$P_r\left[OE_{4,t_{s_2}}\right]$	$P_r\left[OE_{r_{4-r_1}}^{t_{s_1}} \cup OE_{r_{4-4}}^{t_{s_2}}\right]$
	t_{s_3} and t_{s_4}	$P_r\left[OE_{4,t_{s_4}}\right]$	$P_r\left[OE_{r_{3-r_2}}^{t_{s_3}} \cup OE_{r_{4-r_2}}^{t_{s_3}} \cup OE_{r_{4-4}}^{t_{s_4}}\right]$

The conditions for communication interruption or outage event of the users in the various time sub-slots are given in Table 5.12. An outage event may occur if one or more of the following conditions hold:

i. If a user cannot detect the signals of higher-powered users.
ii. If a relay cannot detect the signals of higher-powered users.
iii. If a relay cannot detect the signals of the users connected to it.
iv. If the user throughput is not able to achieve the target rate

The table reads as follows; for UE_2 in t_{s_3} and t_{s_4}:

i. Relay r_2 cannot detect the signals of UE_2,UE_3, and UE_4 in t_{s_3}
ii. UE_2 cannot detect the signal of UE_4 in t_{s_4}
iii. Throughput is not able to achieve the target rate in t_{s_3}

Table 5.12: Outage event conditions

UE	Time Sub-Slot	User or Relay	Failed Signal Detection	Failed Throughput in time sub-slot
UE_1	t_{s_1}	UE_1	UE_2, UE_3, and UE_4	t_{s_1}
	t_{s_3}			t_{s_3}
UE_2	t_{s_1}	UE_2	UE_3 and UE_4	t_{s_1}
	t_{s_3} and t_{s_4}	r_2	UE_2, UE_3, and UE_4 in t_{s_3}	t_{s_3}
		UE_2	UE_4 in t_{s_4}	
UE_3	t_{s_1} and t_{s_2}	r_2	UE_3 and UE_4 in t_{s_1}	t_{s_2}

	t_{s_3} and t_{s_4}	r_1	UE_3 in t_{s_3}	t_{s_4}
UE_4	t_{s_1} and t_{s_2}	r_1	UE_4 in t_{s_1}	t_{s_2}
	t_{s_3} and t_{s_4}	r_2	UE_3 and UE_4 in t_{s_3}	t_{s_4}

The final outage probability expressions with the implemented outage events for each user in each time sub-slot is given in Table 5.13. The outage probability of each user must fall within the boundary conditions, or else an outage event occurs is guaranteed.

Table 5.13: Outage probability

OP for UE_1 in t_{s_1}
$P_{1,t_{s_1}} = \begin{cases} 1-e^{\frac{-\beta^{t_{s_1}}\sigma^2}{\lambda_1^{BS}P_s}\left[\frac{1}{P_1^{t_{s_1}}}+\frac{1}{P_2^{t_{s_1}}-P_1^{t_{s_1}}\beta^{t_{s_1}}}+\frac{1}{P_3^{t_{s_1}}-\left(\sum_{j=1}^{2}P_j^{t_{s_1}}\right)\beta^{t_{s_1}}}+\frac{1}{P_4^{t_{s_1}}-\left(\sum_{j=1}^{3}P_j^{t_{s_1}}\right)\beta^{t_{s_1}}}\right]}, \\ 0<\beta^{t_{s_1}}<\left\{\frac{P_4^{t_{s_1}}}{\sum_{j=1}^{3}P_j^{t_{s_1}}}\bigcup\frac{P_3^{t_{s_1}}}{\sum_{j=1}^{2}P_j^{t_{s_1}}}\bigcup\frac{P_2^{t_{s_1}}}{P_1^{t_{s_1}}}\right\} \\ 1, \text{else} \end{cases}$ (5.65)
OP for UE_1 in t_{s_3}
$P_{1,t_{s_3}} = \begin{cases} 1-e^{\frac{-\beta^{t_{s_3}}\sigma^2}{\lambda_1^{BS}P_s}\left[\frac{1}{P_1^{t_{s_3}}}+\frac{1}{P_2^{t_{s_3}}-P_1^{t_{s_3}}\beta^{t_{s_3}}}+\frac{1}{P_3^{t_{s_3}}-\left(\sum_{j=1}^{2}P_j^{t_{s_3}}+P_4^{t_{s_3}}\right)\beta^{t_{s_3}}}+\frac{1}{P_4^{t_{s_3}}-\left(\sum_{j=1}^{2}P_j^{t_{s_3}}\right)\beta^{t_{s_3}}}\right]}, \\ 0<\beta^{t_{s_3}}<\left\{\frac{P_4^{t_{s_3}}}{\sum_{j=1}^{2}P_j^{t_{s_3}}}\bigcup\frac{P_3^{t_{s_3}}}{\sum_{j=1}^{2}P_j^{t_{s_3}}+P_4^{t_{s_3}}}\bigcup\frac{P_2^{t_{s_3}}}{P_1^{t_{s_3}}}\right\} \\ 1, \text{else} \end{cases}$ (5.66)
OP for UE_2 in t_{s_1}

$$P_{2,t_{s_1}} = \begin{cases} 1-e^{\frac{-\beta^{t_{s_1}}\sigma^2}{\lambda_2^{BS}P_s}\left[\frac{1}{P_2^{t_{s_1}}-P_1^{t_{s_1}}\beta^{t_{s_1}}}+\frac{1}{P_3^{t_{s_1}}-\left(\sum_{j=1}^{2}P_j^{t_{s_1}}\right)\beta^{t_{s_1}}}+\frac{1}{P_4^{t_{s_1}}-\left(\sum_{j=1}^{3}P_j^{t_{s_1}}\right)\beta^{t_{s_1}}}\right]}, \\ 0<\beta^{t_{s_1}}<\left\{\frac{P_4^{t_{s_1}}}{\sum_{j=1}^{3}P_j^{t_{s_1}}}\bigcup\frac{P_3^{t_{s_1}}}{\sum_{j=1}^{2}P_j^{t_{s_1}}}\bigcup\frac{P_2^{t_{s_1}}}{P_1^{t_{s_1}}}\right\} \\ 1, \text{else} \end{cases} \quad (5.67)$$

OP for UE_2 in t_{s_3} and t_{s_4}

$$P_{2,t_{s_4}} = \begin{cases} 1-e^{-\sigma^2\left[\frac{\beta^{t_{s_4}}}{\lambda_2^{r_2}P_{r_2}}\left(\frac{1}{P_2^{t_{s_4}}}+\frac{1}{\left[P_4^{t_{s_4}}-P_2^{t_{s_4}}\beta^{t_{s_4}}\right]}\right)+\frac{\beta^{t_{s_3}}}{\lambda_{r_2}^{BS}P_s}\left(\frac{1}{\left[P_2^{t_{s_3}}-P_1^{t_{s_3}}\beta^{t_{s_3}}\right]}+\frac{1}{\left[P_4^{t_{s_3}}-\sum_{j=1}^{2}P_j^{t_{s_3}}\beta^{t_{s_3}}\right]}+\frac{1}{\left[P_3^{t_{s_3}}-\left(\sum_{j=1}^{2}P_j^{t_{s_3}}+P_4^{t_{s_3}}\right)\beta^{t_{s_3}}\right]}\right)\right]}, \\ 0<\beta^{t_{s_4}}<\frac{P_4^{t_{s_4}}}{P_2^{t_{s_4}}}\bigcup\beta^{t_{s_3}}<\left\{\frac{P_2^{t_{s_3}}}{P_1^{t_{s_3}}}\bigcup\frac{P_4^{t_{s_3}}}{\sum_{j=1}^{2}P_j^{t_{s_3}}}\bigcup\frac{P_3^{t_{s_3}}}{\sum_{j=1}^{2}P_j^{t_{s_3}}+P_4^{t_{s_3}}}\right\} \\ 1, \text{else} \end{cases} \quad (5.68)$$

OP for UE_3 in t_{s_1} and t_{s_2}

$$P_{3,t_{s_2}} = \begin{cases} 1-e^{-\sigma^2\left[\frac{\beta^{t_{s_2}}}{\lambda_3^{r_2}P_3^{t_{s_2}}P_{r_2}}+\frac{\beta^{t_{s_1}}}{\lambda_{r_2}^{BS}P_s}\left(\frac{1}{\left[P_3^{t_{s_1}}-\left(\sum_{j=1}^{2}P_j^{t_{s_1}}\right)\beta^{t_{s_1}}\right]}+\frac{1}{\left[P_4^{t_{s_1}}-\left(\sum_{j=1}^{3}P_j^{t_{s_1}}\right)\beta^{t_{s_1}}\right]}\right)\right]}, \\ 0<\beta^{t_{s_2}}\bigcup\beta^{t_{s_1}}<\left(\frac{P_3^{t_{s_1}}}{\sum_{j=1}^{2}P_j^{t_{s_1}}}\bigcup\frac{P_4^{t_{s_1}}}{\sum_{j=1}^{3}P_j^{t_{s_1}}}\right) \\ 1, \text{else} \end{cases} \quad (5.69)$$

OP for UE_3 in t_{s_3} and t_{s_4}

$$P_{3,t_{s_4}} = \begin{cases} 1-e^{-\sigma^2\left[\frac{\beta^{t_{s_4}}}{\lambda_3^{r_1}P_3^{t_{s_4}}P_{r_1}}+\frac{\beta^{t_{s_3}}}{\lambda_{r_1}^{BS}P_s}\left(\frac{1}{\left[P_3^{t_{s_3}}-\left(\sum_{j=1}^{2}P_j^{t_{s_3}}+P_4^{t_{s_3}}\right)\beta^{t_{s_3}}\right]}\right)\right]}, \\ 0<\beta^{t_{s_4}}\bigcup\beta^{t_{s_3}}<\frac{P_3^{t_{s_3}}}{\sum_{j=1}^{2}P_j^{t_{s_3}}+P_4^{t_{s_3}}} \\ 1, \text{else} \end{cases} \quad (5.70)$$

OP for UE_4 in t_{s_1} and t_{s_2}

$$P_{4,t_{s_2}} = \begin{cases} 1-e^{-\sigma^2\left[\frac{\beta^{t_{s2}}}{\lambda_4^{r_1} P_4^{t_{s2}} P_{r_1}} + \frac{\beta^{t_{s1}}}{\lambda_{r_1}^{BS} P_s}\left(\frac{1}{\left[P_4^{t_{s1}} - \left(\sum_{j=1}^{3} P_j^{t_{s1}}\right)\beta^{t_{s1}}\right]}\right)\right]}, \\ 0 < \beta^{t_{s2}} \bigcup \beta^{t_{s1}} < \dfrac{P_4^{t_{s1}}}{\sum_{j=1}^{3} P_j^{t_{s1}}} \\ 1, \text{else} \end{cases} \tag{5.71}$$

OP for UE_4 in t_{s_3} and t_{s_4}

$$P_{4,t_{s_4}} = \begin{cases} 1-e^{-\sigma^2\left[\frac{\beta^{t_{s4}}}{\lambda_4^{r_2} P_{r_2}\left[P_4^{t_{s4}} - P_2^{t_{s4}}\beta^{t_{s4}}\right]} + \frac{\beta^{t_{s3}}}{\lambda_{r_2}^{BS} P_s}\left(\frac{1}{\left[P_4^{t_{s3}} - \left(\sum_{j=1}^{2} P_j^{t_{s3}}\right)\beta^{t_{s3}}\right]} + \frac{1}{\left[P_3^{t_{s3}} - \left(\sum_{j=1}^{2} P_j^{t_{s3}} + P_4^{t_{s3}}\right)\beta^{t_{s3}}\right]}\right)\right]}, \\ 0 < \beta^{t_{s4}} < \dfrac{P_4^{t_{s4}}}{P_2^{t_{s4}}} \bigcup \beta^{t_{s3}} < \left\{\dfrac{P_4^{t_{s3}}}{\sum_{j=1}^{2} P_j^{t_{s3}}} \bigcup \dfrac{P_3^{t_{s3}}}{\sum_{j=1}^{2} P_j^{t_{s3}} + P_4^{t_{s3}}}\right\} \\ 1, \text{else} \end{cases} \tag{5.72}$$

The total system outage event is the condition when no user can achieve detection; the total outage probability is given by equation (5.73)

$$P_T = 1 - \prod_{n=1}^{4}\left(1 - P_{n,t_{s_1}}\right)\prod_{n=1}^{4}\left(1 - P_{n,t_{s_3}}\right) \tag{5.73}$$

Error! Reference source not found. gives the outage probability derivations of all the UEs.

5.4. Ergodic Rate

The ergodic rate of the UE in the sub-slot *t* is given by

$$E_{UE}^{t} = \frac{t}{\log_2}\int_0^{\infty} \log(1+y)\, f_Y(y)\, dy = \frac{t}{\log_2}\int_0^{\infty} \frac{1-F_Y(y)}{(1+y)}\, dy \tag{5.74}$$

Where $f_Y(y)$ and $F_Y(y)$ denotes the probability density function (PDF) and cumulative distribution function (CDF) and *y* denotes the SINR of the UE.

The ergodic rate of UE_1 in time sub-slot t_{s_1}, it is assumed that UE_1 successfully decoded the signals of UE_2, UE_3, and UE_4 thus, using equation (5.74) the $E_1^{t_{s1}}$ is given by equation (5.75)

$$E_1^{t_{s1}} = \frac{t}{\log_2}\int_0^{\infty} \frac{1-F_{SINR_{t_{s_1}}^{1-1}}(y)}{(1+y)}\, dy \tag{5.75}$$

The SINR is denoted by *y*, where $F_{SINR_{t_{s_1}}^{1-1}}$ denotes the CDF of $SINR_{t_{s_1}}^{1-1}$ as seen by equation (5.76)

$$F_{SINR_{t_{s_1}}^{1-1}}(y) = P\left(\frac{P_1^{t_{s1}} P_s \left|h_1^{BS}\right|^2}{\sigma^2} \le y\right) = P\left(\left|h_1^{BS}\right|^2 \le \frac{y\sigma^2}{P_1^{t_{s1}} P_s}\right) \tag{5.76}$$

The channel is a complex Gaussian distribution and $\left|h_1^{BS}\right|^2$ is exponentially distributed with $1/\lambda_1^{BS}$ thus, the CDF is given by equation (5.77)

$$F_{SINR_{t_{s_1}}^{1-1}}(y) = 1 - e^{\frac{-y\sigma^2}{P_1^{t_{s1}} P_s \lambda_1^{BS}}} \tag{5.77}$$

Finally, the ergodic rate of UE_1 in time sub-slot t_{s_1} is given by equation (5.78), where $Ei(x) = \int_{-\infty}^{x} \frac{e^t}{t}\, dt$

$$E_1^{t_{s1}} = -\frac{t_{s_1}}{\log_2} Ei\left(\frac{-1}{P_1^{t_{s1}} P_s \lambda_1^{BS}}\right) e^{\frac{1}{P_1^{t_{s1}} P_s \lambda_1^{BS}}} \tag{5.78}$$

Table 5.14 gives the ergodic rates for UE_1, UE_2, UE_3, and UE_4 in the time sub-slots. The detailed derivations of the ergodic rates for all the users can be found in **Error! Reference source not found.**

$$E_1^{t_{s_1}} = -\frac{t_{s_1}}{\log_2} Ei\left(\frac{-1}{P_1^{t_{s_1}} P_s \lambda_1^{BS}}\right) e^{\frac{1}{P_1^{t_{s_1}} P_s \lambda_1^{BS}}} \tag{5.79}$$

Table 5.14: Ergodic rates

UE	Time Sub-Slot	Ergodic Rate
UE_1	t_{s_1}	$E_1^{t_{s_1}} = -\frac{t_{s_1}}{\log_2} Ei\left(\frac{-1}{P_1^{t_{s_1}} P_s \lambda_1^{BS}}\right) e^{\frac{1}{P_1^{t_{s_1}} P_s \lambda_1^{BS}}}$ (5.80)
	t_{s_3}	$E_1^{t_{s_3}} = -\frac{t_{s_3}}{\log_2} Ei\left(\frac{-1}{P_1^{t_{s_3}} P_s \lambda_1^{BS}}\right) e^{\frac{1}{P_1^{t_{s_3}} P_s \lambda_1^{BS}}}$ (5.81)
UE_2	t_{s_1}	$E_2^{t_{s_1}} = -\frac{t_{s_1}}{\log_2} Ei\left(-\frac{1}{P_s}\left(\frac{1}{\lambda_1^{BS}} + \frac{1}{\lambda_2^{BS}}\right)\right) e^{\frac{1}{P_s}\left(\frac{1}{\lambda_1^{BS}} + \frac{1}{\lambda_2^{BS}}\right)}$ (5.82)
	$t_{s_{3-4}}$	$E_2^{t_{s_{3-4}}} = \frac{t_{s_3}}{\log_2}\left[Ei(a) - Ei(ab+a)\right]e^a$ (5.83) $a = \sigma^2\left(\frac{1}{P_s\lambda_1^{BS}} + \frac{1}{P_s\lambda_{r_2}^{BS}} + \frac{1}{P_2^{t_{s_4}} P_{r_2}\lambda_2^{r_2}}\right), b = \frac{P_2^{t_{s_3}}}{P_1^{t_{s_3}}}$
UE_3	$t_{s_{1-2}}$	$E_3^{t_{s_{1-2}}} = \frac{t_{s_1}}{\log_2}\left[Ei(a) - Ei(ab+a)\right]e^a$ (5.84) $a = \sigma^2\left(\frac{1}{P_s\lambda_1^{BS}} + \frac{1}{P_s\lambda_2^{BS}} + \frac{1}{P_s\lambda_{r_2}^{BS}} + \frac{1}{P_3^{t_{s_2}} P_{r_2}\lambda_3^{r_2}}\right), b = \frac{P_3^{t_{s_1}}}{\sum_{j=1}^{2} P_j^{t_{s_1}}}$
	$t_{s_{3-4}}$	$E_3^{t_{s_{3-4}}} = \frac{t_{s_3}}{\log_2}\left[Ei(a) - Ei(ab+a)\right]e^a$ … (5.85)

		$a = \sigma^2 \left(\frac{1}{P_s \lambda_1^{BS}} + \frac{1}{P_s \lambda_{r_2}^{BS}} + \frac{1}{P_s \lambda_{r_1}^{BS}} + \frac{1}{P_3^{t_{s_4}} P_{r_1} \lambda_3^{r_1}} \right)$ $b = \frac{P_3^{t_{s_3}}}{\sum_{j=1}^{2} P_j^{t_{s_3}} + P_4^{t_{s_3}}}$
UE_4	$t_{s_{1-2}}$	$E_4^{t_{s_{1-2}}} = \frac{t_{s_1}}{\log_2} [Ei(a) - Ei(ab+a)] e^a$ (5.86) $a = \sigma^2 \left(\frac{1}{P_s \lambda_1^{BS}} + \frac{1}{P_s \lambda_2^{BS}} + \frac{1}{P_s \lambda_{r_1}^{BS}} + \frac{1}{P_s \lambda_{r_2}^{BS}} + \frac{1}{P_4^{t_{s_2}} P_{r_1} \lambda_4^{r_1}} \right)$ $b = \frac{P_4^{t_{s_1}}}{\sum_{j=1}^{3} P_j^{t_{s_1}}}$
	$t_{s_{3-4}}$	$E_4^{t_{s_{3-4}}} = \frac{t_{s_3}}{\log_2} [Ei(ab+a) - Ei(ac+a)] e^a$ (5.87) $a = \sigma^2 \left(\frac{1}{P_s \lambda_1^{BS}} + \frac{1}{P_s \lambda_{r_2}^{BS}} + \frac{1}{P_{r_2} \lambda_2^{r_2}} + \frac{1}{P_{r_2} \lambda_4^{r_2}} \right)$ $b = \frac{P_4^{t_{s_3}}}{\sum_{j=1}^{2} P_j^{t_{s_3}}}, c = \frac{P_4^{t_{s_4}}}{P_2^{t_{s_4}}}$

$$E = E_1^{t_{s_{1-2}}} + E_1^{t_{s_{3-4}}} + E_2^{t_{s_{1-2}}} + E_2^{t_{s_{3-4}}} + E_3^{t_{s_{1-2}}} + E_3^{t_{s_{3-4}}} + E_4^{t_{s_{1-2}}} + E_4^{t_{s_{3-4}}} \quad (5.88)$$

5.5. Algorithm

Using the equation below, the power coefficient matrix denoted by pc_m is generated

$$\begin{bmatrix} P_1^{t_{s1}} + P_2^{t_{s1}} + P_3^{t_{s1}} + P_4^{t_{s1}} = 1 \\ P_3^{t_{s2}} + P_4^{t_{s2}} = 1 \\ P_1^{t_{s3}} + P_2^{t_{s3}} + P_3^{t_{s3}} + P_4^{t_{s3}} = 1 \\ P_2^{t_{s4}} + P_3^{t_{s4}} + P_4^{t_{s4}} = 1 \end{bmatrix} \tag{5.89}$$

1. Initialise the number of users n and time sub-slots k. The power matrix $p\_m = zeros(n,k)$. The $pc\_m = zeros(n,k)$ and time matrix $t\_m = zeros(n,1)$
2. Find the number of cell center users (n_c) and cell edge users (n_e)
3. Calculate $P_{n,t_{s_k}}$
4. For $j = 1:n$
5. If $FI > FI_F$
6. If $(n_c > n_e)$
7. $FI = FI - a, 0.5 \le a \le FI$
8. Else $n_c \ll n_e$
9. $p\_m(j,:) = pc\_m(j,:), t\_m(j,:) = t_{s_j}$
10. End
11. Else $FI < FI_F$
12. If $n_c < n_e$
13. $FI = FI + (FI - FI_F) = 2FI - FI_F$
14. $p\_m(j,:) = pc\_m(j,:), t\_m(j,:) = t_{s_j}$
15. End
16. End
17. Allocation Matrix $= [t\_m \quad p\_m]$

The algorithm checks the number of cell center users and cell-edge users. When cell center users are more, the fairness index must be less than 0.5.

5.6. Simulation Results

The simulation model is shown in Figure 5.1 and Figure 5.2; the model has one BS, three relays $(r_1, r_2, \text{and } r_3)$, and four users $(UE_1, UE_2, UE_3, \text{and } UE_4)$. The relay works in half-duplex mode. For t_{s_1} and t_{s_2} time sub-slots UE_1 and UE_2 are cell center users while UE_3 and UE_4 are cell edge users using relays r_2 and r_1. For t_{s_3} and t_{s_4} time sub-slots UE_1 is a cell center user while $UE_2, UE_3,$ and UE_4 are cell edge users. The UE_2 and UE_4 are connected to relay r_2 and UE_3 is connected to relay r_1. The system parameters are given in Table 5.15.

Table 5.15: System parameters

Base station power	$P_s = 25 \sim 50$ dB
Relay r_2 power	$P_{r_2} = 12.5 \sim 25$ dB
Relay r_1 power	$P_{r_1} = 0.3P_s$
'Channel variances (Figure 5.1)'	$\lambda_1^{BS} = 1^{-4}, \lambda_2^{BS} = 0.8^{-4}, \lambda_{r_1}^{BS} = 0.4^{-4},$ $\lambda_{r_2}^{BS} = 0.5^{-4}, \lambda_3^{r_2} = 0.3^{-4}, \lambda_4^{r_1} = 0.3^{-4}$
'Channel variances (Figure 5.2)'	$\lambda_1^{BS} = 1^{-4}, \lambda_{r_1}^{BS} = 0.4^{-4}, \lambda_{r_2}^{BS} = 0.5^{-4},$ $\lambda_2^{r_2} = 0.3^{-4}, \lambda_3^{r_1} = 0.3^{-4}, \lambda_4^{r_2} = 0.4^{-4}$
Target rate	$R = 0.3$ bps/Hz
Fairness index factor	$FI_F = 0.5$

The power allocation algorithm is adapted from (Fang, Zhang, Cheng, Roy, et al., 2017). The user's theoretical and simulated rates are compared in Figure 5.3 for $FI_F = 0.5$; the theoretical and simulated values of rates are closer to each other. An increase in the transmission power of each user increases the corresponding rates. The rates of user UE_1 increases in all the time sub-slots as it is always a cell centre user.

In sub-slots t_{s_3} and t_{s_4}, the situation for UE_2 changes as it is a cell-edge user now, resulting in a slower growth rate in these time slots. For UE_3 and UE_4, the rate growth is slow in sub-slots as they are always cell edge users.

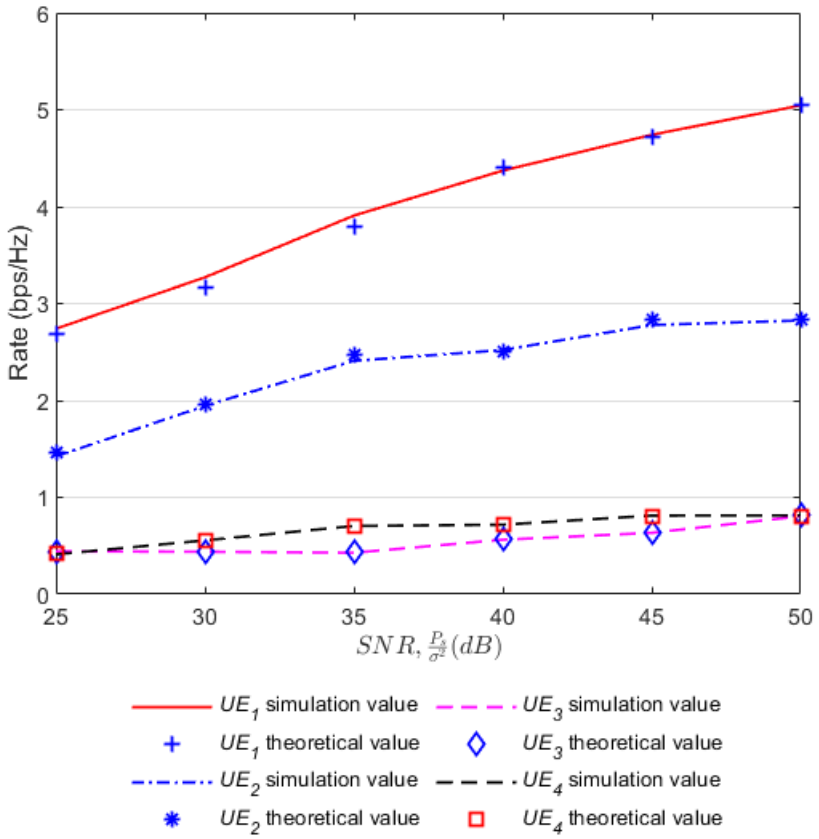

Figure 5.3: Users theoretical and simulated results

The user's outage probability and transmission power are compared in Figure 5.4. Different transmission power requires different power allocation adopted from (Fang, Zhang, Cheng, Roy, et al., 2017). The plot of outage probability with transmission power is non-linear for fairness $FI_F = 0.5$.

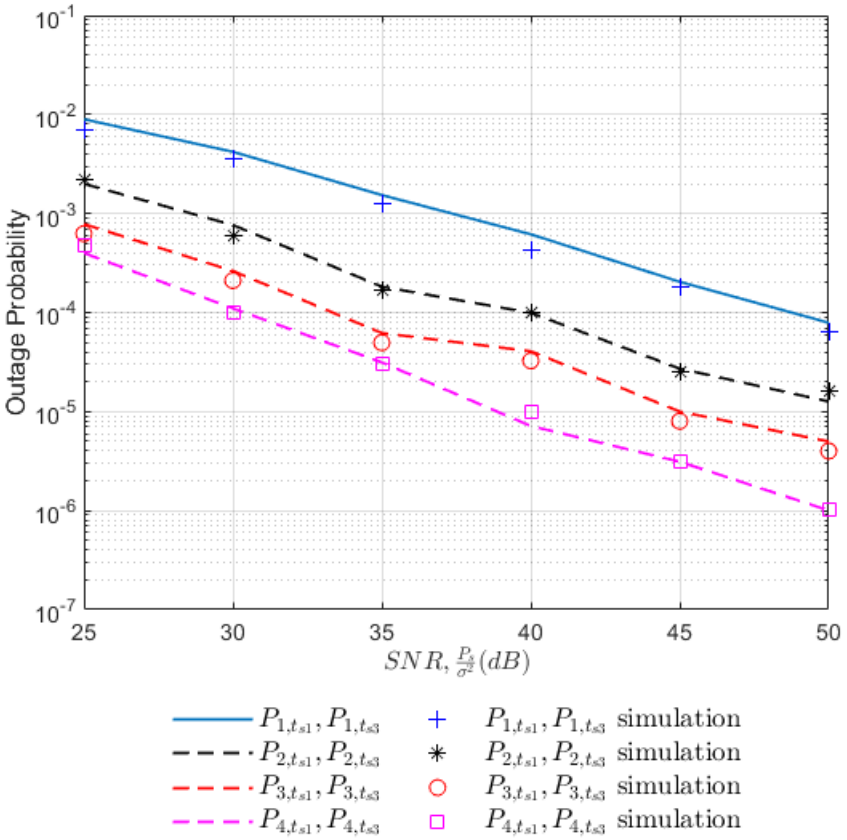

Figure 5.4: User's outage probability and transmission power

The outage probability of the system is compared with the equal-time transmission approach in Figure 5.5. When transmission power is lower, the outage probability of the proposed system is low, while the performance of the two systems is closer when the transmission power is high.

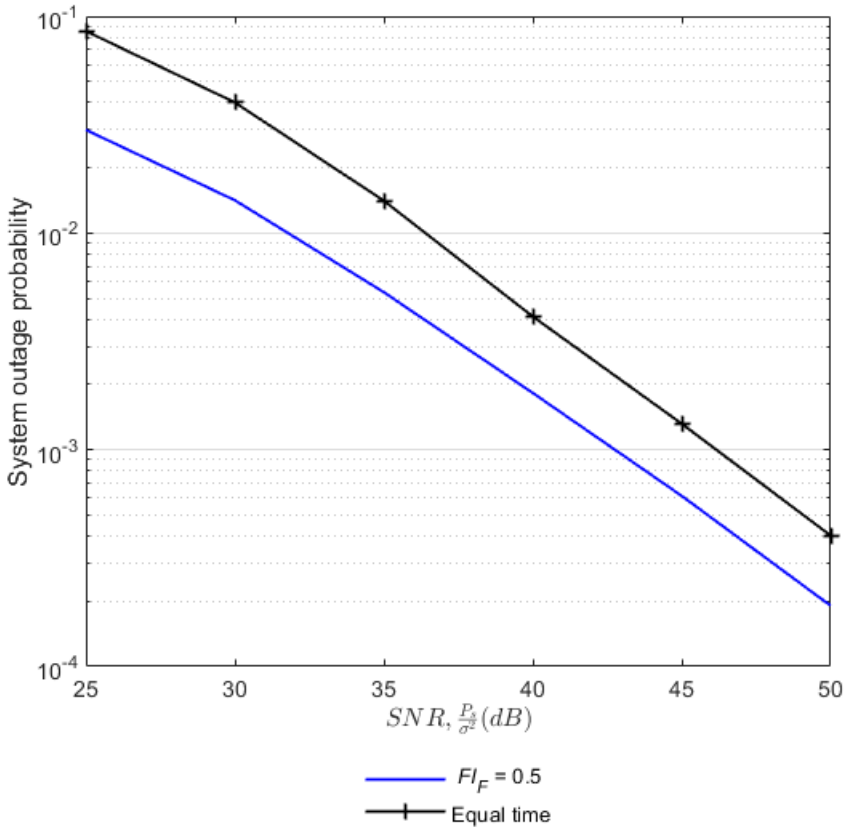

Figure 5.5: Outage probability of the system

The user rates of the system are compared with the variation in the fairness index in Figure 5.6 with a maximum transmission power of all devices. The rates of cell center users decrease with the increase in the fairness index while the rates of cell edge users increase. For UE_1 rate decreases with an increase in FI. For UE_2 in the first two sub-slots, the rate decreases and increases in the last two sub-slots. The system also decreases at a lesser rate in the last two sub-slots.

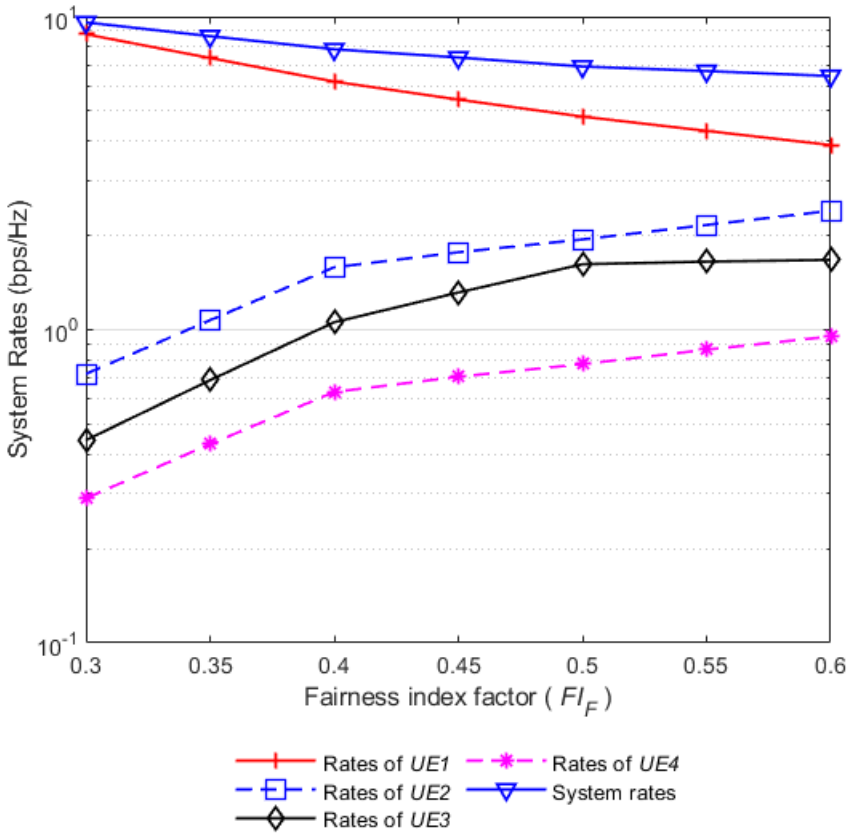

Figure 5.6: User rate and fairness index

5.7. Summary

This chapter explores the core of the research by implementing a power allocation scheme into a four-user NOMA based MIMO system. The system utilises relays to aid downlink communication between the base station and users, where a connection with a relay depends on the channel conditions between a user and the base station. The system model explores four time slots and derives each user's SINR, outage probability, and ergodic rate, along with a power allocation algorithm focusing on user fairness. Simulation results reveal the performance of the power allocation algorithm in terms of outage probability and system rates.

Chapter 6

ENERGY HARVESTING

6.1. Introduction

Energy harvesting in wireless communication networks has garnered much attention recently; it is a proposed solution to self-sustaining and lifetime extension of wireless networks. It is argued that battery replacement and charging can be done; however, it can be costly and inconvenient, especially if the location of the batteries is not ideal. There are environmental energy harvesting techniques such as wind, solar, and vibration; however, radio frequency (RF) wireless energy transfer (WET) is a more controlled, convenient, and safer way to harvest energy from the environment. RF signals contain information and energy; thus, an energy harvesting node can simultaneously harvest and process information. A relay in a cooperative wireless network needs to have sufficient energy to stay active; therefore, a relay node with energy harvesting capabilities is an excellent advantage in a wireless network (Shi et al., 2017; Nasir et al., 2013). This chapter is an adaptation of the paper published by (Balyan & Daniels, 2020), which utilises the exact system model, however, with the added implementation of energy harvesting relays.

6.2. Relaying Protocols

There are two main relaying protocols in energy harvesting: time-switching relaying (TSR) and power splitting relaying (PSR) protocols.

6.2.1. Time-Switching Relaying

In the TSR protocol, the relay utilises the first time slot to harvest energy from the signal and then utilises the remaining time to process the information, as seen in Figure 6.1. The relay expends all the harvested energy to forward the signal to its destination.

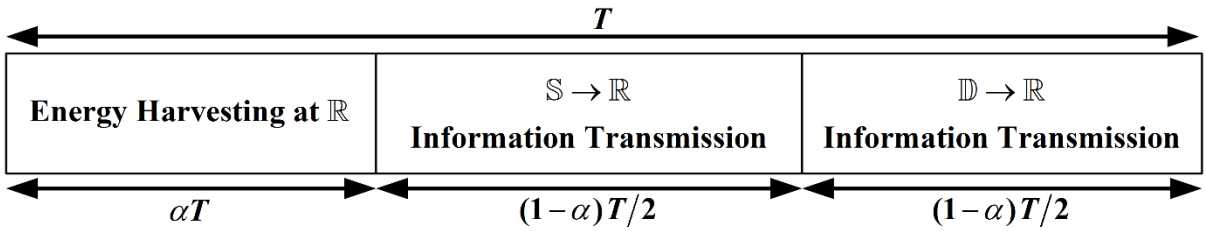

Figure 6.1: TSR protocol

In the TSR diagram, the denotations are as follows:

- $\mathbb{S}$ - the source node
- $\mathbb{R}$ - the relay node
- $\mathbb{D}$ - the destination node
- T - the block time in which information transmission from source to destination node occurs
- α - the fraction of block time in which the energy harvesting occurs
- $(1-\alpha)T/2$ - the remaining block time for information transmission

6.2.2. Power-Splitting Relaying

In the PSR protocol, the relay harvests a portion of the received signal's power, and the remainder of the power is used to process the information, as seen in Figure 6.2.

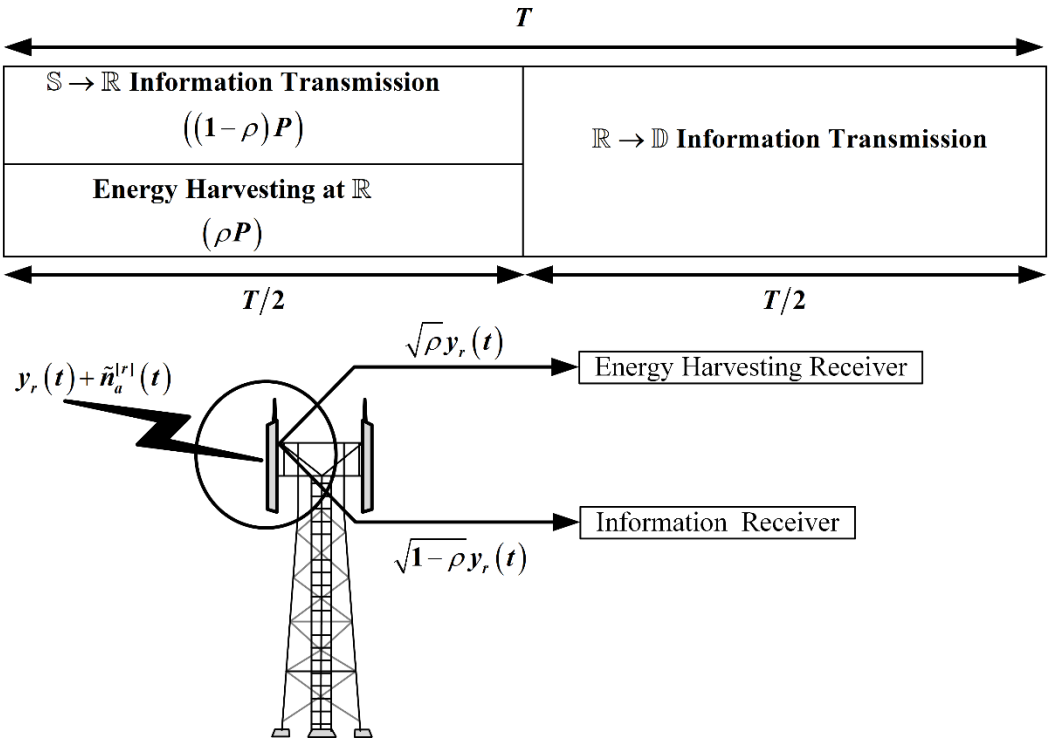

Figure 6.2: PSR protocol

In the PSR diagram, the denotations are as follows:

- $\mathbb{S}$ - the source node
- $\mathbb{R}$ - the relay node
- $\mathbb{D}$ - the destination node
- P - the received signal's power
- T - the total block-time
- ρ - the power splitting coefficient
- $(1-\rho)P$ - remainder of signal's power

In the first block of time, the relay harvests a fraction of the received signal's power ρP, with the remainder of the power $(1-\rho)P$ used for information transmission in the second block time. Also, the relay expends all the harvested energy in information forwarding. The value of the power splitting coefficient affects the system throughput with a value between 0 and 1.

6.3. System Model

An investigation into energy harvesting nodes further improves the MIMO system's energy efficiency, thus reducing power consumption. Research shows the benefits of energy harvesting, specifically in cooperative networks (Du et al., 2015). Thus, this system model is that of Chapter 5; however, these relays employ energy harvesting capabilities. The relays utilise the PSR protocol to harvest energy and amplify-and-forward (AF) protocol to forward the signals to the connected UEs. This system focuses on the broadcast MIMO channel explored in section 5.2.

6.3.1. Time Sub-slot t_{s_1} :

In this time sub-slot, the UE connections remain the same as section 5.2.1, with the following connections:

a) UE_1 and UE_2 are cell center users connected directly to the base station
b) UE_3 and UE_4 are cell edge users connected to relay r_2 and r_1, respectively.

As stated before in section 5.2.1:

i. The base station transmits the superimposed signal to the connected UEs given by equation (5.1).
ii. The received signals at $UE_1, UE_2, r_1,$ and r_2 are given by equations (5.2) to (5.5)
iii. The decoded SINRs at UE_1 are given by equations (5.6) to (5.9).
iv. The decoded SINRs at UE_2 are given by equations (5.10) to (5.12).
v. The energy harvesting does not affect UE_1 and UE_2, as it is not connected to a relay.

The PSR splits the received superimposed signal by a portion $\sqrt{\rho}y_{r_i}\left(t_{s_1}\right)$ utilised by the energy harvesting receiver, given by equations (6.1) and (6.2). With the remaining power of the received signal $\sqrt{(1-\rho)}y_{r_i}\left(t_{s_1}\right)$ utilised by the information receiver, given by equations (6.3) and (6.4).

$$\sqrt{\rho}y_{r_1}\left(t_{s_1}\right)=\sqrt{\rho P_1^{t_{s_1}}P_s}x_1\left(t_{s_1}\right)h_{r_1}^{BS}+\sqrt{\rho P_2^{t_{s_1}}P_s}x_2\left(t_{s_1}\right)h_{r_1}^{BS}+\sqrt{\rho P_3^{t_{s_1}}P_s}x_3\left(t_{s_1}\right)h_{r_1}^{BS}+\sqrt{\rho P_4^{t_{s_1}}P_s}x_4\left(t_{s_1}\right)h_{r_1}^{BS}+\sqrt{\rho}N_{r_1} \quad (6.1)$$

$$\sqrt{\rho}y_{r_2}\left(t_{s_1}\right)=\sqrt{\rho P_1^{t_{s_1}}P_s}x_1\left(t_{s_1}\right)h_{r_2}^{BS}+\sqrt{\rho P_2^{t_{s_1}}P_s}x_2\left(t_{s_1}\right)h_{r_2}^{BS}+\sqrt{\rho P_3^{t_{s_1}}P_s}x_3\left(t_{s_1}\right)h_{r_2}^{BS}+\sqrt{\rho P_4^{t_{s_1}}P_s}x_4\left(t_{s_1}\right)h_{r_2}^{BS}+\sqrt{\rho}N_{r_2} \quad (6.2)$$

$$\sqrt{(1-\rho)}y_{r_1}\left(t_{s_1}\right)=\sqrt{(1-\rho)P_1^{t_{s_1}}P_s}x_1\left(t_{s_1}\right)h_{r_1}^{BS}+\sqrt{(1-\rho)P_2^{t_{s_1}}P_s}x_2\left(t_{s_1}\right)h_{r_1}^{BS}+\sqrt{(1-\rho)P_3^{t_{s_1}}P_s}x_3\left(t_{s_1}\right)h_{r_1}^{BS}+\sqrt{(1-\rho)P_4^{t_{s_1}}P_s}x_4\left(t_{s_1}\right)h_{r_1}^{BS}+\sqrt{(1-\rho)}N_{r_1} \quad (6.3)$$

$$\sqrt{(1-\rho)}y_{r_2}\left(t_{s_1}\right)=\sqrt{(1-\rho)P_1^{t_{s_1}}P_s}x_1\left(t_{s_1}\right)h_{r_2}^{BS}+\sqrt{(1-\rho)P_2^{t_{s_1}}P_s}x_2\left(t_{s_1}\right)h_{r_2}^{BS}+\sqrt{(1-\rho)P_3^{t_{s_1}}P_s}x_3\left(t_{s_1}\right)h_{r_2}^{BS}+\sqrt{(1-\rho)P_4^{t_{s_1}}P_s}x_4\left(t_{s_1}\right)h_{r_2}^{BS}+\sqrt{(1-\rho)}N_{r_2} \quad (6.4)$$

Table 6.1 gives the decoded SINR at relays r_1 and r_2, respectively.

Table 6.1:SINR at relays

Relay r_1 and r_2	
$SINR_{t_{s_1}}^{4-r_1}=\frac{(1-\rho)P_4^{t_{s_1}}P_s\left\|h_{r_1}^{BS}\right\|^2}{\sum_{j=1}^{3}(1-\rho)P_j^{t_{s_1}}P_s\left\|h_{r_1}^{BS}\right\|^2+(1-\rho)\sigma_{r_1}^2}$	(6.5)
$SINR_{t_{s_1}}^{4-r_2}=\frac{(1-\rho)P_4^{t_{s_1}}P_s\left\|h_{r_2}^{BS}\right\|^2}{\sum_{j=1}^{3}(1-\rho)P_j^{t_{s_1}}P_s\left\|h_{r_2}^{BS}\right\|^2+(1-\rho)\sigma_{r_2}^2}$	(6.6)

$$SINR_{t_{s1}}^{3-r_2} = \frac{(1-\rho) P_3^{t_{s1}} P_s \left| h_{r_2}^{BS} \right|^2}{\sum_{j=1}^{2} (1-\rho) P_j^{t_{s1}} P_s \left| h_{r_2}^{BS} \right|^2 + (1-\rho)\sigma_{r_2}^2} \quad (6.7)$$

In the first block-time, the energy harvesting receiver at r_1 and r_2 harvests the energy from the received signal given by equations (6.8) and (6.11). The energy conversion efficiency is η with values between $0 < \eta < 1$. The harvested energy is used to power the relays; thus, the relay power is given by equations (6.9) and (6.12). Table 6.2 shows all the harvesting-related equations.

Table 6.2: Harvesting at relay 1 and 2

r_1	r_2
$EH_{r_1} = \eta\rho P_s \left\| h_{r_1}^{BS} \right\|^2 T/2$ (6.8)	$EH_{r_2} = \eta\rho P_s \left\| h_{r_2}^{BS} \right\|^2 T/2$ (6.11)
$P_{r_1} = \frac{EH_{r_1}}{T/2} = \eta\rho P_s \left\| h_{r_1}^{BS} \right\|^2$ (6.9)	$P_{r_2} = \frac{EH_{r_2}}{T/2} = \eta\rho P_s \left\| h_{r_2}^{BS} \right\|^2$ (6.12)
$G_{r_1} = \frac{1}{(1-\rho) P_s \left\| h_{r_1}^{BS} \right\|^2 + \sigma_{R_1}^2}$ (6.10)	$G_{r_2} = \frac{1}{(1-\rho) P_s \left\| h_{r_2}^{BS} \right\|^2 + \sigma_{R_2}^2}$ (6.13)

6.3.2. Time Sub-slot t_{s_2}:

In the second block-time, the AF protocol utilises an amplifying factor G_{r_i} given by equations (6.10) and (6.13). The relays regenerate the signals for the users connected to it with the amplification given by equations (6.14) and (6.15).

$$x_{s_{r_1}}(t_{s_2}) = \sqrt{(1-\rho) P_4^{t_{s2}} G_{r_1} P_s P_{r_1}}\, x_4(t_{s_1}) h_{r_1}^{BS} \quad (6.14)$$

$$x_{s_{r_2}}(t_{s_2}) = \sqrt{(1-\rho) P_3^{t_{s2}} G_{r_2} P_s P_{r_2}}\, x_3(t_{s_1}) h_{r_2}^{BS} \quad (6.15)$$

The received signals of UE_3 and UE_4 are the same as section 5.2.2.1 given by equations (5.19) and (5.20). Combining the equations in Table 6.2, the decoded SINR at UE_3 and UE_4 are shown in Table 6.3.

Table 6.3: SINR at UE_3 and UE_4

UE	SINR
UE_3	$SINR_{t_{s_2}}^{3-3} = \frac{(1-\rho)\eta\rho P_3^{t_{s_2}} P_s^2 \left(\left\|h_{r_2}^{BS}\right\|^2\right)^2 \left\|h_3^{r_2}\right\|^2}{(1-\rho) P_s \left\|h_{r_2}^{BS}\right\|^2 \sigma_3^2 + \sigma_{R_2}^2 \sigma_3^2}$ (6.16)
UE_4	$SINR_{t_{s_2}}^{4-4} = \frac{(1-\rho)\eta\rho P_4^{t_{s_2}} P_s^2 \left(\left\|h_{r_1}^{BS}\right\|^2\right)^2 \left\|h_4^{r_1}\right\|^2}{(1-\rho) P_s \left\|h_{r_1}^{BS}\right\|^2 \sigma_4^2 + \sigma_{R_1}^2 \sigma_4^2}$ (6.17)

6.3.3. Time Sub-slot t_{s_3} :

In this time sub-slot, the UE connections remain the same as section 5.2.3, with the following connections:

a) UE_1 is a cell center user connected directly to the base station.
b) UE_2, UE_3, and UE_4 are cell edge users with UE_3 connected to r_1, and UE_2 and UE_4 connected to r_2.

As stated before in section 5.2.3:

i. The base station transmits the superimposed signal to the connected UEs given by equation (5.33).
ii. The received signals at $UE_1, r_1,$ and r_2 are given by equations (5.34) to (5.36).
iii. The decoded SINRs at UE_1 are given by equations (5.37) to (5.40).

As previously stated in section 6.3.1, the PSR protocol splits the received signal by $\rho:(1-\rho)$, resulting in equations (6.18) to (6.21).

$$\sqrt{\rho}y_{r_1}\left(t_{s_3}\right)=\sqrt{\rho P_1^{t_{s_3}}P_s}x_1\left(t_{s_3}\right)h_{r_1}^{BS}+\sqrt{\rho P_2^{t_{s_3}}P_s}x_2\left(t_{s_3}\right)h_{r_1}^{BS}$$
$$+\sqrt{\rho P_3^{t_{s_3}}P_s}x_3\left(t_{s_3}\right)h_{r_1}^{BS}+\sqrt{\rho P_4^{t_{s_3}}P_s}x_4\left(t_{s_3}\right)h_{r_1}^{BS} \quad (6.18)$$
$$+\sqrt{\rho}N_{r_1}$$

$$\sqrt{\rho}y_{r_2}\left(t_{s_3}\right)=\sqrt{\rho P_1^{t_{s_3}}P_s}x_1\left(t_{s_3}\right)h_{r_2}^{BS}+\sqrt{\rho P_2^{t_{s_3}}P_s}x_2\left(t_{s_3}\right)h_{r_2}^{BS}$$
$$+\sqrt{\rho P_3^{t_{s_3}}P_s}x_3\left(t_{s_3}\right)h_{r_2}^{BS}+\sqrt{\rho P_4^{t_{s_3}}P_s}x_4\left(t_{s_3}\right)h_{r_2}^{BS} \quad (6.19)$$
$$+\sqrt{\rho}N_{r_2}$$

$$\sqrt{(1-\rho)}y_{r_1}\left(t_{s_3}\right)=\sqrt{(1-\rho)P_1^{t_{s_3}}P_s}x_1\left(t_{s_3}\right)h_{r_1}^{BS}+\sqrt{(1-\rho)P_2^{t_{s_3}}P_s}x_2\left(t_{s_3}\right)h_{r_1}^{BS}$$
$$+\sqrt{(1-\rho)P_3^{t_{s_3}}P_s}x_3\left(t_{s_3}\right)h_{r_1}^{BS}+\sqrt{(1-\rho)P_4^{t_{s_3}}P_s}x_4\left(t_{s_3}\right)h_{r_1}^{BS} \quad (6.20)$$
$$+\sqrt{(1-\rho)}N_{r_1}$$

$$\sqrt{(1-\rho)}y_{r_2}\left(t_{s_3}\right)=\sqrt{(1-\rho)P_1^{t_{s_3}}P_s}x_1\left(t_{s_3}\right)h_{r_2}^{BS}+\sqrt{(1-\rho)P_2^{t_{s_3}}P_s}x_2\left(t_{s_3}\right)h_{r_2}^{BS}$$
$$+\sqrt{(1-\rho)P_3^{t_{s_3}}P_s}x_3\left(t_{s_3}\right)h_{r_2}^{BS}+\sqrt{(1-\rho)P_4^{t_{s_3}}P_s}x_4\left(t_{s_3}\right)h_{r_2}^{BS} \quad (6.21)$$
$$+\sqrt{(1-\rho)}N_{r_2}$$

Table 6.4 gives the decoded SINR at the relays in time sub-slot t_{s_3}.

Table 6.4: SINR at relays in t_{s_3}

Relay r_1 and r_2	
$SINR_{t_{s_3}}^{3-r_1}=\frac{(1-\rho)P_3^{t_{s_3}}P_s\left\|h_{r_1}^{BS}\right\|^2}{\sum_{j=1}^{2}(1-\rho)P_j^{t_{s_3}}P_s\left\|h_{r_1}^{BS}\right\|^2+(1-\rho)P_4^{t_{s_3}}P_s\left\|h_{r_1}^{BS}\right\|^2+(1-\rho)\sigma_{r_1}^2}$	(6.22)
$SINR_{t_{s_3}}^{3-r_2}=\frac{(1-\rho)P_3^{t_{s_3}}P_s\left\|h_{r_2}^{BS}\right\|^2}{\sum_{j=1}^{2}(1-\rho)P_j^{t_{s_3}}P_s\left\|h_{r_2}^{BS}\right\|^2+(1-\rho)P_4^{t_{s_3}}P_s\left\|h_{r_2}^{BS}\right\|^2+(1-\rho)\sigma_{r_2}^2}$	(6.23)

$$SINR_{t_{s3}}^{4-r_2} = \frac{(1-\rho) P_4^{t_{s3}} P_s \left| h_{r_2}^{BS} \right|^2}{\sum_{j=1}^{2} (1-\rho) P_j^{t_{s3}} P_s \left| h_{r_2}^{BS} \right|^2 + (1-\rho)\sigma_{r_2}^2} \quad (6.24)$$

$$SINR_{t_{s3}}^{2-r_2} = \frac{(1-\rho) P_2^{t_{s3}} P_s \left| h_{r_2}^{BS} \right|^2}{(1-\rho) P_1^{t_{s3}} P_s \left| h_{r_2}^{BS} \right|^2 + (1-\rho)\sigma_{r_2}^2} \quad (6.25)$$

The energy harvesting equations in Table 6.2 are not time-dependent; thus, they are utilised in this time sub-slot as well.

6.3.4. Time sub-slot t_{s_4} :

The relays regenerate the signals for the users connected to it, given by equations (6.26) and (6.27).

$$x_{s_{r_1}}\left(t_{s_4}\right) = \sqrt{(1-\rho) P_3^{t_{s4}} G_{r_1} P_s P_{r_1}}\, x_3\left(t_{s_3}\right) h_{r_1}^{BS} \quad (6.26)$$

$$x_{s_{r_2}}\left(t_{s_4}\right) = \sqrt{(1-\rho) P_2^{t_{s4}} G_{r_2} P_s P_{r_2}}\, x_2\left(t_{s_3}\right) h_{r_2}^{BS} + \sqrt{(1-\rho) P_4^{t_{s4}} G_{r_2} P_s P_{r_2}}\, x_4\left(t_{s_3}\right) h_{r_2}^{BS} \quad (6.27)$$

The received signals of UE_2,UE_3 and UE_4 are the same as section 5.2.4.1, given by equations (5.47) to (5.49). Table 6.5 gives the decoded SINRs at UE_2,UE_3 and UE_4.

Table 6.5: SINR at UEs

UE	SINR
UE_2	$SINR_{t_{s4}}^{4-2} = \frac{(1-\rho)\eta\rho P_4^{t_{s4}} P_s^2 \left(\left| h_{r_2}^{BS} \right|^2 \right)^2 \left| h_2^{r_2} \right|^2}{(1-\rho)\eta\rho P_2^{t_{s4}} P_s^2 \left(\left| h_{r_2}^{BS} \right|^2 \right)^2 \left| h_2^{r_2} \right|^2 + (1-\rho) P_s \left| h_{r_2}^{BS} \right|^2 \sigma_2^2 + \sigma_{R_2}^2 \sigma_2^2}$ (6.28)

	$$SINR_{t_{s_4}}^{2-2} = \frac{(1-\rho)\eta\rho P_2^{t_{s_4}} P_s^2 \left(\left|h_{r_2}^{BS}\right|^2\right)^2 \left|h_2^{r_2}\right|^2}{(1-\rho) P_s \left|h_{r_2}^{BS}\right|^2 \sigma_2^2 + \sigma_{R_2}^2 \sigma_2^2} \quad (6.29)$$
UE_3	$$SINR_{t_{s_4}}^{3-3} = \frac{(1-\rho)\eta\rho P_3^{t_{s_4}} P_s^2 \left(\left|h_{r_1}^{BS}\right|^2\right)^2 \left|h_3^{r_1}\right|^2}{(1-\rho) P_s \left|h_{r_1}^{BS}\right|^2 \sigma_3^2 + \sigma_{R_1}^2 \sigma_3^2} \quad (6.30)$$
UE_4	$$SINR_{t_{s_4}}^{4-4} = \frac{(1-\rho) P_4^{t_{s_4}} \eta\rho P_s^2 \left(\left|h_{r_2}^{BS}\right|^2\right)^2 \left|h_4^{r_2}\right|^2}{(1-\rho)\eta\rho P_2^{t_{s_4}} P_s^2 \left(\left|h_{r_2}^{BS}\right|^2\right)^2 \left|h_4^{r_2}\right|^2 + (1-\rho) P_s \left|h_{r_2}^{BS}\right|^2 \sigma_4^2 + \sigma_{R_2}^2 \sigma_4^2} \quad (6.31)$$

6.4. Energy Harvesting Outage Probability

The energy harvesting outage probability of the users are given in Table 6.6.

Table 6.6: Energy harvested outage probability

OP for UE_1 in t_{s_1} is the same as equation (5.65)
OP for UE_1 in t_{s_3} is the same as equation (5.66)
OP for UE_2 in t_{s_1} is the same as equation (5.67)
OP for UE_2 in t_{s_3} and t_{s_4}

$$P_{2,t_{s_4}}=\begin{cases}1-e^{-\lambda_{r_2}^{BS}P_s\sigma^2\left[\left(\frac{\beta^{t_{s_4}}}{\eta\rho\left|h_2^{r_2}\right|^2}\left(\frac{1}{P_2^{t_{s_4}}}+\frac{1}{\left[P_4^{t_{s_4}}-P_2^{t_{s_4}}\beta^{t_{s_4}}\right]}\right)+\beta^{t_{s_3}}\left(\frac{1}{\left[P_2^{t_{s_3}}-P_1^{t_{s_3}}\beta^{t_{s_3}}\right]}+\frac{1}{\left[P_4^{t_{s_3}}-\sum_{j=1}^{2}P_j^{t_{s_3}}\beta^{t_{s_3}}\right]}+\frac{1}{\left[P_3^{t_{s_3}}-\left(\sum_{j=1}^{2}P_j^{t_{s_3}}+P_4^{t_{s_3}}\right)\beta^{t_{s_3}}\right]}\right)\right)\right]}, & 0<\beta^{t_{s_4}}<\frac{P_4^{t_{s_4}}}{P_2^{t_{s_4}}}\bigcup\beta^{t_{s_3}}<\left\{\frac{P_2^{t_{s_3}}}{P_1^{t_{s_3}}}\bigcup\frac{P_4^{t_{s_3}}}{\sum_{j=1}^{2}P_j^{t_{s_3}}}\bigcup\frac{P_3^{t_{s_3}}}{\sum_{j=1}^{2}P_j^{t_{s_3}}+P_4^{t_{s_3}}}\right\} \\ 1, \text{else}\end{cases} \tag{6.32}$$

OP for UE_3 in t_{s_1} and t_{s_2}

$$P_{3,t_{s_2}}=\begin{cases}1-e^{-\sigma^2\left[\frac{\beta^{t_{s_2}}}{\lambda_3^{r_2}P_s\eta\rho P_3^{t_{s_2}}\left|h_{r_2}^{BS}\right|^2}+\frac{\beta^{t_{s_1}}}{\lambda_{r_2}^{BS}P_s}\left(\frac{1}{\left[P_3^{t_{s_1}}-\sum_{j=1}^{2}P_j^{t_{s_1}}\beta^{t_{s_1}}\right]}+\frac{1}{\left[P_4^{t_{s_1}}-\sum_{j=1}^{3}P_j^{t_{s_1}}\beta^{t_{s_1}}\right]}\right)\right]}, & 0<\beta^{t_{s_2}}\bigcup\beta^{t_{s_1}}<\left\{\frac{P_3^{t_{s_1}}}{\sum_{j=1}^{2}P_j^{t_{s_1}}}\bigcup\frac{P_4^{t_{s_1}}}{\sum_{j=1}^{3}P_j^{t_{s_1}}}\right\} \\ 1, \text{else}\end{cases} \tag{6.33}$$

OP for UE_3 in t_{s_3} and t_{s_4}

$$P_{3,t_{s_4}}=\begin{cases}1-e^{-\sigma^2\left[\frac{\beta^{t_{s_4}}}{\lambda_3^{r_1}P_s\left[\eta\rho P_3^{t_{s_4}}\left|h_{r_1}^{BS}\right|^2\right]}+\frac{\beta^{t_{s_3}}}{\lambda_{r_1}^{BS}P_s}\left(\frac{1}{\left[P_3^{t_{s_3}}-\left(\sum_{j=1}^{2}P_j^{t_{s_3}}+P_4^{t_{s_3}}\right)\beta^{t_{s_3}}\right]}\right)\right]}, & 0<\beta^{t_{s_4}}\bigcup\beta^{t_{s_3}}<\frac{P_3^{t_{s_3}}}{\sum_{j=1}^{2}P_j^{t_{s_3}}+P_4^{t_{s_3}}} \\ 1, \text{else}\end{cases} \tag{6.34}$$

OP for UE_4 in t_{s_1} and t_{s_2}

$$P_{4,t_{s_2}}=\begin{cases}1-e^{-\sigma^2\left[\frac{\beta^{t_{s_2}}}{\lambda_4^{r_1}P_s\eta\rho P_4^{t_{s_2}}\left|h_{r_1}^{BS}\right|^2}+\frac{\beta^{t_{s_1}}}{\lambda_{r_1}^{BS}P_s}\left(\frac{1}{\left[P_4^{t_{s_1}}-\sum_{j=1}^{3}P_j^{t_{s_1}}\beta^{t_{s_1}}\right]}\right)\right]}, & 0<\beta^{t_{s_2}}\bigcup\beta^{t_{s_1}}<\frac{P_4^{t_{s_1}}}{\sum_{j=1}^{3}P_j^{t_{s_1}}} \\ 1, \text{else}\end{cases} \tag{6.35}$$

OP for UE_4 in t_{s_3} and t_{s_4}

$$P_{4,t_{s_4}} = \begin{cases} 1-e^{-\sigma^2\left[\frac{\beta^{t_{s_4}}}{\lambda_4^{r_2} P_s \eta\rho \left|h_{r_2}^{BS}\right|^2}\left(\frac{1}{\left[P_4^{t_{s_4}} - P_2^{t_{s_4}}\beta^{t_{s_4}}\right]}\right)+ \frac{\beta^{t_{s_3}}}{\lambda_{r_2}^{BS} P_s}\left(\frac{1}{\left[P_4^{t_{s_3}} - \sum_{j=1}^{2} P_j^{t_{s_3}}\beta^{t_{s_3}}\right]}+\frac{1}{\left[P_3^{t_{s_3}} - \left(\sum_{j=1}^{2} P_j^{t_{s_3}} + P_4^{t_{s_3}}\right)\beta^{t_{s_3}}\right]}\right)\right]}, \\ 0 < \beta^{t_{s_4}} < \frac{P_4^{t_{s_4}}}{P_2^{t_{s_4}}} \bigcup \beta^{t_{s_3}} < \left\{\frac{P_4^{t_{s_3}}}{\sum_{j=1}^{2} P_j^{t_{s_3}}} \bigcup \frac{P_3^{t_{s_3}}}{\sum_{j=1}^{2} P_j^{t_{s_3}} + P_4^{t_{s_3}}}\right\} \\ 1, \text{else} \end{cases} \quad (6.36)$$

6.5. Simulation Results

The simulation model is shown in Figure 5.1and Figure 5.2, with the energy harvesting relay capabilities from Chapter 5. The system model has one BS, three relays $(r_1, r_2, \text{and } r_3)$, and four users $(UE_1, UE_2, UE_3, \text{ and } UE_4)$. The relay works in half-duplex mode. For t_{s_1} and t_{s_2} time sub-slots UE_1 and UE_2 are cell center users while UE_3 and UE_4 are cell edge users using relays r_2 and r_1. For t_{s_3} and t_{s_4} time sub-slots UE_1 is a cell center user while $UE_2, UE_3,$ and UE_4 are cell edge users. The UE_2 and UE_4 are connected to relay r_2 and UE_3 is connected to relay r_1. The relays harvest energy from the received signal and employ the amplify and forward protocol to forward the intended signals to the connected users. The system parameters for the energy harvesting NOMA-based system are given in Table 6.7. Simulation results compare the four-user NOMA-based network with and with energy harvesting relay capabilities.

Table 6.7: Energy harvesting system parameters

$P_s = 25 \sim 50$ dB	Base station power
$\lambda_1^{BS} = 1^{-4}, \lambda_2^{BS} = 0.8^{-4}, \lambda_{r_1}^{BS} = 0.4^{-4},$ $\lambda_{r_2}^{BS} = 0.5^{-4}, \lambda_3^{r_2} = 0.3^{-4}, \lambda_4^{r_1} = 0.3^{-4}$	Figure 5.1 channel variances
$\lambda_1^{BS} = 1^{-4}, \lambda_{r_1}^{BS} = 0.4^{-4}, \lambda_{r_2}^{BS} = 0.5^{-4},$ $\lambda_2^{r_2} = 0.3^{-4}, \lambda_3^{r_1} = 0.3^{-4}, \lambda_4^{r_2} = 0.4^{-4}$	Figure 5.2 channel variances
$R = 0.3$ bps/Hz	Target rate
$\rho = 0.5$	Power splitting coefficient
$\eta = 1$	Energy conversion efficiency
$P_s = 10 \sim 20$ dB	Transmit power

The simulation results show the outage probability of UEs in the various time sub-slots. Figure 6.3 shows the outage probability of UE_1 in t_{s_1} and t_{s_3}, with and without energy harvesting relays. The energy harvesting does not affect UE_1 as it is always a cell-center user and connects directly to the base station. Due to the changes in mobility of users 2, 3, and 4 from t_{s_1} to t_{s_3}, their channel conditions change, thus changing all the users' power allocation. Therefore the figure also shows a slight change in the outage probability of UE_1 from t_{s_1} to t_{s_3}.

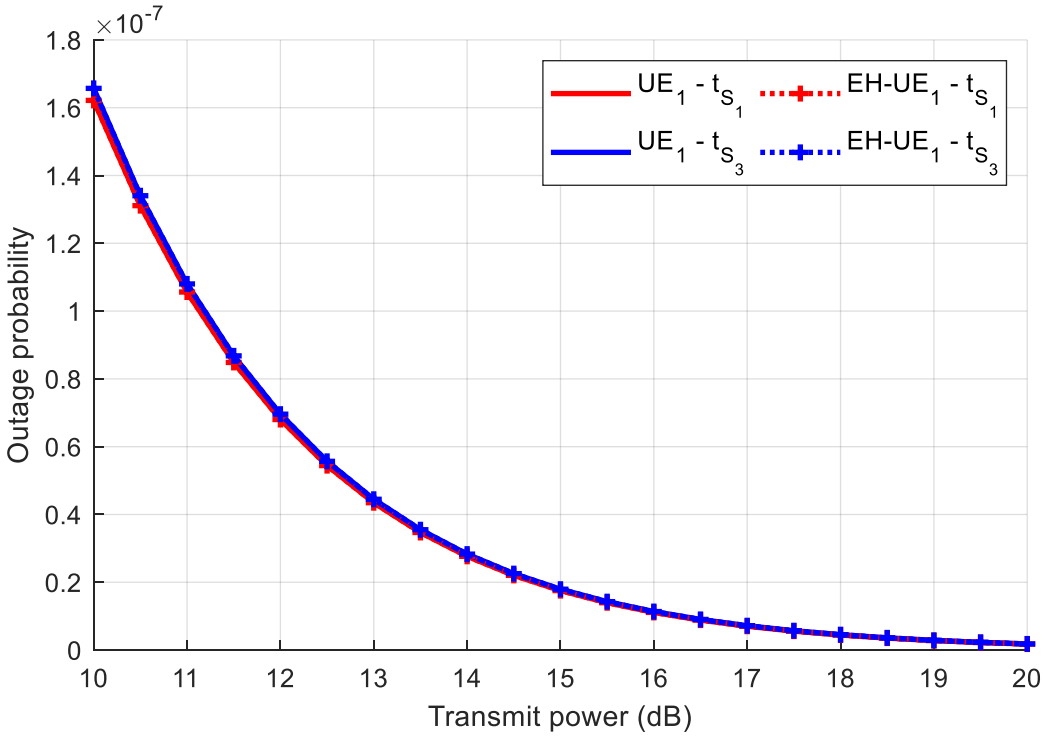

Figure 6.3: Outage probability of user 1

Figure 6.4 shows the outage probability of UE_2 in t_{s_1} and $t_{s_{3-4}}$. During time sub-slot 1, UE_2 is a cell center user, and therefore the energy harvesting does not affect this user. However, for time sub-slot $t_{s_{3-4}}$, the outage probability of UE_2 improves; because UE_2 is a cell-edge user and connected to an energy harvesting relay.

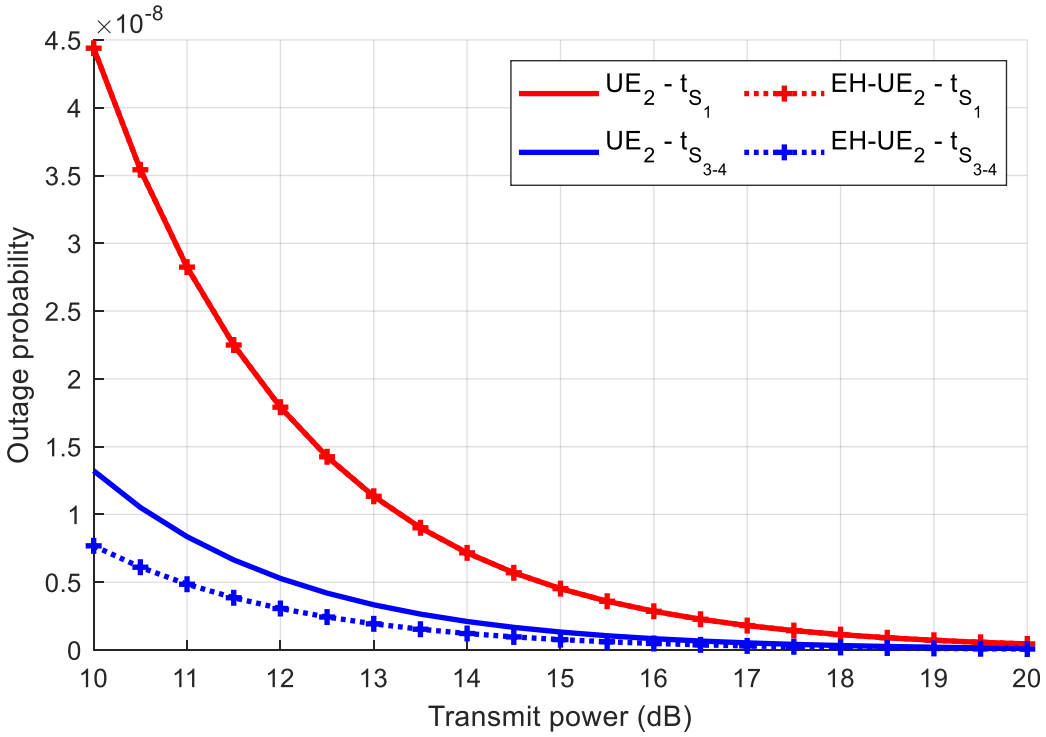

Figure 6.4 Outage probability of user 2

Figure 6.5 and Figure 6.6 show the outage probability of UE_3 and UE_4, respectively. These UEs are cell edge users in both time slots; therefore, they benefit from the energy harvesting relays where their outage probabilities improve. The change in positions shows a noticeable difference between the outage probability of UE_3 and UE_4. For the first time slot $\left(t_{s_{1-2}}\right)$ UE_3 is connected to relay 2 with the second highest allocated power, whereas UE_4 is connected to relay 1 with the highest allocated power. However, in time slot $\left(t_{s_{3-4}}\right)$ UE_3 is connected to relay 1 with the highest allocated power and UE_4 shares a relay with UE_2.

The results simply show the impact of the power allocations on the outage probability of the users as well as their positions in the network. The cell edge users connected to the relays benefit from the harvested energy by receiving more power than the network without harvesting, which can be seen in the figures.

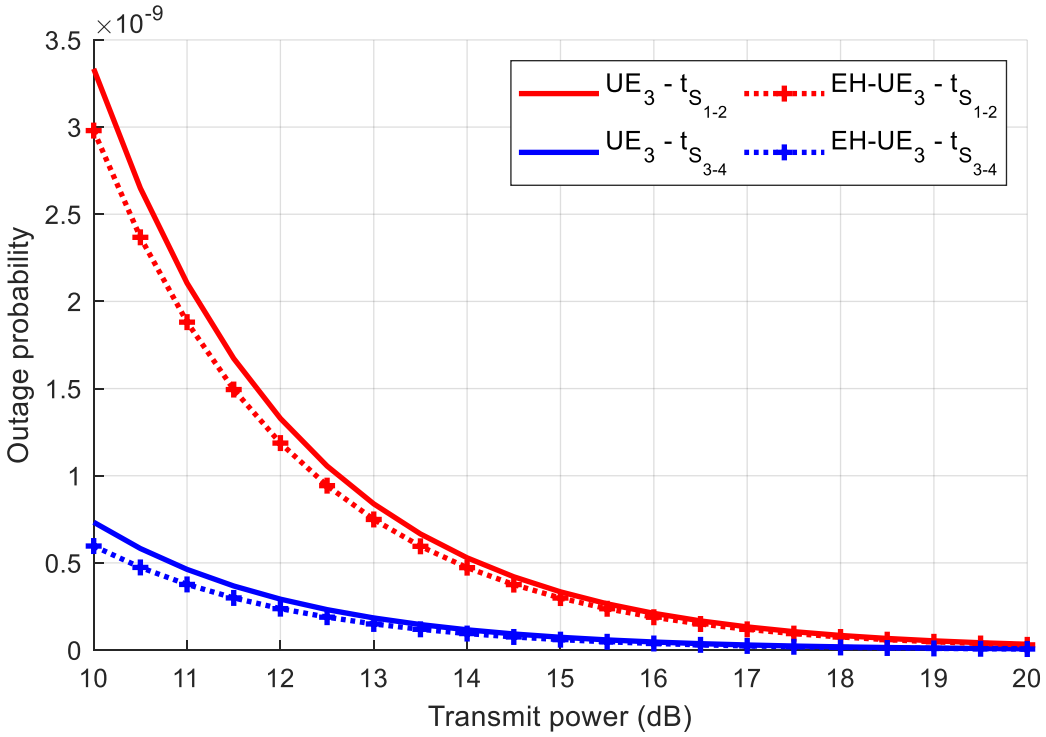

Figure 6.5: Outage probability of user 3

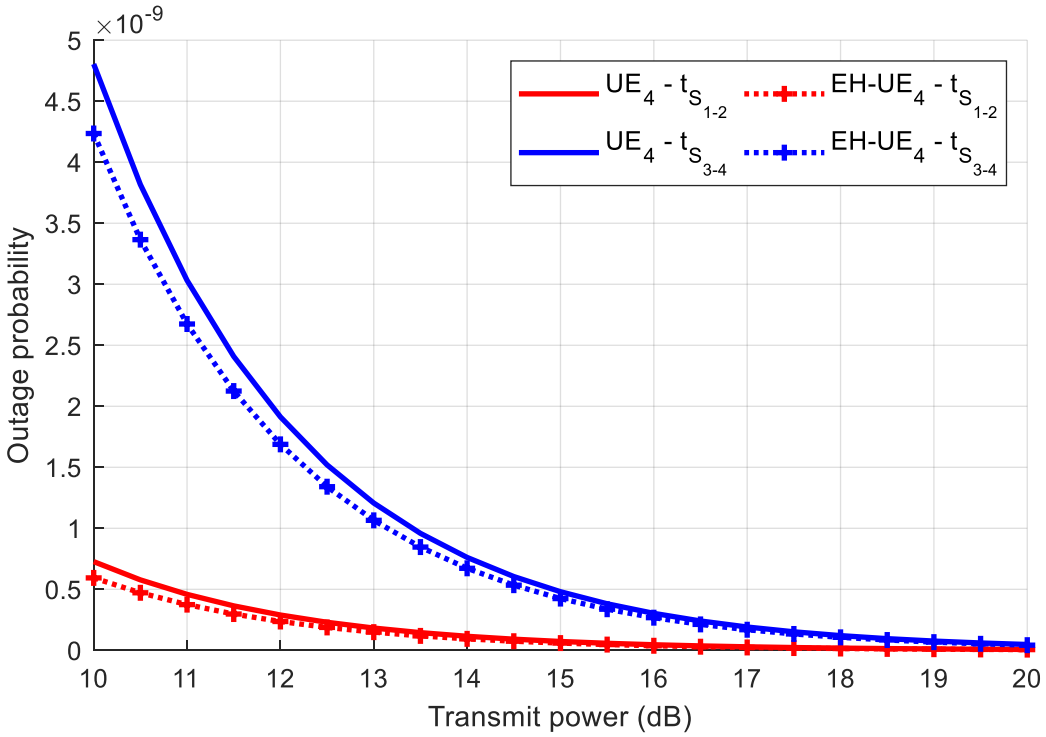

Figure 6.6: Outage probability of user 4

6.6. Summary

A brief introduction to energy harvesting shows its applications and benefits, such as self-sustaining and prolonged wireless networks. The implementation of energy harvesting into the relay nodes presented in chapter 5 utilises the PSR protocol to harvest energy from the received signal and the AF protocol to forward signals to the connected UE. The section follows the methodology in chapter 5, focusing on each user's energy harvested outage probability in the various time slots. Simulation results show the benefits of energy harvesting relaying nodes.

Chapter 7

FUTURE WORK AND CONCLUSION

7.1. Conclusion

This research introduces the MIMO communication system and highlights its advantages and disadvantages, thus resulting in the power consumption problem of the system. An extensive literature review gives the current schemes and methodologies to improve the energy efficiency of the respective systems. A history of mobile communication technology shows the progression of the mobile generations and their evolving technologies, specifically the multiple access techniques. An in-depth discussion shows the MIMO concept and channel models. A review of 5G shows the drivers, possible technologies and applications of this technology, resulting in NOMA as a promising technology. A focus on NOMA explains the concept and benefits, specifically the operations of NOMA in uplink and downlink communications. The study and evaluation of current power allocations schemes led to the design and simulation of the proposed power allocation scheme, utilising MATLAB.

Finally, this research explores resource allocation in a broadcast MIMO NOMA-based relay network, where cell center UEs connect directly to the BS and cell-edge UEs connect via relays. The utilisation of the relays reduces outage probability in the two-hop communication and improves the system's spectral efficiency. The SIC capabilities of NOMA successfully cancel interfering UE's signals at the user and relay. The outage probability and ergodic rate expressions of the UEs in the different time slots are derived. A power allocation algorithm allocates user power while considering user fairness. The simulation results show the effect of fairness on the cell center and cell-edge users, where the system's rate significantly improves when considering fairness among users. The energy harvesting simulation results show the advantage of employing energy harvesting relay nodes in the NOMA system.

The utilisation of MIMO improves the physical layer performance of the mobile communication system by utilising spatial multiplexing. NOMA proves to be an excellent candidate for 5G applications with its superposition coding and successive interference cancellation. It also improves the system performance by improving efficiency, thus reducing power consumption.

7.2. Future Work

Future work might explore the ergodic rate of the energy harvesting system and physical layer security, where implementing a jamming signal increases the security of the physical layer of a network. Further research into NOMA 5G applications combined with MIMO multiple access channels is another route to explore.

BIBLIOGRAPHY

Ahmadi, S. 2019. *5G NR: Architecture, Technology, Implementation, and Operation of 3GPP New Radio Standards*. Academic Press.

Alexiou, A. 2017. *5G Wireless Technologies*. Institution of Engineering and Technology.

Alsharoa, A., Ghazzai, H., Kamal, A.E. & Kadri, A. 2017. Near Optimal Power Splitting Protocol for Energy Harvesting Based Two Way Multiple Relay Systems. IEEE. doi:10.1109/WCNC.2017.7925700.

Asif, S. 2018. *5G Mobile Communications: Concepts and Technologies*. CRC Press. doi:10.1007/978-3-319-34208-5.

Balyan, V. 2020. Outage Probability of Cognitive Radio Network Utilizing Non Orthogonal Multiple Access. IEEE. doi:10.1109/SPIN48934.2020.9071401.

Balyan, V. & Daniels, R. 2020. Resource allocation for NOMA based networks using relays: cell centre and cell edge users. *International Journal on Smart Sensing and Intelligent Systems*, vol.13(1): pp. 1–18. doi:10.21307/ijssis-2020-031.

Belleschi, M. 2008. *Cross-layer optimization protocols in Ad-hoc networks: analysis and practical implementation of transport and network layers*. KTH Electrical Engineering.

Bizaki, H.K. 2016. *Towards 5G Wireless Networks: A Physical Layer Perspective*. IntechOpen.

Brown, T., Kyritsi, P. & De Carvalho, E. 2012. *Practical Guide to MIMO Radio Channel: with MATLAB Examples*. John Wiley & Sons. doi:10.1002/9781119944966.

Cai, Y., Ke, C., Ni, Y., Zhang, J. & Zhu, H. 2021. Power allocation for NOMA in D2D relay communications. *China Communications*, vol.18(1): pp. 61–69. doi:10.23919/JCC.2021.01.006.

Chinnadurai, S., Selvaprabhu, P. & Lee, M.H. 2017. A novel joint user pairing and dynamic power allocation scheme in MIMO-NOMA system. IEEE. doi:10.1109/ICTC.2017.8190822.

Choi, J. 2017a. Effective Capacity of NOMA and a Suboptimal Power Control Policy With Delay QoS. *IEEE Transactions on Communications*, vol.65(4): pp. 1849–1858. doi:10.1109/TCOMM.2017.2661763.

Choi, J. 2017b. NOMA: Principles and recent results. IEEE. doi:10.1109/ISWCS.2017.8108138.

Cox, C. 2014. *An Introduction to LTE: LTE, LTE-Advanced, SAE, VoLTE and 4G Mobile Communications*. 2nd ed. John Wiley & Sons.

Dahlman, E., Parkvall, S. & Skold, J. 2011. *4G: LTE/LTE-Advanced for Mobile Broadband*. Academic Press.

Dahlman, E., Parkvall, S. & Sköld, J. 2016. *4G, LTE-Advanced Pro and The Road to 5G*. 3rd ed. Academic Press.

Das, S.K. 2017. *Mobile Terminal Receiver Design: LTE and LTE-Advanced*. illustrate. Singapore: John Wiley & Sons. doi:10.1002/9781119107422.

Di, B., Song, L. & Li, Y. 2016. Sub-Channel Assignment, Power Allocation, and User Scheduling for Non-Orthogonal Multiple Access Networks. *IEEE Transactions on Wireless Communications*, vol.15(11): pp. 7686–7698. doi:10.1109/TWC.2016.2606100.

Ding, Z., Adachi, F. & Poor, H.V. 2016. The Application of MIMO to Non-Orthogonal Multiple Access. *IEEE Transactions on Wireless Communications*, vol.15(1): pp. 537–552. doi:10.1109/TWC.2015.2475746.

Du, G., Xiong, K. & Qiu, Z. 2015. Outage Analysis of Cooperative Transmission with Energy Harvesting Relay: Time Switching versus Power Splitting W. Xiao, ed. *Mathematical Problems in Engineering*, vol.2015: pp. 598290. doi:10.1155/2015/598290.

Fang, F., Zhang, H., Cheng, J. & Leung, V.C.M. 2017. Energy-efficient resource scheduling for NOMA systems with imperfect channel state information. IEEE. doi:10.1109/ICC.2017.7996360.

Fang, F., Zhang, H., Cheng, J., Roy, S. & Leung, V.C.M. 2017. Joint User Scheduling and Power Allocation Optimization for Energy-Efficient NOMA Systems With Imperfect CSI. *IEEE Journal on Selected Areas in Communications*, vol.35(12): pp. 2874–2885. doi:10.1109/JSAC.2017.2777672.

Guo, C., Xin, J., Zhao, L. & Chu, X. 2019. Performance analysis of cooperative NOMA with energy harvesting in multi-cell networks. *China Communications*, vol.16(11): pp. 120–129. doi:10.23919/JCC.2019.11.010.

Huang, H., Papadias, C.B. & Venkatesan, S. 2011. *MIMO Communications for Cellular Networks*. Illustrate. Springer Science & Business Media, 2011.

Huang, K., Wang, Z., Wan, X., Fan, Z. & Xu, Y. 2019. Max-Min Energy Efficiency Optimization Algorithm for Wireless Power Transfer Enabled Massive MIMO Systems. *2019 IEEE 5th International Conference on Computer and Communications, ICCC 2019*, (ii): pp. 2029–2033. doi:10.1109/ICCC47050.2019.9064265.

Huang, R., Wan, D., Ji, F., Qing, H., Li, J., Yu, H. & Chen, F. 2020. Performance analysis of NOMA-based cooperative networks with relay selection. *China Communications*, vol.17(11): pp. 111–119. doi:10.23919/JCC.2020.11.010.

Jia, B., Hu, H., Zeng, Y., Xu, T. & Chen, H.-H. 2018. Joint User Pairing and Power Allocation in Virtual MIMO Systems. *IEEE Transactions on Wireless Communications*, vol.17(6): pp. 3697–3708. doi:10.1109/TWC.2018.2814048.

Kaur, J. & Singh, M.L. 2019. User assisted cooperative relaying in beamspace massive MIMO NOMA based systems for millimeter wave communications. *China Communications*, vol.16(6): pp. 103–113. doi:10.23919/j.cc.2019.06.009.

Le, T.A. & Kong, H.Y. 2019. Evaluating the Performance of Cooperative NOMA with Energy Harvesting Under Physical Layer Security. *Wireless Personal Communications*, vol.108(2): pp. 1037–1054. doi:10.1007/s11277-019-06452-5.

Li, F., Jiang, H., Fan, R. & Tan, P. 2019. Cognitive Non-Orthogonal Multiple Access With Energy Harvesting: An Optimal Resource Allocation Approach. *IEEE Transactions on Vehicular Technology*, vol.68(7): pp. 7080–7095. doi:10.1109/TVT.2019.2919261.

Li, H., Cheng, J., Wang, Z. & Wang, H. 2019. Joint Antenna Selection and Power Allocation for an Energy-efficient Massive MIMO System. *IEEE Wireless Communications Letters*, vol.8(1): pp. 257–260. doi:10.1109/LWC.2018.2869152.

Liu, Q., Lv, T. & Lin, Z. 2018. Energy-efficient transmission design in cooperative relaying systems using NOMA. *IEEE Communications Letters*, vol.22(3): pp. 594–597. doi:10.1109/LCOMM.2018.2790379.

Luo, F.-L. & Zhang, J.C. 2016. *Signal Processing for 5G: Algorithms and Implementations*. John Wiley & Sons. doi:10.1002/9781119116493.ch3.

Manglayev, T., Kizilirmak, R.C. & Kho, Y.H. 2016. Optimum power allocation for non-

orthogonal multiple access (NOMA). IEEE. doi:10.1109/ICAICT.2016.7991730.

McDonough, C. 2009. Mobile Broadband. In Springer Science & Business Media: 74–86. doi:10.4018/978-1-4666-1981-4.ch005.

Mishra, D. & Alexandropoulos, G.C. 2018. Jointly Optimal Spatial Channel Assignment and Power Allocation for MIMO SWIPT Systems. *IEEE Wireless Communications Letters*, vol.7(2): pp. 214–217. doi:10.1109/LWC.2017.2765320.

Mondal, S., Dharroy, S. & Kundu, S. 2020. Adaptive Energy Harvesting with Relay Selection Schemes in an Ordered NOMA network. *2020 National Conference on Communications (NCC)*: pp. 1–6. doi:10.1109/NCC48643.2020.9056072.

Nasir, A.A., Zhou, X., Durrani, S. & Kennedy, R.A. 2013. Relaying Protocols for Wireless Energy Harvesting and Information Processing. *IEEE Transactions on Wireless Communications*, vol.12(17): pp. 3622–3636. doi:10.1109/TWC.2013.062413.122042.

Nasser, A., Muta, O., Elsabrouty, M. & Gacanin, H. 2019. Interference Mitigation and Power Allocation Scheme for Downlink MIMO–NOMA HetNet. *IEEE Transactions on Vehicular Technology*, vol.68(7): pp. 6805–6816. doi:10.1109/TVT.2019.2918336.

Oestges, C. & Clerckx, B. 2007. *MIMO Wireless Communications: From Real-World Propagation to Space-Time Code Design*. Academic Press. doi:eISBN: 9780123850560 pISBN: 9780123850553.

Osseiran, A., Monserrat, J.F. & Marsch, P. 2016. *5G Mobile and Wireless Communications Technology*. Cambridge University Press.

Oviedo, J.A. & Sadjadpour, H.R. 2018. On the Power Allocation Limits for Downlink Multi-User NOMA with QoS. IEEE. doi:10.1109/ICC.2018.8422366.

Rodriguez, J. 2015. *Fundamentals of 5G Mobile Networks*. John Wiley & Sons.

Saatlou, O., Ahmad, M.O. & Swamy, M.N.S. 2019. Joint Data and Pilot Power Allocation for Massive MU-MIMO Downlink TDD Systems. *IEEE Transactions on Circuits and Systems II: Express Briefs*, vol.66(3): pp. 512–516. doi:10.1109/TCSII.2018.2866111.

Salem, A., Musavian, L., Jorswieck, E. & Aissa, S. 2020. Secrecy Outage Probability of Energy-Harvesting Cooperative NOMA Transmissions with Relay Selection. *IEEE Transactions on Green Communications and Networking*, vol.4(4): pp. 1130–1148.

doi:10.1109/TGCN.2020.2999815.

Sauter, M. 2014. *From GSM to LTE-advanced: An Introduction to Mobile Networks and Mobile Broadband*. revised. John Wiley & Sons Incorporated.

Sboui, L., Rezki, Z. & Alouini, M.-S. 2017. Energy-Efficient Power Allocation for MIMO-SVD Systems. *IEEE Access*, vol.5: pp. 9774–9784. doi:10.1109/ACCESS.2017.2707550.

Shi, J., Yu, W., Ni, Q., Liang, W., Li, Z. & Xiao, P. 2019. Energy Efficient Resource Allocation in Hybrid Non-Orthogonal Multiple Access Systems. *IEEE Transactions on Communications*, vol.67(5): pp. 3496–3511. doi:10.1109/TCOMM.2019.2893304.

Shi, L., Zhao, L. & Liang, K. 2017. Power allocation for wireless powered MIMO transmissions with non-linear RF energy conversion models. *China Communications*, vol.14(2): pp. 57–64. doi:10.1109/CC.2017.7868175.

Shrestha, A.P., Tao Han, Zhiquan Bai, Kim, J.M. & Kwak, K.S. 2016. Performance of transmit antenna selection in non-orthogonal multiple access for 5G systems. IEEE. doi:10.1109/ICUFN.2016.7536954.

Song, Q., Jin, S. & Zheng, F.-C. 2018. Joint Power Allocation and Beamforming for UAV-Enabled Relaying Systems with Channel Estimation Errors. IEEE. doi:10.1109/VTCSpring.2018.8417734.

Sun, Q., Han, S., I, C.-L. & Pan, Z. 2015. On the Ergodic Capacity of MIMO NOMA Systems. *IEEE Wireless Communications Letters*, vol.4(4): pp. 405–408. doi:10.1109/LWC.2015.2426709.

Timotheou, S. & Krikidis, I. 2015. Fairness for Non-Orthogonal Multiple Access in 5G Systems. *IEEE Signal Processing Letters*, vol.22(10): pp. 1647–1651. doi:10.1109/LSP.2015.2417119.

Vaezi, M., Ding, Z. & Vincent Poor, H. 2018. *Multiple access techniques for 5G wireless networks and beyond*. Springer. doi:10.1007/978-3-319-92090-0.

Wang, T., Lu, G., Ye, Y. & Ren, Y. 2018. Dynamic Power Splitting Strategy for SWIPT Based Two-Way Multiplicative AF Relay Networks with Nonlinear Energy Harvesting Model. *Wireless Communications and Mobile Computing*, vol.2018: pp. 1–9. doi:10.1155/2018/1802063.

Xiang, W., Zheng, K. & (Sherman) Shen, X. 2016. *5G Mobile Communications*. illustrate. Springer. doi:10.1007/978-3-319-34208-5.

Xie, S., Zhang, B., Guo, D. & Zhao, B. 2019. Performance Analysis and Power Allocation for NOMA-Based Hybrid Satellite-Terrestrial Relay Networks With Imperfect Channel State Information. *IEEE Access*, vol.7: pp. 136279–136289. doi:10.1109/ACCESS.2019.2942167.

Xie, X., Bi, Y. & Nie, X. 2020. Performance Analysis of Uplink Cooperative NOMA System with an AF Relay. *2020 IEEE 20th International Conference on Communication Technology (ICCT)*: pp. 178–181. doi:10.1109/ICCT50939.2020.9295870.

Xu, P. & Cumanan, K. 2017. Optimal Power Allocation Scheme for Non-Orthogonal Multiple Access With $\alpha $ -Fairness. *IEEE Journal on Selected Areas in Communications*, vol.35(10): pp. 2357–2369. doi:10.1109/JSAC.2017.2729780.

Xu, Y., Cheng, J., Wang, G. & Leung, V.C.M. 2021. Coordinated Direct and Relay Transmission for Multiuser Networks: NOMA or Hybrid Multiple Access? *IEEE Wireless Communications Letters*, vol.10(5): pp. 976–980. doi:10.1109/LWC.2021.3052894.

Yang, Y., Xu, J., Shi, G. & Wang, C.-X. 2017. *5G Wireless Systems: Simulation and Evaluation Techniques*. Springer. doi:10.1007/978-3-319-61869-2.

Yang, Z., Ding, Z., Fan, P. & Al-Dhahir, N. 2016. A General Power Allocation Scheme to Guarantee Quality of Service in Downlink and Uplink NOMA Systems. *IEEE Transactions on Wireless Communications*, vol.15(11): pp. 7244–7257. doi:10.1109/TWC.2016.2599521.

Young Bae Song, Hyeon Su Kang & Duk Kyung Kim. 2016. 5G cellular systems with D2D assisted NOMA relay. *2016 URSI Asia-Pacific Radio Science Conference (URSI AP-RASC)*: pp. 1–3. doi:10.1109/URSIAP-RASC.2016.7883540.

Yuan, Z., Li, X. & Lv, G. 2019. Energy Efficient Power Allocation for Multi-carrier Non-orthogonal Multiple Access (NOMA) Systems with Proportional Rate Constraints. IEEE. doi:10.1109/ITNEC.2019.8729390.

Zarrinkoub, H. 2014. *Understanding LTE with MATLAB: From Mathematical Modeling to Simulation and Prototyping*. John Wiley & Sons.

Zeng, M. & Fodor, V. 2018. Energy-efficient Resource Allocation for NOMA-assisted Mobile

Edge Computing. IEEE. doi:10.1109/PIMRC.2018.8580984.

Zeng, M., Hao, W., Dobre, O.A. & Poor, H.V. 2019. Energy-Efficient Power Allocation in Uplink mmWave Massive MIMO With NOMA. *IEEE Transactions on Vehicular Technology*, vol.68(3): pp. 3000–3004. doi:10.1109/TVT.2019.2891062.

Zeng, M., Yadav, A., Dobre, O.A. & Poor, H.V. 2018a. Energy-Efficient Power Allocation for Hybrid Multiple Access Systems. IEEE. doi:10.1109/ICCW.2018.8403619.

Zeng, M., Yadav, A., Dobre, O.A. & Poor, H.V. 2018b. Energy-Efficient Power Allocation for MIMO-NOMA With Multiple Users in a Cluster. *IEEE Access*, vol.6: pp. 5170–5181. doi:10.1109/ACCESS.2017.2779855.

Zhai, D., Li, H., Tang, X., Zhang, R., Ding, Z. & Yu, F.R. 2021. Height Optimization and Resource Allocation for NOMA Enhanced UAV-Aided Relay Networks. *IEEE Transactions on Communications*, vol.69(2): pp. 962–975. doi:10.1109/TCOMM.2020.3037345.

Zhang, M., Tan, W., Gao, J. & Jin, S. 2018. Spectral efficiency and power allocation for mixed-ADC massive MIMO system. *China Communications*, vol.15(3): pp. 112–127. doi:10.1109/CC.2018.8331995.

Zhang, X., Zhu, X. & Zhu, H. 2019. Joint User Clustering and Multi-Dimensional Resource Allocation in Downlink MIMO–NOMA Networks. *IEEE Access*, vol.7: pp. 81783–81793. doi:10.1109/ACCESS.2019.2923713.

Zhang, Y., Wang, H.M., Zheng, T.X. & Yang, Q. 2017. Energy-Efficient Transmission Design in Non-orthogonal Multiple Access. *IEEE Transactions on Vehicular Technology*, vol.66(3): pp. 2852–2857. doi:10.1109/TVT.2016.2578949.

Zhao, L., Zhao, H., Zheng, K. & Xiang, W. 2017. *Massive MIMO in 5G Networks: Selected Applications*. Springer.

Zhao, S., Mei, C. & Zhu, Q. 2019. Joint Time and Power Allocation Algorithm in NOMA Relaying Network. *Mobile Information Systems*, vol.2019: pp. 1–14. doi:10.1155/2019/7842987.

Zuo, H. & Tao, X. 2017. Power allocation optimization for uplink non-orthogonal multiple access systems. IEEE. doi:10.1109/WCSP.2017.8171176.

APPENDICES

Appendix A

OP for UE_1 in t_{s_1} :

$$\begin{aligned} P_{1,t_{s_1}} &= P_r\left[OE_{1,t_{s_1}}\right] = P_r\left[OE_{r_{4-1}}^{t_{s_1}} \cup OE_{r_{3-1}}^{t_{s_1}} \cup OE_{r_{2-1}}^{t_{s_1}} \cup OE_{r_{1-1}}^{t_{s_1}}\right] \\ &= P_r\left[\left(R_{r_{4-1}}^{t_{s_1}} < R\right) \cup \left(R_{r_{3-1}}^{t_{s_1}} < R\right) \cup \left(R_{r_{2-1}}^{t_{s_1}} < R\right) \cup \left(R_{r_{1-1}}^{t_{s_1}} < R\right)\right] \\ &= 1 - \left[1 - F_{R_{r_{4-1}}^{t_{s_1}}}(R)\right]\left[1 - F_{R_{r_{3-1}}^{t_{s_1}}}(R)\right]\left[1 - F_{R_{r_{2-1}}^{t_{s_1}}}(R)\right]\left[1 - F_{R_{r_{1-1}}^{t_{s_1}}}(R)\right] \end{aligned} \quad (A.1)$$

In time sub-slot 1 $\beta^{t_{s_1}} = 2^{\frac{R}{t_{s_1}}} - 1$

$$\begin{aligned} F_{R_{r_{1-1}}^{t_{s_1}}}(R) &= P_r\left(R_{r_{1-1}}^{t_{s_1}} < R\right) = P_r\left(t_{s_1}\log_2\left(1 + SINR_{t_{s_1}}^{1-1}\right) < R\right) \\ &= \begin{cases} 1 - e^{\frac{-\beta^{t_{s_1}}\sigma_1^2}{\lambda_1^{BS} P_1^{t_{s_1}} P_s}}, 0 < \beta^{t_{s_1}} \\ 1, \text{else} \end{cases} \end{aligned} \quad (A.2)$$

$$\begin{aligned} F_{R_{r_{2-1}}^{t_{s_1}}}(R) &= P_r\left(R_{r_{2-1}}^{t_{s_1}} < R\right) = P_r\left(t_{s_1}\log_2\left(1 + SINR_{t_{s_1}}^{2-1}\right) < R\right) \\ &= \begin{cases} 1 - e^{\frac{-\beta^{t_{s_1}}\sigma_1^2}{\lambda_1^{BS} P_s\left[P_2^{t_{s_1}} - P_1^{t_{s_1}}\beta^{t_{s_1}}\right]}}, 0 < \beta^{t_{s_1}} < \frac{P_2^{t_{s_1}}}{P_1^{t_{s_1}}} \\ 1, \text{else} \end{cases} \end{aligned} \quad (A.3)$$

$$\begin{aligned} F_{R_{r_{3-1}}^{t_{s_1}}}(R) &= P_r\left(R_{r_{3-1}}^{t_{s_1}} < R\right) = P_r\left(t_{s_1}\log_2\left(1 + SINR_{t_{s_1}}^{3-1}\right) < R\right) \\ &= \begin{cases} 1 - e^{\frac{-\beta^{t_{s_1}}\sigma_1^2}{\lambda_1^{BS} P_s\left[P_3^{t_{s_1}} - \left(\sum_{j=1}^{2} P_j^{t_{s_1}}\right)\beta^{t_{s_1}}\right]}}, 0 < \beta^{t_{s_1}} < \frac{P_3^{t_{s_1}}}{P_1^{t_{s_1}} + P_2^{t_{s_1}}} \\ 1, \text{else} \end{cases} \end{aligned} \quad (A.4)$$

$$\begin{aligned} F_{R_{r_{4-1}}^{t_{s_1}}}(R) &= P_r\left(R_{r_{4-1}}^{t_{s_1}} < R\right) = P_r\left(t_{s_1}\log_2\left(1 + SINR_{t_{s_1}}^{4-1}\right) < R\right) \\ &= \begin{cases} 1 - e^{\frac{-\beta^{t_{s_1}}\sigma_1^2}{\lambda_1^{BS} P_s\left[P_4^{t_{s_1}} - \left(\sum_{j=1}^{3} P_j^{t_{s_1}}\right)\beta^{t_{s_1}}\right]}}, 0 < \beta^{t_{s_1}} < \frac{P_4^{t_{s_1}}}{\sum_{j=1}^{3} P_j^{t_{s_1}}} \\ 1, \text{else} \end{cases} \end{aligned} \quad (A.5)$$

$$P_{1,t_{s_1}} = \left\{ \begin{array}{l} 1-e^{\frac{-\beta^{t_{s_1}}\sigma^2}{\lambda_1^{BS}P_s}\left[\frac{1}{P_1^{t_{s_1}}}+\frac{1}{P_2^{t_{s_1}}-P_1^{t_{s_1}}\beta^{t_{s_1}}}+\frac{1}{P_3^{t_{s_1}}-\left(\sum_{j=1}^{2}P_j^{t_{s_1}}\right)\beta^{t_{s_1}}}+\frac{1}{P_4^{t_{s_1}}-\left(\sum_{j=1}^{3}P_j^{t_{s_1}}\right)\beta^{t_{s_1}}}\right]}, \\ 0<\beta^{t_{s_1}}<\left\{\frac{P_4^{t_{s_1}}}{\sum_{j=1}^{3}P_j^{t_{s_1}}}\bigcup\frac{P_3^{t_{s_1}}}{\sum_{j=1}^{2}P_j^{t_{s_1}}}\bigcup\frac{P_2^{t_{s_1}}}{P_1^{t_{s_1}}}\right\} \\ 1, \text{else} \end{array} \right\} \quad \text{(A.6)}$$

OP for UE_1 in t_{s_3}:

In time sub-slot 3 $\beta^{t_{s_3}} = 2^{\frac{R}{t_{s_3}}}-1$

$$\begin{aligned} P_{1,t_{s_3}} &= P_r\left[OE_{1,t_{s_3}}\right] = P_r\left[OE_{r_{3-1}}^{t_{s_3}}\bigcup OE_{r_{4-1}}^{t_{s_3}}\bigcup OE_{r_{2-1}}^{t_{s_3}}\bigcup OE_{r_{1-1}}^{t_{s_3}}\right] \\ &= P_r\left[\left(R_{r_{3-1}}^{t_{s_3}}<R\right)\bigcup\left(R_{r_{4-1}}^{t_{s_3}}<R\right)\bigcup\left(R_{r_{2-1}}^{t_{s_3}}<R\right)\bigcup\left(R_{r_{1-1}}^{t_{s_3}}<R\right)\right] \\ &= 1-\left[1-F_{R_{r_{3-1}}^{t_{s_3}}}(R)\right]\left[1-F_{R_{r_{4-1}}^{t_{s_3}}}(R)\right]\left[1-F_{R_{r_{2-1}}^{t_{s_3}}}(R)\right]\left[1-F_{R_{r_{1-1}}^{t_{s_3}}}(R)\right] \end{aligned} \quad \text{(A.7)}$$

$$\begin{aligned} F_{R_{r_{1-1}}^{t_{s_3}}}(R) &= P_r\left(R_{r_{1-1}}^{t_{s_3}}<R\right) = P_r\left(t_{s_3}\log_2\left(1+SINR_{t_{s_3}}^{1-1}\right)<R\right) \\ &= \left\{ \begin{array}{l} 1-e^{\frac{-\beta^{t_{s_3}}\sigma_1^{\,2}}{\lambda_1^{BS}P_1^{t_{s_3}}P_s}}, 0<\beta^{t_{s_3}} \\ 1, \text{else} \end{array} \right\} \end{aligned} \quad \text{(A.8)}$$

$$\begin{aligned} F_{R_{r_{2-1}}^{t_{s_3}}}(R) &= P_r\left(R_{r_{2-1}}^{t_{s_3}}<R\right) = P_r\left(t_{s_3}\log_2\left(1+SINR_{t_{s_3}}^{2-1}\right)<R\right) \\ &= \left\{ \begin{array}{l} 1-e^{\frac{-\beta^{t_{s_3}}\sigma_1^{\,2}}{\lambda_1^{BS}P_s\left[P_2^{t_{s_3}}-P_1^{t_{s_3}}\beta^{t_{s_3}}\right]}}, 0<\beta^{t_{s_3}}<\frac{P_2^{t_{s_3}}}{P_1^{t_{s_3}}} \\ 1, \text{else} \end{array} \right\} \end{aligned} \quad \text{(A.9)}$$

$$\begin{aligned} F_{R_{r_{3-1}}^{t_{s_3}}}(R) &= P_r\left(R_{r_{3-1}}^{t_{s_3}}<R\right) = P_r\left(t_{s_3}\log_2\left(1+SINR_{t_{s_3}}^{3-1}\right)<R\right) \\ &= \left\{ \begin{array}{l} 1-e^{\frac{-\beta^{t_{s_3}}\sigma_1^{\,2}}{\lambda_1^{BS}P_s\left[P_3^{t_{s_3}}-\left(\sum_{j=1}^{2}P_j^{t_{s_3}}+P_4^{t_{s_3}}\right)\beta^{t_{s_3}}\right]}}, 0<\beta^{t_{s_3}}<\frac{P_3^{t_{s_3}}}{\sum_{j=1}^{2}P_j^{t_{s_3}}+P_4^{t_{s_3}}} \\ 1, \text{else} \end{array} \right\} \end{aligned} \quad \text{(A.10)}$$

$$F_{R_{r_{4-1}}^{t_{s3}}}(R)=P_r\left(R_{r_{4-1}}^{t_{s3}}<R\right)=P_r\left(t_{s_1}\log_2\left(1+SINR_{t_{s3}}^{4-1}\right)<R\right)$$
$$=\left\{\begin{array}{l}1-e^{\frac{-\beta^{t_{s3}}\sigma_1^{\,2}}{\lambda_1^{BS}P_s\left[P_4^{\,t_{s3}}-\left(\sum_{j=1}^{2}P_j^{\,t_{s3}}\right)\beta^{t_{s3}}\right]}},0<\beta^{t_{s3}}<\dfrac{P_4^{t_{s3}}}{\sum_{j=1}^{2}P_j^{\,t_{s3}}}\\ 1,\text{else}\end{array}\right\} \quad (A.11)$$

$$P_{1,t_{s3}}=\left\{\begin{array}{l}1-e^{\frac{-\beta^{t_{s3}}\sigma^2}{\lambda_1^{BS}P_s}\left[\frac{1}{P_1^{t_{s3}}}+\frac{1}{P_2^{t_{s3}}-P_1^{t_{s3}}\beta^{t_{s3}}}+\frac{1}{P_3^{t_{s3}}-\left(\sum_{j=1}^{2}P_j^{t_{s3}}+P_4^{t_{s3}}\right)\beta^{t_{s3}}}+\frac{1}{P_4^{t_{s3}}-\left(\sum_{j=1}^{2}P_j^{t_{s3}}\right)\beta^{t_{s3}}}\right]},\\ 0<\beta^{t_{s3}}<\left\{\dfrac{P_4^{t_{s3}}}{\sum_{j=1}^{2}P_j^{t_{s3}}}\bigcup\dfrac{P_3^{t_{s3}}}{\sum_{j=1}^{2}P_j^{t_{s3}}+P_4^{t_{s3}}}\bigcup\dfrac{P_2^{t_{s3}}}{P_1^{t_{s3}}}\right\}\\ 1,\text{else}\end{array}\right\} \quad (A.12)$$

OP for UE_2 in t_{s_1} :

$$\begin{aligned}P_{2,t_{s_1}}&=P_r\left[OE_{2,t_{s_1}}\right]=P_r\left[OE_{r_{4-2}}^{t_{s_1}}\bigcup OE_{r_{3-2}}^{t_{s_1}}\bigcup OE_{r_{2-2}}^{t_{s_1}}\right]\\&=P_r\left[\left(R_{r_{4-2}}^{t_{s_1}}<R\right)\bigcup\left(R_{r_{3-2}}^{t_{s_1}}<R\right)\bigcup\left(R_{r_{2-2}}^{t_{s_1}}<R\right)\right]\\&=1-\left[1-F_{R_{r_{4-2}}^{t_{s_1}}}(R)\right]\left[1-F_{R_{r_{3-2}}^{t_{s_1}}}(R)\right]\left[1-F_{R_{r_{2-2}}^{t_{s_1}}}(R)\right]\end{aligned} \quad (A.13)$$

$$F_{R_{r_{2-2}}^{t_{s_1}}}(R)=P_r\left(R_{r_{2-2}}^{t_{s_1}}<R\right)=P_r\left(t_{s_1}\log_2\left(1+SINR_{t_{s_1}}^{2-2}\right)<R\right)$$
$$=\left\{\begin{array}{l}1-e^{\frac{-\beta^{t_{s_1}}\sigma_2^{\,2}}{\lambda_2^{BS}P_s\left[P_2^{\,t_{s_1}}-P_1^{t_{s_1}}\beta^{t_{s_1}}\right]}},0<\beta^{t_{s_1}}<\dfrac{P_2^{t_{s_1}}}{P_1^{t_{s_1}}}\\ 1,\text{else}\end{array}\right\} \quad (A.14)$$

$$F_{R_{r_{3-2}}^{t_{s_1}}}(R)=P_r\left(R_{r_{3-2}}^{t_{s_1}}<R\right)=P_r\left(t_{s_1}\log_2\left(1+SINR_{t_{s_1}}^{3-2}\right)<R\right)$$
$$=\left\{\begin{array}{l}1-e^{\frac{-\beta^{t_{s_1}}\sigma_2^{\,2}}{\lambda_2^{BS}P_s\left[P_3^{\,t_{s_1}}-\left(\sum_{j=1}^{2}P_j^{\,t_{s_1}}\right)\beta^{t_{s_1}}\right]}},0<\beta^{t_{s_1}}<\dfrac{P_3^{t_{s_1}}}{\sum_{j=1}^{2}P_j^{\,t_{s_1}}}\\ 1,\text{else}\end{array}\right\} \quad (A.15)$$

$$F_{R_{r_{4-2}}^{t_{s_1}}}(R)=P_r\left(R_{r_{4-2}}^{t_{s_1}}<R\right)=P_r\left(t_{s_1}\log_2\left(1+SINR_{t_{s_1}}^{4-2}\right)<R\right)$$
$$=\begin{Bmatrix}1-e^{\frac{-\beta^{t_{s_1}}{\sigma_2}^2}{\lambda_2^{BS}P_s\left[P_4^{t_{s_1}}-\left(\sum_{j=1}^{3}P_j^{t_{s_1}}\right)\beta^{t_{s_1}}\right]}},0<\beta^{t_{s_1}}<\frac{P_4^{t_{s_1}}}{\sum_{j=1}^{3}P_j^{t_{s_1}}}\\ 1,\text{else}\end{Bmatrix} \quad (A.16)$$

$$P_{2,t_{s_1}}=\begin{Bmatrix}1-e^{\frac{-\beta^{t_{s_1}}\sigma^2}{\lambda_2^{BS}P_s}\left[\frac{1}{P_2^{t_{s_1}}-P_1^{t_{s_1}}\beta^{t_{s_1}}}+\frac{1}{P_3^{t_{s_1}}-\left(\sum_{j=1}^{2}P_j^{t_{s_1}}\right)\beta^{t_{s_1}}}+\frac{1}{P_4^{t_{s_1}}-\left(\sum_{j=1}^{3}P_j^{t_{s_1}}\right)\beta^{t_{s_1}}}\right]},\\ 0<\beta^{t_{s_1}}<\left\{\frac{P_4^{t_{s_1}}}{\sum_{j=1}^{3}P_j^{t_{s_1}}}\bigcup\frac{P_3^{t_{s_1}}}{\sum_{j=1}^{2}P_j^{t_{s_1}}}\bigcup\frac{P_2^{t_{s_1}}}{P_1^{t_{s_1}}}\right\}\\ 1,\text{else}\end{Bmatrix} \quad (A.17)$$

OP for UE_2 in $t_{s_{3-4}}$:

$$P_{2,t_{s_4}}=P_r\left[OE_{2,t_{s_4}}\right]=P_r\left[OE_{r_{3-r_2}}^{t_{s_3}}\bigcup OE_{r_{4-r_2}}^{t_{s_3}}\bigcup OE_{r_{2-r_2}}^{t_{s_3}}\bigcup OE_{r_{4-2}}^{t_{s_4}}\bigcup OE_{r_{2-2}}^{t_{s_4}}\right]$$
$$=P_r\left[\left(R_{r_{3-r_2}}^{t_{s_3}}<R\right)\bigcup\left(R_{r_{4-r_2}}^{t_{s_3}}<R\right)\bigcup\left(R_{r_{2-r_2}}^{t_{s_3}}<R\right)\bigcup\left(R_{r_{4-2}}^{t_{s_4}}<R\right)\bigcup\left(R_{r_{2-2}}^{t_{s_4}}<R\right)\right] \quad (A.18)$$
$$=1-\left[1-F_{R_{r_{3-r_2}}^{t_{s_3}}}(R)\right]\left[1-F_{R_{r_{4-r_2}}^{t_{s_3}}}(R)\right]\left[1-F_{R_{r_{2-r_2}}^{t_{s_3}}}(R)\right]\left[1-F_{R_{r_{4-2}}^{t_{s_4}}}(R)\right]\left[1-F_{R_{r_{2-2}}^{t_{s_4}}}(R)\right]$$

In time sub-slot 4 $\beta^{t_{s_4}}=2^{\frac{R}{t_{s_4}}}-1$

$$F_{R_{r_{2-2}}^{t_{s_4}}}(R)=P_r\left(R_{r_{2-2}}^{t_{s_4}}<R\right)=P_r\left(t_{s_4}\log_2\left(1+SINR_{t_{s_4}}^{2-2}\right)<R\right)$$
$$=\begin{Bmatrix}1-e^{\frac{-\beta^{t_{s_4}}{\sigma_2}^2}{\lambda_2^{r_2}P_2^{t_{s_4}}P_{r_2}}},0<\beta^{t_{s_4}}\\ 1,\text{else}\end{Bmatrix} \quad (A.19)$$

$$F_{R_{r_{4-2}}^{t_{s_4}}}(R)=P_r\left(R_{r_{4-2}}^{t_{s_4}}<R\right)=P_r\left(t_{s_4}\log_2\left(1+SINR_{t_{s_4}}^{4-2}\right)<R\right)$$
$$=\begin{Bmatrix}1-e^{\frac{-\beta^{t_{s_4}}{\sigma_2}^2}{\lambda_2^{r_2}P_{r_2}\left[P_4^{t_{s_4}}-P_2^{t_{s_4}}\beta^{t_{s_4}}\right]}},0<\beta^{t_{s_4}}<\frac{P_4^{t_{s_4}}}{P_2^{t_{s_4}}}\\ 1,\text{else}\end{Bmatrix} \quad (A.20)$$

$$F_{R_{r_{2-r_2}}^{t_{s3}}}(R)=P_r\left(R_{r_{2-r_2}}^{t_{s3}}<R\right)=P_r\left(t_{s_3}\log_2\left(1+SINR_{t_{s3}}^{2-r_2}\right)<R\right)$$

$$=\begin{Bmatrix}1-e^{\frac{-\beta^{t_{s3}}\sigma_{r_2}{}^2}{\lambda_{r_2}^{BS}P_s\left[P_2^{t_{s3}}-P_1^{t_{s3}}\beta^{t_{s3}}\right]}},0<\beta^{t_{s3}}<\frac{P_2^{t_{s3}}}{P_1^{t_{s3}}}\\ 1,\text{else}\end{Bmatrix} \quad (A.21)$$

$$F_{R_{r_{4-r_2}}^{t_{s3}}}(R)=P_r\left(R_{r_{4-r_2}}^{t_{s3}}<R\right)=P_r\left(t_{s_3}\log_2\left(1+SINR_{t_{s3}}^{4-r_2}\right)<R\right)$$

$$=\begin{Bmatrix}1-e^{\frac{-\beta^{t_{s3}}\sigma_{r_2}{}^2}{\lambda_{r_2}^{BS}P_s\left[P_4^{t_{s3}}-\sum_{j=1}^{2}P_j^{t_{s3}}\beta^{t_{s3}}\right]}},0<\beta^{t_{s3}}<\frac{P_4^{t_{s3}}}{\sum_{j=1}^{2}P_j^{t_{s3}}}\\ 1,\text{else}\end{Bmatrix} \quad (A.22)$$

$$F_{R_{r_{3-r_2}}^{t_{s3}}}(R)=P_r\left(R_{r_{3-r_2}}^{t_{s3}}<R\right)=P_r\left(t_{s_3}\log_2\left(1+SINR_{t_{s3}}^{3-r_2}\right)<R\right)$$

$$=\begin{Bmatrix}1-e^{\frac{-\beta^{t_{s3}}\sigma_{r_2}{}^2}{\lambda_{r_2}^{BS}P_s\left[P_3^{t_{s3}}-\left(\sum_{j=1}^{2}P_j^{t_{s3}}+P_4^{t_{s3}}\right)\beta^{t_{s3}}\right]}},0<\beta^{t_{s3}}<\frac{P_3^{t_{s3}}}{\sum_{j=1}^{2}P_j^{t_{s3}}+P_4^{t_{s3}}}\\ 1,\text{else}\end{Bmatrix} \quad (A.23)$$

$$P_{2,t_{s_4}}=\begin{Bmatrix}1-e^{-\sigma^2\left[\frac{\beta^{t_{s4}}}{\lambda_2^{r_2}P_{r_2}}\left(\frac{1}{P_2^{t_{s4}}}+\frac{1}{\left[P_4^{t_{s4}}-P_2^{t_{s4}}\beta^{t_{s4}}\right]}\right)+\frac{\beta^{t_{s3}}}{\lambda_{r_2}^{BS}P_s}\left(\frac{1}{\left[P_2^{t_{s3}}-P_1^{t_{s3}}\beta^{t_{s3}}\right]}+\frac{1}{\left[P_4^{t_{s3}}-\sum_{j=1}^{2}P_j^{t_{s3}}\beta^{t_{s3}}\right]}+\frac{1}{\left[P_3^{t_{s3}}-\left(\sum_{j=1}^{2}P_j^{t_{s3}}+P_4^{t_{s3}}\right)\beta^{t_{s3}}\right]}\right)\right]},\\ 0<\beta^{t_{s4}}<\frac{P_4^{t_{s4}}}{P_2^{t_{s4}}}\bigcup\beta^{t_{s3}}<\left\{\frac{P_2^{t_{s3}}}{P_1^{t_{s3}}}\bigcup\frac{P_4^{t_{s3}}}{\sum_{j=1}^{2}P_j^{t_{s3}}}\bigcup\frac{P_3^{t_{s3}}}{\sum_{j=1}^{2}P_j^{t_{s3}}+P_4^{t_{s3}}}\right\}\\ 1,\text{else}\end{Bmatrix} \quad (A.24)$$

OP for UE_3 in $t_{s_{1-2}}$:

$$P_{3,t_{s_2}}=P_r\left[OE_{3,t_{s_2}}\right]=P_r\left[OE_{r_{4-r_2}}^{t_{s1}}\bigcup OE_{r_{3-r_2}}^{t_{s1}}\bigcup OE_{r_{3-3}}^{t_{s2}}\right]$$

$$=P_r\left[\left(R_{r_{4-r_2}}^{t_{s1}}<R\right)\bigcup\left(R_{r_{3-r_2}}^{t_{s1}}<R\right)\bigcup\left(R_{r_{3-3}}^{t_{s2}}<R\right)\right] \quad (A.25)$$

$$=1-\left[1-F_{R_{r_{4-r_2}}^{t_{s1}}}(R)\right]\left[1-F_{R_{r_{3-r_2}}^{t_{s1}}}(R)\right]\left[1-F_{R_{r_{3-3}}^{t_{s2}}}(R)\right]$$

In time sub-slot $\beta^{t_{s2}}=2^{\frac{R}{t_{s2}}}-1$

$$F_{R_{r_{3-3}}^{t_{s_2}}}(R)=P_r\left(R_{r_{3-3}}^{t_{s_2}}<R\right)=P_r\left(t_{s_2}\log_2\left(1+SINR_{t_{s_2}}^{3-3}\right)<R\right)$$
$$=\begin{Bmatrix}1-e^{\frac{-\beta^{t_{s_2}}{\sigma_3}^2}{\lambda_3^{r_2}P_3^{t_{s_2}}P_{r_2}}},0<\beta^{t_{s_2}}>0\\1,\text{else}\end{Bmatrix} \quad (A.26)$$

$$F_{R_{r_{3-r_2}}^{t_{s_1}}}(R)=P_r\left(R_{r_{3-r_2}}^{t_{s_1}}<R\right)=P_r\left(t_{s_1}\log_2\left(1+SINR_{t_{s_1}}^{3-r_2}\right)<R\right)$$
$$=\begin{Bmatrix}1-e^{\frac{-\beta^{t_{s_1}}{\sigma_{r_2}}^2}{\lambda_{r_2}^{BS}P_s\left[P_3^{t_{s_1}}-\left(\sum_{j=1}^{2}P_j^{t_{s_1}}\right)\beta^{t_{s_1}}\right]}},0<\beta^{t_{s_1}}<\frac{P_3^{t_{s_1}}}{\sum_{j=1}^{2}P_j^{t_{s_1}}}\\1,\text{else}\end{Bmatrix} \quad (A.27)$$

$$F_{R_{r_{4-r_2}}^{t_{s_1}}}(R)=P_r\left(R_{r_{4-r_2}}^{t_{s_1}}<R\right)=P_r\left(t_{s_1}\log_2\left(1+SINR_{t_{s_1}}^{4-r_2}\right)<R\right)$$
$$=\begin{Bmatrix}1-e^{\frac{-\beta^{t_{s_1}}{\sigma_{r_2}}^2}{\lambda_{r_2}^{BS}P_s\left[P_4^{t_{s_1}}-\left(\sum_{j=1}^{3}P_j^{t_{s_1}}\right)\beta^{t_{s_1}}\right]}},0<\beta^{t_{s_1}}<\frac{P_4^{t_{s_1}}}{\sum_{j=1}^{3}P_j^{t_{s_1}}}\\1,\text{else}\end{Bmatrix} \quad (A.28)$$

$$P_{3,t_{s_2}}=\begin{Bmatrix}1-e^{-\sigma^2\left[\frac{\beta^{t_{s_2}}}{\lambda_3^{r_2}P_3^{t_{s_2}}P_{r_2}}+\frac{\beta^{t_{s_1}}}{\lambda_{r_2}^{BS}P_s}\left(\frac{1}{\left[P_3^{t_{s_1}}-\left(\sum_{j=1}^{2}P_j^{t_{s_1}}\right)\beta^{t_{s_1}}\right]}+\frac{1}{\left[P_4^{t_{s_1}}-\left(\sum_{j=1}^{3}P_j^{t_{s_1}}\right)\beta^{t_{s_1}}\right]}\right)\right]},\\0<\beta^{t_{s_2}}\cup\beta^{t_{s_1}}<\left(\frac{P_3^{t_{s_1}}}{\sum_{j=1}^{2}P_j^{t_{s_1}}}\cup\frac{P_4^{t_{s_1}}}{\sum_{j=1}^{3}P_j^{t_{s_1}}}\right)\\1,\text{else}\end{Bmatrix} \quad (A.29)$$

OP for UE_3 in $t_{s_{3-4}}$:

$$P_{3,t_{s_4}}=P_r\left[OE_{3,t_{s_4}}\right]=P_r\left[OE_{r_{3-\eta}}^{t_{s_3}}\cup OE_{r_{3-3}}^{t_{s_4}}\right]$$
$$=P_r\left[\left(R_{r_{3-\eta}}^{t_{s_3}}<R\right)\cup\left(R_{r_{3-3}}^{t_{s_4}}<R\right)\right] \quad (A.30)$$
$$=1-\left[1-F_{R_{r_{3-\eta}}^{t_{s_3}}}(R)\right]\left[1-F_{R_{r_{3-3}}^{t_{s_4}}}(R)\right]$$

$$F_{R_{r_{3-3}}^{t_{s_4}}}(R)=P_r\left(R_{r_{3-3}}^{t_{s_4}}<R\right)=P_r\left(t_{s_4}\log_2\left(1+SINR_{t_{s_4}}^{3-3}\right)<R\right)$$
$$=\begin{Bmatrix}1-e^{\frac{-\beta^{t_{s_4}}{\sigma_3}^2}{\lambda_3^{\eta}P_3^{t_{s_4}}P_{\eta}}},0<\beta^{t_{s_4}}\\1,\text{else}\end{Bmatrix} \quad (A.31)$$

$$F_{R_{r_{3-r_1}}^{t_{s3}}}(R)=P_r\left(R_{r_{3-r_1}}^{t_{s3}}<R\right)=P_r\left(t_{s_3}\log_2\left(1+SINR_{t_{s3}}^{3-r_1}\right)<R\right)$$

$$=\left\{\begin{array}{l}1-e^{\frac{-\beta^{t_{s3}}{\sigma_{r_1}}^2}{\lambda_{r_1}^{BS}P_s\left[P_3^{t_{s3}}-\left(\sum_{j=1}^{2}P_j^{t_{s3}}+P_4^{t_{s3}}\right)\beta^{t_{s3}}\right]}},0<\beta^{t_{s3}}<\frac{P_3^{t_{s3}}}{\sum_{j=1}^{2}P_j^{t_{s3}}+P_4^{t_{s3}}}\\1,\text{else}\end{array}\right\} \quad (A.32)$$

$$P_{3,t_{s_4}}=\left\{\begin{array}{l}1-e^{-\sigma^2\left[\frac{\beta^{t_{s4}}}{\lambda_3^{r_1}P_3^{t_{s4}}P_{r_1}}+\frac{\beta^{t_{s3}}}{\lambda_{r_1}^{BS}P_s}\left(\frac{1}{\left[P_3^{t_{s3}}-\left(\sum_{j=1}^{2}P_j^{t_{s3}}+P_4^{t_{s3}}\right)\beta^{t_{s3}}\right]}\right)\right]},\\0<\beta^{t_{s4}}\bigcup\beta^{t_{s3}}<\frac{P_3^{t_{s3}}}{\sum_{j=1}^{2}P_j^{t_{s3}}+P_4^{t_{s3}}}\\1,\text{else}\end{array}\right\} \quad (A.33)$$

OP for UE_4 in $t_{s_{1-2}}$:

$$\begin{aligned}P_{4,t_{s_2}}&=P_r\left[OE_{4,t_{s_2}}\right]=P_r\left[OE_{r_{4-r_1}}^{t_{s1}}\bigcup OE_{r_{4-4}}^{t_{s2}}\right]\\&=P_r\left[\left(R_{r_{4-r_1}}^{t_{s1}}<R\right)\bigcup\left(R_{r_{4-4}}^{t_{s2}}<R\right)\right]\\&=1-\left[1-F_{R_{r_{4-r_1}}^{t_{s1}}}(R)\right]\left[1-F_{R_{r_{4-4}}^{t_{s2}}}(R)\right]\end{aligned} \quad (A.34)$$

$$F_{R_{r_{4-4}}^{t_{s2}}}(R)=P_r\left(R_{r_{4-4}}^{t_{s2}}<R\right)=P_r\left(t_{s_2}\log_2\left(1+SINR_{t_{s2}}^{4-4}\right)<R\right)$$

$$=\left\{\begin{array}{l}1-e^{\frac{-\beta^{t_{s2}}{\sigma_4}^2}{\lambda_4^{r_1}P_4^{t_{s2}}P_{r_1}}},0<\beta^{t_{s2}}\\1,\text{else}\end{array}\right\} \quad (A.35)$$

$$F_{R_{r_{4-r_1}}^{t_{s1}}}(R)=P_r\left(R_{r_{4-r_1}}^{t_{s1}}<R\right)=P_r\left(t_{s_1}\log_2\left(1+SINR_{t_{s1}}^{4-r_1}\right)<R\right)$$

$$=\left\{\begin{array}{l}1-e^{\frac{-\beta^{t_{s1}}{\sigma_{r_1}}^2}{\lambda_{r_1}^{BS}P_s\left[P_4^{t_{s1}}-\left(\sum_{j=1}^{3}P_j^{t_{s1}}\right)\beta^{t_{s1}}\right]}},0<\beta^{t_{s1}}<\frac{P_4^{t_{s1}}}{\sum_{j=1}^{3}P_j^{t_{s1}}}\\1,\text{else}\end{array}\right\} \quad (A.36)$$

$$P_{4,t_{s_2}} = \begin{cases} 1-e^{-\sigma^2\left[\frac{\beta^{t_{s_2}}}{\lambda_4^{\eta} P_4^{t_{s_2}} P_{r_1}}+\frac{\beta^{t_{s_1}}}{\lambda_{r_1}^{BS} P_s}\left(\frac{1}{\left[P_4^{t_{s_1}}-\left(\sum_{j=1}^{3} P_j^{t_{s_1}}\right)\beta^{t_{s_1}}\right]}\right)\right]}, \\ 0<\beta^{t_{s_2}} \bigcup \beta^{t_{s_1}} < \frac{P_4^{t_{s_1}}}{\sum_{j=1}^{3} P_j^{t_{s_1}}} \\ 1, \text{else} \end{cases} \tag{A.37}$$

OP for UE_4 in $t_{s_{3-4}}$:

$$\begin{aligned} P_{4,t_{s_4}} &= P_r\left[OE_{4,t_{s_4}}\right] = P_r\left[OE_{r_{3-r_2}}^{t_{s_3}} \bigcup OE_{r_{4-r_2}}^{t_{s_3}} \bigcup OE_{r_{4-4}}^{t_{s_4}}\right] \\ &= P_r\left[\left(R_{r_{3-r_2}}^{t_{s_3}} < R\right) \bigcup \left(R_{r_{4-r_2}}^{t_{s_3}} < R\right) \bigcup \left(R_{r_{4-4}}^{t_{s_4}} < R\right)\right] \\ &= 1-\left[1-F_{R_{r_{3-r_2}}^{t_{s_3}}}(R)\right]\left[1-F_{R_{r_{4-r_2}}^{t_{s_3}}}(R)\right]\left[1-F_{R_{r_{4-4}}^{t_{s_4}}}(R)\right] \end{aligned} \tag{A.38}$$

$$\begin{aligned} F_{R_{r_{4-4}}^{t_{s_4}}}(R) &= P_r\left(R_{r_{4-4}}^{t_{s_4}} < R\right) = P_r\left(t_{s_4}\log_2\left(1+SINR_{t_{s_4}}^{4-4}\right) < R\right) \\ &= \begin{cases} 1-e^{\frac{-\beta^{t_{s_4}}\sigma_4^2}{\lambda_4'^2 P_{r_2}\left[P_4^{t_{s_4}}-P_2^{t_{s_4}}\beta^{t_{s_4}}\right]}}, 0<\beta^{t_{s_4}} < \frac{P_4^{t_{s_4}}}{P_2^{t_{s_4}}} \\ 1, \text{else} \end{cases} \end{aligned} \tag{A.39}$$

$$\begin{aligned} F_{R_{r_{4-r_2}}^{t_{s_3}}}(R) &= P_r\left(R_{r_{4-r_2}}^{t_{s_3}} < R\right) = P_r\left(t_{s_3}\log_2\left(1+SINR_{t_{s_3}}^{4-r_2}\right) < R\right) \\ &= \begin{cases} 1-e^{\frac{-\beta^{t_{s_3}}\sigma_{r_1}^2}{\lambda_{r_2}^{BS} P_s\left[P_4^{t_{s_3}}-\left(\sum_{j=1}^{2} P_j^{t_{s_3}}\right)\beta^{t_{s_3}}\right]}}, 0<\beta^{t_{s_3}} < \frac{P_4^{t_{s_3}}}{\sum_{j=1}^{2} P_j^{t_{s_3}}} \\ 1, \text{else} \end{cases} \end{aligned} \tag{A.40}$$

$$\begin{aligned} F_{R_{r_{3-r_2}}^{t_{s_3}}}(R) &= P_r\left(R_{r_{3-r_2}}^{t_{s_3}} < R\right) = P_r\left(t_{s_3}\log_2\left(1+SINR_{t_{s_3}}^{3-r_2}\right) < R\right) \\ &= \begin{cases} 1-e^{\frac{-\beta^{t_{s_3}}\sigma_{r_2}^2}{\lambda_{r_2}^{BS} P_s\left[P_3^{t_{s_3}}-\left(\sum_{j=1}^{2} P_j^{t_{s_3}}+P_4^{t_{s_3}}\right)\beta^{t_{s_3}}\right]}}, 0<\beta^{t_{s_3}} < \frac{P_3^{t_{s_3}}}{\sum_{j=1}^{2} P_j^{t_{s_3}}+P_4^{t_{s_3}}} \\ 1, \text{else} \end{cases} \end{aligned} \tag{A.41}$$

$$P_{4,t_{s4}} = \begin{cases} 1-e^{-\sigma^2\left[\frac{\beta^{t_{s4}}}{\lambda_4^{r2}P_{r_2}\left[P_4^{t_{s4}}-P_2^{t_{s4}}\beta^{t_{s4}}\right]^+}+\frac{\beta^{t_{s3}}}{\lambda_{r_2}^{BS}P_s}\left(\frac{1}{\left[P_4^{t_{s3}}-\left(\sum_{j=1}^{2}P_j^{t_{s3}}\right)\beta^{t_{s3}}\right]^+}+\frac{1}{\left[P_3^{t_{s3}}-\left(\sum_{j=1}^{2}P_j^{t_{s3}}+P_4^{t_{s3}}\right)\beta^{t_{s3}}\right]}\right)\right]}, \\ 0<\beta^{t_{s4}}<\frac{P_4^{t_{s4}}}{P_2^{t_{s4}}}\bigcup\beta^{t_{s3}}<\left\{\frac{P_4^{t_{s3}}}{\sum_{j=1}^{2}P_j^{t_{s3}}}\bigcup\frac{P_3^{t_{s3}}}{\sum_{j=1}^{2}P_j^{t_{s3}}+P_4^{t_{s3}}}\right\} \\ 1, \text{else} \end{cases} \quad \text{(A.42)}$$

Appendix B

Ergodic Rate of UE_1 in t_{s_3}:

In t_{s_3}, if UE_1 can perform SIC for UE_2,UE_3 and UE_4 successfully, then

$$F_{SINR_{t_{s_3}}^{1-1}}(y)=1-e^{\frac{-y\sigma^2}{P_1^{t_{s_3}}P_s\lambda_1^{BS}}} \tag{B.1}$$

$$E_1^{t_{s_3}}=-\frac{t_{s_3}}{\log_2}Ei\left(\frac{-1}{P_1^{t_{s_3}}P_s\lambda_1^{BS}}\right)e^{\frac{1}{P_1^{t_{s_3}}P_s\lambda_1^{BS}}} \tag{B.2}$$

Ergodic Rate of UE_2 in t_{s_1}:

$$a_2^{t_{s_1}}=\min\left(SINR_{t_{s_1}}^{2-2},SINR_{t_{s_1}}^{2-1}\right)$$

$$F_{SINR_{t_{s_1}}^2}(y)=P\left(a_2^{t_{s_1}}\le y\right)=\left[\left(1-F_{SINR_{t_{s_1}}^{2-2}}(y)\right)\left(1-F_{SINR_{t_{s_1}}^{2-1}}(y)\right)\right] \tag{B.3}$$

$$F_{SINR_{t_{s_1}}^{2-1}}(y)=P\left(\frac{P_2^{t_{s_1}}P_s\left|h_1^{BS}\right|^2}{P_1^{t_{s_1}}P_s\left|h_1^{BS}\right|^2+{\sigma_1}^2}\le y\right)=1-e^{\frac{-y{\sigma_1}^2}{\left(P_2^{t_{s_1}}-yP_1^{t_{s_1}}\right)P_s\lambda_1^{BS}}} \tag{B.4}$$

$$F_{SINR_{t_{s_1}}^{2-2}}(y)=P\left(\frac{P_2^{t_{s_1}}P_s\left|h_2^{BS}\right|^2}{P_1^{t_{s_1}}P_s\left|h_2^{BS}\right|^2+{\sigma_2}^2}\le y\right)=1-e^{\frac{-y{\sigma_2}^2}{\left(P_2^{t_{s_1}}-yP_1^{t_{s_1}}\right)P_s\lambda_2^{BS}}} \tag{B.5}$$

$$F_{SINR_{t_{s_1}}^2}(y)=\begin{cases}1-e^{\frac{-y{\sigma_2}^2}{\left(P_2^{t_{s_1}}-yP_1^{t_{s_1}}\right)P_s}\left(\frac{1}{\lambda_1^{BS}}+\frac{1}{\lambda_2^{BS}}\right)}, y>0\\ 1, y\le 0\end{cases} \tag{B.6}$$

The closed-form expression of $F_{SINR_{t_{s_1}}^2}(y)$ can be obtained by considering a high SINR situation for which the transmission power of the BS is infinite, i.e. $P_s\to\infty$, which changes

$$F_{SINR_{t_{s_1}}^2}(y)=\begin{cases}1-e^{-\frac{y{\sigma_2}^2}{P_s}\left(\frac{1}{\lambda_1^{BS}}+\frac{1}{\lambda_2^{BS}}\right)}, 0<y<\frac{P_2^{t_{s_1}}}{P_1^{t_{s_1}}}\\ 1, \text{else}\end{cases} \tag{B.7}$$

$$E_2^{t_{s_1}}=-\frac{t_{s_1}}{\log_2}Ei\left(-\frac{1}{P_s}\left(\frac{1}{\lambda_1^{BS}}+\frac{1}{\lambda_2^{BS}}\right)\right)e^{\frac{1}{P_s}\left(\frac{1}{\lambda_1^{BS}}+\frac{1}{\lambda_2^{BS}}\right)} \tag{B.8}$$

Ergodic Rate UE_2 in $t_{s_{3-4}}$:

$$P_2^{t_{s3}} + P_4^{t_{s3}} = 1$$

$$a_2^{t_{s4}} = \min\left(SINR_{t_{s3}}^{2-1}, SINR_{t_{s3}}^{2-r_2}, SINR_{t_{s4}}^{2-2} \right)$$

$$F_{SINR_{t_{s4}}^2}(y) = P\left(a_2^{t_{s4}} \le y\right) = \left[1 - \left(1 - F_{SINR_{t_{s4}}^{2-2}}(y)\right)\left(1 - F_{SINR_{t_{s3}}^{2-1}}(y)\right)\left(1 - F_{SINR_{t_{s3}}^{2-r_2}}(y)\right)\right] \quad \text{(B.9)}$$

$$F_{SINR_{t_{s3}}^{2-1}}(y) = P\left(\frac{P_2^{t_{s3}} P_s \left|h_1^{BS}\right|^2}{P_1^{t_{s3}} P_s \left|h_1^{BS}\right|^2 + {\sigma_1}^2} \le y\right) = 1 - e^{\frac{-y{\sigma_1}^2}{\left(P_2^{t_{s3}} - yP_1^{t_{s3}}\right)P_s\lambda_1^{BS}}} \quad \text{(B.10)}$$

$$F_{SINR_{t_{s3}}^{2-r_2}}(y) = P\left(\frac{P_2^{t_{s3}} P_s \left|h_{r_2}^{BS}\right|^2}{P_1^{t_{s3}} P_s \left|h_{r_2}^{BS}\right|^2 + {\sigma_{r_2}}^2} \le y\right) = 1 - e^{\frac{-y{\sigma_{r_2}}^2}{\left(P_2^{t_{s3}} - yP_1^{t_{s3}}\right)P_s\lambda_{r_2}^{BS}}} \quad \text{(B.11)}$$

$$F_{SINR_{t_{s4}}^{2-2}}(y) = P\left(\frac{P_2^{t_{s4}} P_{r_2} \left|h_2^{r_2}\right|^2}{{\sigma_2}^2} \le y\right) = 1 - e^{\frac{-y{\sigma_2}^2}{P_2^{t_{s4}} P_{r_2}\lambda_2^{r_2}}} \quad \text{(B.12)}$$

$$F_{SINR_{t_{s3-4}}^2}(y) = \begin{cases} 1 - e^{-y{\sigma_1}^2\left(\frac{1}{P_s\lambda_1^{BS}} + \frac{1}{P_s\lambda_{r_2}^{BS}} + \frac{1}{P_2^{t_{s4}} P_{r_2}\lambda_2^{r_2}}\right)}, 0 < y < \frac{P_2^{t_{s3}}}{P_1^{t_{s3}}} \\ 1, \text{else} \end{cases} \quad \text{(B.13)}$$

To find the closed-form expression of $F_{SINR_{t_{s3-4}}^2}(y)$ with $P_s \to \infty$ and $P_{r_2} \to \infty$, and assuming $\frac{P_2^{t_{s3}}}{P_1^{t_{s3}}} = b$ and $\sigma^2\left(\frac{1}{P_s\lambda_1^{BS}} + \frac{1}{P_s\lambda_{r_2}^{BS}} + \frac{1}{P_2^{t_{s4}} P_{r_2}\lambda_2^{r_2}}\right) = a$.

$$E_2^{t_{s3-4}} = \frac{t_{s_3}}{\log_2}\left[Ei(a) - Ei(ab + a)\right]e^a \quad \text{(B.14)}$$

Ergodic Rate UE_3 in $t_{s_{1-2}}$

$$a_3^{t_{s2}} = \min\left(SINR_{t_{s1}}^{3-1}, SINR_{t_{s1}}^{3-2}, SINR_{t_{s1}}^{3-r_2}, SINR_{t_{s2}}^{3-3} \right)$$

$$F_{SINR_{t_{s2}}^3}(y) = P\left(a_3^{t_{s2}} \le y\right) = \left[1 - \left(1 - F_{SINR_{t_{s1}}^{3-1}}(y)\right)\left(1 - F_{SINR_{t_{s1}}^{3-2}}(y)\right)\left(1 - F_{SINR_{t_{s1}}^{3-r_2}}(y)\right)\left(1 - F_{SINR_{t_{s2}}^{3-3}}(y)\right)\right] \quad \text{(B.15)}$$

$$F_{SINR_{t_{s_1}}^{3-1}}(y)=P\left(\frac{P_3^{t_{s_1}}P_s\left|h_1^{BS}\right|^2}{\sum_{j=1}^{2}P_j^{t_{s_1}}P_s\left|h_1^{BS}\right|^2+{\sigma_1}^2}\le y\right)=1-e^{\frac{-y{\sigma_1}^2}{\left(P_3^{t_{s_1}}-y\sum_{j=1}^{2}P_j^{t_{s_1}}\right)P_s\lambda_1^{BS}}} \tag{B.16}$$

$$F_{SINR_{t_{s_1}}^{3-2}}(y)=P\left(\frac{P_3^{t_{s_1}}P_s\left|h_2^{BS}\right|^2}{\sum_{j=1}^{2}P_j^{t_{s_1}}P_s\left|h_2^{BS}\right|^2+{\sigma_2}^2}\le y\right)=1-e^{\frac{-y{\sigma_2}^2}{\left(P_3^{t_{s_1}}-y\sum_{j=1}^{2}P_j^{t_{s_1}}\right)P_s\lambda_2^{BS}}} \tag{B.17}$$

$$F_{SINR_{t_{s_1}}^{3-r_2}}(y)=P\left(\frac{P_3^{t_{s_1}}P_s\left|h_{r_2}^{BS}\right|^2}{\sum_{j=1}^{2}P_j^{t_{s_1}}P_s\left|h_{r_2}^{BS}\right|^2+{\sigma_{r_2}}^2}\le y\right)=1-e^{\frac{-y{\sigma_{r_2}}^2}{\left(P_3^{t_{s_1}}-y\sum_{j=1}^{2}P_j^{t_{s_1}}\right)P_s\lambda_{r_2}^{BS}}} \tag{B.18}$$

$$F_{SINR_{t_{s_2}}^{3-3}}(y)=P\left(\frac{P_3^{t_{s_2}}P_{r_2}\left|h_3^{r_2}\right|^2}{{\sigma_3}^2}\le y\right)=1-e^{\frac{-y{\sigma_3}^2}{P_3^{t_{s_2}}P_{r_2}\lambda_3^{r_2}}} \tag{B.19}$$

$$F_{SINR_{t_{s_{1-2}}}^{3}}(y)=\begin{Bmatrix}1-e^{-y\sigma^2\left(\frac{1}{P_s\lambda_1^{BS}}+\frac{1}{P_s\lambda_2^{BS}}+\frac{1}{P_s\lambda_{r_2}^{BS}}+\frac{1}{P_3^{t_{s_2}}P_{r_2}\lambda_3^{r_2}}\right)}, 0<y<\frac{P_3^{t_{s_1}}}{\sum_{j=1}^{2}P_j^{t_{s_1}}}\\ 1,\text{else}\end{Bmatrix} \tag{B.20}$$

To find the closed-form expression of $F_{SINR_{t_{s_{1-2}}}^{3}}(y)$ with $P_s\to\infty, P_{r_1}\to\infty$ and $P_{r_2}\to\infty$, and assuming $\frac{P_3^{t_{s_1}}}{\sum_{j=1}^{2}P_j^{t_{s_1}}}=b$ and $\sigma^2\left(\frac{1}{P_s\lambda_1^{BS}}+\frac{1}{P_s\lambda_2^{BS}}+\frac{1}{P_s\lambda_{r_2}^{BS}}+\frac{1}{P_3^{t_{s_2}}P_{r_2}\lambda_3^{r_2}}\right)=a$

$$E_3^{t_{s_{1-2}}}=\frac{t_{s_1}}{\log_2}[Ei(a)-Ei(ab+a)]e^a \tag{B.21}$$

Ergodic Rate UE_3 in $t_{s_{3-4}}$:

$$a_3^{t_{s_4}}=\min\left(SINR_{t_{s_3}}^{3-1},SINR_{t_{s_3}}^{3-r_1},SINR_{t_{s_3}}^{3-r_2},SINR_{t_{s_4}}^{3-3}\right)$$

$$\begin{aligned}F_{SINR_{t_{s_{3-4}}}^{3}}(y)&=P\left(a_3^{t_{s_4}}\le y\right)\\&=\left[1-\left(1-F_{SINR_{t_{s_3}}^{3-1}}(y)\right)\left(1-F_{SINR_{t_{s_3}}^{3-r_1}}(y)\right)\left(1-F_{SINR_{t_{s_3}}^{3-r_2}}(y)\right)\left(1-F_{SINR_{t_{s_4}}^{3-3}}(y)\right)\right]\end{aligned} \tag{B.22}$$

$$F_{SINR_{t_{s3}}^{3-1}}(y)=P\left(\frac{P_3^{t_{s3}}P_s\left|h_1^{BS}\right|^2}{\sum_{j=1}^{2}P_j^{t_{s3}}P_s\left|h_1^{BS}\right|^2+P_4^{t_{s3}}P_s\left|h_1^{BS}\right|^2+{\sigma_1}^2}\le y\right) \tag{B.23}$$
$$=1-e^{\frac{-y{\sigma_1}^2}{\left(P_3^{t_{s3}}-y\left(\sum_{j=1}^{2}P_j^{t_{s3}}+P_4^{t_{s3}}\right)\right)P_s\lambda_1^{BS}}}$$

$$F_{SINR_{t_{s3}}^{3-r_2}}(y)=P\left(\frac{P_3^{t_{s3}}P_s\left|h_{r_2}^{BS}\right|^2}{\sum_{j=1}^{2}P_j^{t_{s3}}P_s\left|h_{r_2}^{BS}\right|^2+P_4^{t_{s3}}P_s\left|h_{r_2}^{BS}\right|^2+{\sigma_{r_2}}^2}\le y\right) \tag{B.24}$$
$$=1-e^{\frac{-y{\sigma_{r_2}}^2}{\left(P_3^{t_{s3}}-y\left(\sum_{j=1}^{2}P_j^{t_{s3}}+P_4^{t_{s3}}\right)\right)P_s\lambda_{r_2}^{BS}}}$$

$$F_{SINR_{t_{s3}}^{3-r_1}}(y)=P\left(\frac{P_3^{t_{s3}}P_s\left|h_{r_1}^{BS}\right|^2}{\sum_{j=1}^{2}P_j^{t_{s3}}P_s\left|h_{r_1}^{BS}\right|^2+P_4^{t_{s3}}P_s\left|h_{r_1}^{BS}\right|^2+{\sigma_{r_1}}^2}\le y\right) \tag{B.25}$$
$$=1-e^{\frac{-y{\sigma_{r_1}}^2}{\left(P_3^{t_{s3}}-y\left(\sum_{j=1}^{2}P_j^{t_{s3}}+P_4^{t_{s3}}\right)\right)P_s\lambda_{r_1}^{BS}}}$$

$$F_{SINR_{t_{s4}}^{3-3}}(y)=P\left(\frac{P_3^{t_{s4}}P_{r_1}\left|h_3^{r_1}\right|^2}{{\sigma_3}^2}\le y\right)=1-e^{\frac{-y{\sigma_3}^2}{P_3^{t_{s4}}P_{r_1}\lambda_3^{r_1}}} \tag{B.26}$$

$$F_{SINR_{t_{s3-4}}^{3}}(y)=\begin{cases}1-e^{-y\sigma^2\left(\frac{1}{P_s\lambda_1^{BS}}+\frac{1}{P_s\lambda_{r_2}^{BS}}+\frac{1}{P_s\lambda_{r_1}^{BS}}+\frac{1}{P_3^{t_{s4}}P_{r_1}\lambda_3^{r_1}}\right)}, 0<y<\frac{P_3^{t_{s3}}}{\sum_{j=1}^{2}P_j^{t_{s3}}+P_4^{t_{s3}}}\\ 1, \text{else}\end{cases} \tag{B.27}$$

To find the closed-form expression $F_{SINR_{t_{s3-4}}^{3}}(y)$ with $P_s\to\infty, P_{r_1}\to\infty$ and $P_{r_2}\to\infty$, and assuming $\frac{P_3^{t_{s3}}}{\sum_{j=1}^{2}P_j^{t_{s3}}+P_4^{t_{s3}}}=b$ and $\sigma^2\left(\frac{1}{P_s\lambda_1^{BS}}+\frac{1}{P_s\lambda_{r_2}^{BS}}+\frac{1}{P_s\lambda_{r_1}^{BS}}+\frac{1}{P_3^{t_{s4}}P_{r_1}\lambda_3^{r_1}}\right)=a$

$$E_3^{t_{s3-4}}=\frac{t_{s_3}}{\log_2}[Ei(a)-Ei(ab+a)]e^a \tag{B.28}$$

Ergodic Rate UE_4 in $t_{s_{1-2}}$:

$$a_4^{t_{s_2}}=\min\left(SINR_{t_{s_1}}^{4-1}, SINR_{t_{s_1}}^{4-2}, SINR_{t_{s_1}}^{4-r_1}, SINR_{t_{s_1}}^{4-r_2}, SINR_{t_{s_2}}^{4-4}\right)$$

$$F_{SINR^{4}_{t_{s_{1-2}}}}(y)=P\left(a_4^{t_{s_2}}\le y\right)$$

$$=\begin{bmatrix}1-\left(1-F_{SINR^{4-1}_{t_{s_1}}}(y)\right)\left(1-F_{SINR^{4-2}_{t_{s_1}}}(y)\right)\left(1-F_{SINR^{4-\eta}_{t_{s_1}}}(y)\right)\\ \left(1-F_{SINR^{4-r_2}_{t_{s_1}}}(y)\right)\left(1-F_{SINR^{4-4}_{t_{s_2}}}(y)\right)\end{bmatrix} \tag{B.29}$$

$$F_{SINR^{4-1}_{t_{s_1}}}(y)=P\left(\frac{P_4^{t_{s_1}}P_s\left|h_1^{BS}\right|^2}{\sum_{j=1}^{3}P_j^{t_{s_1}}P_s\left|h_1^{BS}\right|^2+{\sigma_1}^2}\le y\right)=1-e^{\frac{-y{\sigma_1}^2}{\left(P_4^{t_{s_1}}-y\sum_{j=1}^{3}P_j^{t_{s_1}}\right)P_s\lambda_1^{BS}}} \tag{B.30}$$

$$F_{SINR^{4-2}_{t_{s_1}}}(y)=P\left(\frac{P_4^{t_{s_1}}P_s\left|h_2^{BS}\right|^2}{\sum_{j=1}^{3}P_j^{t_{s_1}}P_s\left|h_2^{BS}\right|^2+{\sigma_2}^2}\le y\right)=1-e^{\frac{-y{\sigma_2}^2}{\left(P_4^{t_{s_1}}-y\sum_{j=1}^{3}P_j^{t_{s_1}}\right)P_s\lambda_2^{BS}}} \tag{B.31}$$

$$F_{SINR^{4-\eta}_{t_{s_1}}}(y)=P\left(\frac{P_4^{t_{s_1}}P_s\left|h_{r_1}^{BS}\right|^2}{\sum_{j=1}^{3}P_j^{t_{s_1}}P_s\left|h_{r_1}^{BS}\right|^2+{\sigma_{r_1}}^2}\le y\right)=1-e^{\frac{-y{\sigma_\eta}^2}{\left(P_4^{t_{s_1}}-y\sum_{j=1}^{3}P_j^{t_{s_1}}\right)P_s\lambda_\eta^{BS}}} \tag{B.32}$$

$$F_{SINR^{4-r_2}_{t_{s_1}}}(y)=P\left(\frac{P_4^{t_{s_1}}P_s\left|h_{r_2}^{BS}\right|^2}{\sum_{j=1}^{3}P_j^{t_{s_1}}P_s\left|h_{r_2}^{BS}\right|^2+{\sigma_{r_2}}^2}\le y\right)=1-e^{\frac{-y{\sigma_\eta}^2}{\left(P_4^{t_{s_1}}-y\sum_{j=1}^{3}P_j^{t_{s_1}}\right)P_s\lambda_{r_2}^{BS}}} \tag{B.33}$$

$$F_{SINR^{4-4}_{t_{s_2}}}(y)=P\left(\frac{P_4^{t_{s_2}}P_{r_1}\left|h_4^{r_1}\right|^2}{{\sigma_4}^2}\le y\right)=1-e^{\frac{-y{\sigma_4}^2}{P_4^{t_{s_2}}P_{r_1}\lambda_4^{r_1}}} \tag{B.34}$$

$$F_{SINR^{4}_{t_{s_{1-2}}}}(y)=\begin{Bmatrix}1-e^{-y\sigma^2\left(\frac{1}{P_s\lambda_1^{BS}}+\frac{1}{P_s\lambda_2^{BS}}+\frac{1}{P_s\lambda_{r_1}^{BS}}+\frac{1}{P_s\lambda_{r_2}^{BS}}+\frac{1}{P_4^{t_{s_2}}P_{r_1}\lambda_4^{r_1}}\right)},0<y<\dfrac{P_4^{t_{s_1}}}{\sum_{j=1}^{3}P_j^{t_{s_1}}}\\ 1,\text{else}\end{Bmatrix} \tag{B.35}$$

The find the closed-form expression $F_{SINR^{4}_{t_{s_{1-2}}}}(y)$ with $P_s\to\infty, P_{r_1}\to\infty$ and $P_{r_2}\to\infty$, and assuming $\dfrac{P_4^{t_{s_1}}}{\sum_{j=1}^{3}P_j^{t_{s_1}}}=b$ and $\sigma^2\left(\dfrac{1}{P_s\lambda_1^{BS}}+\dfrac{1}{P_s\lambda_2^{BS}}+\dfrac{1}{P_s\lambda_{r_1}^{BS}}+\dfrac{1}{P_s\lambda_{r_2}^{BS}}+\dfrac{1}{P_4^{t_{s_2}}P_{r_1}\lambda_4^{r_1}}\right)=a$

$$E_4^{t_{s_{1-2}}}=\frac{t_{s_1}}{\log_2}[Ei(a)-Ei(ab+a)]e^a \tag{B.36}$$

Ergodic Rate UE_4 in $t_{s_{3-4}}$:

$$a_4^{t_{s4}} = \min\left(SINR_{t_{s3}}^{4-1}, SINR_{t_{s3}}^{4-r_2}, SINR_{t_{s4}}^{4-2}, SINR_{t_{s4}}^{4-4} \right)$$

$$\begin{aligned} F_{SINR_{t_{s3-4}}^4}(y) &= P\left(a_4^{t_{s4}} \le y\right) \\ &= \left[1-\left(1-F_{SINR_{t_{s3}}^{4-1}}(y)\right)\left(1-F_{SINR_{t_{s3}}^{4-r_2}}(y)\right)\left(1-F_{SINR_{t_{s3}}^{4-2}}(y)\right)\left(1-F_{SINR_{t_{s4}}^{4-4}}(y)\right)\right] \end{aligned} \quad \text{(B.37)}$$

$$F_{SINR_{t_{s3}}^{4-1}}(y) = P\left(\frac{P_4^{t_{s3}} P_s \left|h_1^{BS}\right|^2}{\sum_{j=1}^{2} P_j^{t_{s3}} P_s \left|h_1^{BS}\right|^2 + {\sigma_1}^2} \le y\right) = 1 - e^{\frac{-y{\sigma_1}^2}{\left(P_4^{t_{s3}} - y\sum_{j=1}^{2} P_j^{t_{s3}}\right)P_s \lambda_1^{BS}}} \quad \text{(B.38)}$$

$$F_{SINR_{t_{s3}}^{4-r_2}}(y) = P\left(\frac{P_4^{t_{s3}} P_s \left|h_{r_2}^{BS}\right|^2}{\sum_{j=1}^{2} P_j^{t_{s3}} P_s \left|h_{r_2}^{BS}\right|^2 + {\sigma_{r_2}}^2} \le y\right) = 1 - e^{\frac{-y{\sigma_{r_2}}^2}{\left(P_4^{t_{s3}} - y\sum_{j=1}^{2} P_j^{t_{s3}}\right)P_s \lambda_{r_2}^{BS}}} \quad \text{(B.39)}$$

$$F_{SINR_{t_{s4}}^{4-2}}(y) = P\left(\frac{P_4^{t_{s4}} P_{r_2} \left|h_2^{r_2}\right|^2}{P_2^{t_{s4}} P_{r_2} \left|h_2^{r_2}\right|^2 + {\sigma_2}^2} \le y\right) = 1 - e^{\frac{-y{\sigma_2}^2}{\left(P_4^{t_{s4}} - yP_2^{t_{s4}}\right)P_{r_2} \lambda_2^{r_2}}} \quad \text{(B.40)}$$

$$F_{SINR_{t_{s4}}^{4-4}}(y) = P\left(\frac{P_4^{t_{s4}} P_{r_2} \left|h_4^{r_2}\right|^2}{P_2^{t_{s4}} P_{r_2} \left|h_4^{r_2}\right|^2 + {\sigma_4}^2} \le y\right) = 1 - e^{\frac{-y{\sigma_4}^2}{\left(P_4^{t_{s4}} - yP_2^{t_{s4}}\right)P_{r_2} \lambda_4^{r_2}}} \quad \text{(B.41)}$$

$$F_{SINR_{t_{s3-4}}^4}(y) = \begin{cases} 1 - e^{-y\sigma^2\left(\frac{1}{P_s\lambda_1^{BS}} + \frac{1}{P_s\lambda_{r_2}^{BS}} + \frac{1}{P_{r_2}\lambda_2^{r_2}} + \frac{1}{P_{r_2}\lambda_4^{r_2}}\right)}, 0 < y < \frac{P_4^{t_{s3}}}{\sum_{j=1}^{2} P_j^{t_{s3}}}, 0 < y < \frac{P_4^{t_{s4}}}{P_2^{t_{s4}}} \\ 1, \text{else} \end{cases} \quad \text{(B.42)}$$

To find the closed-form expression $F_{SINR_{t_{s3-4}}^4}(y)$ with $P_s \to \infty, P_{r_1} \to \infty$ and $P_{r_2} \to \infty$, and assuming $\frac{P_4^{t_{s4}}}{P_2^{t_{s4}}} = c, \frac{P_4^{t_{s3}}}{\sum_{j=1}^{2} P_j^{t_{s3}}} = b$ and $\sigma^2\left(\frac{1}{P_s\lambda_1^{BS}} + \frac{1}{P_s\lambda_{r_2}^{BS}} + \frac{1}{P_{r_2}\lambda_2^{r_2}} + \frac{1}{P_{r_2}\lambda_4^{r_2}}\right) = a$

$$E_4^{t_{s3-4}} = \frac{t_{s_3}}{\log_2}\left[Ei(ab+a) - Ei(ac+a)\right]e^a \quad \text{(B.43)}$$

Where $c-b>0, c+1>0, b+1>0$